THE PERFORMANCE AND BEHAVIOR OF DECK-TO-GIRDER CONNECTIONS FOR THE SANDWICH PLATE SYSTEM (SPS) IN BRIDGE DECK APPLICATIONS

by

Joshua T. Boggs

Thesis submitted to the Faculty of the Virginia Polytechnic Institute and State University in partial fulfillment of the requirements for the degree of

MASTER OF SCIENCE

in

CIVIL ENGINEERING

APPROVED:

Thomas E. Cousins, Co-Chairperson	Thomas M. Murray, Co-Chairperson

Elisa D. Sotelino

May 15, 2008
Blacksburg, Virginia

Keywords: Sandwich Plate System, Composite Bridge Decks, Fatigue, Slip-Critical Connection, Weld Stress, Lateral Load Distribution

THE PERFORMANCE AND BEHAVIOR OF DECK-TO-GIRDER CONNECTIONS FOR THE SANDWICH PLATE SYSTEM (SPS) IN BRIDGE DECK APPLICATIONS

Joshua T. Boggs

(ABSTRACT)

An innovative approach to possible construction or rehabilitation of bridge decks can be found in a bridge construction system called the Sandwich Plate System (SPS). The technology developed and patented by Intelligent Engineering Canada Limited in conjunction with an industry partner, Elastogran GmbH, a member of BASF, may be an effective alternative to traditional bridge rehabilitation techniques.

Although the system's behavior has been studied the connection of the SPS deck to the supporting girders has not been investigated. Two types of connection are presented in this research. The use of a bent plate welded to the SPS deck and subsequently bolted to the supporting girder utilizing slip-critical connections has been utilized in the construction of a SPS bridge. A proposed SPS bridge system utilizes the top flange of the supporting girder welded directly to the SPS deck as the deck-to-girder connection.

The fatigue performance of a deck-to-girder connection utilizing a bent plate welded to the deck and bolted to the supporting girder using slip-critical connections was tested in the Virginia Tech Materials and Structures Laboratory. The testing concluded that the fatigue performance of the welded and bolted bent plate connection was limited by the weld details and no slip occurred in the slip-critical connections. Finite element modeling of the two types of deck-to-girder connections was also used to determine influence of the connections on the local and global behavior of a SPS bridge system. A comparison of the different connection details showed that the connection utilizing the flange welded directly to the SPS deck significantly reduces the stresses at location of the welds in the connections, but the connection type has a limited influence on the global behavior of a SPS bridge.

ACKNOWLEDGEMENTS

This is the last page I wrote in my Thesis, an arguably the most important. My experience at Virginia Tech and gratefulness to those who have helped me along the way cannot be summed up in this one page, but here is an attempt.

I would first like to thank my thesis committee. Dr. Cousins, serving as my advisor and Co-chair of my committee, you have provided me with countless hours of mentorship in my studies and in my career pursuits. I appreciate your ability to guide me while allowing me opportunities to thrive on my own. Dr. Murray, also a Co-chair of my committee, I am at awe at your patience and ability to teach and mentor students. I wish you the best of luck with your retirement and am very fortunate to be one your students. Dr. Sotelino, thank you for your continuous support and positive attitude. I only hope that I continue to meet more people like you throughout my career.

To all of those at the Structures Lab, I could not have done it without you. Brett Farmer and Dennis Huffman, I believe I learned as much from the both of you than if I had added another class to my transcript. And to all of the graduate students that have helped me along the way, I wish you the best of luck with the rest of your careers. Take care of the alligators.

Finally, I would like to thank my family and closest friends. Without your constant love and support none of this would have been possible. Thank you for always believing in me and never letting me down.

Table of Contents

Page

Chapter 1: Introduction 1
1.1 Introduction 1
1.2 Objectives and Scope of Study 2
1.2.1 Fatigue resistance testing of SPS deck-to-girder connections 3
1.2.2 Finite Element Modeling 4
Chapter 2: Literature Review 5
2.1 SPS Technology Background 5
2.2 SPS Bridge Inventory 7
2.2.1 Shenley Bridge 7
2.2.2 Martin Branch Bridge 8
2.3 Deck-to-Girder Connections 10
2.4 Fatigue in Steel Bridge Connections 11
2.4.1 AASHTO-LRFD Specifications for Fatigue 12
2.5 Simplified Finite Element Modeling 13
2.5.1 Slab-Girder Finite Element Analysis and Element Selection 14
2.5.2 Boundary Conditions 15
2.5.3 Application of Loading 16
2.6 Live Load Distribution 17
2.6.1 AASHTO Standard Specifications for Load Distribution Factors (LDF) 19
2.6.2 AASHTO-LRFD Specifications (2007) for Load Distribution Factors (LDF) 19
2.7 Summary 21
Chapter 3: Laboratory Testing 23
3.1 General 23
3.2 Load Range Calculation 25
3.3 Testing Setup 27
3.3.1 Overview 27
3.3.2 Load Case 1 Setup 27
3.3.3 Load Case 2 29
3.3.4 Instrumentation 31
3.3.5 Testing 32
Chapter 4: Laboratory Fatigue Test Results 34
4.1 Load Case 1 Results 34
4.1.1 Vertical Deflection Results 35
4.1.2 Weld Failures 38
4.1.3 Strain Gauge Results 40

4.1.4 Slip Displacement Results 46
4.2 Repair of Cracked Welds 46
4.3 Analysis of Load Case 1 Results 47
4.3.1 Load Case 1 Summary 51
4.4 Load Case 2 Results 52
4.4.1 Vertical Deflection Results 52
4.4.2 Weld Failures 55
4.4.3 Strain Gauge Results 58
4.4.4 Slip Displacement Results 64
4.5 Analysis of Load Case 2 Results 64
4.5.1 Load Case 2 Summary 65
4.6 Laboratory Fatigue Testing Summary 65
Chapter 5: Local Behavior Investigation 67
5.1 Introduction 67
5.2 Finite Element Model 68
5.2.1 Validation of Initial Model 71
5.3 Connection Comparisons 75
5.3.1 Deflection Comparison 76
5.3.2 Stress Comparison 76
5.4 Summary 79
Chapter 6: Global Behavior Investigation 81
6.1 Introduction 81
6.2 Development of Initial Models 82
6.2.1 Validation of Initial Models 85
6.2.2 Load Case 1 Validation 85
6.2.3 Load Case 2 Validation 88
6.2.4 Shenley Bridge Validation 89
6.3 Global Response of Connections 93
6.3.1 Shenley Bridge Load Distribution Factors (LDF) 95
6.3.2 Martin Branch Bridge Load Distribution Factors (LDF) 96
6.4 Summary 97
Chapter 7: Conclusions and Recommendations 98
7.1 Conclusions 98
7.1.1 Laboratory Testing Conclusion 98
7.1.2 Local Behavior 99
7.1.3 Global Behavior 99
7.2 Summary 100

7.3 Recommendations for future research 101
References 102
Appendix A: Additional Laboratory Supporting Calculations 105
A.1 Load Calculation Example 105
Appendix B: Additional Local Behavior Results 109
B.1 Displacement contour plots from finite element panels 109
B.2 Average finite element transverse stresses at weld toe 110
Appendix C: Additional Global Behavior Supporting Calculations 114
C.1 Load Distribution Factor calculations 114

List of Tables

Table 2.1: LRFD –LDF for a concrete deck supported by steel girders 20
Table 4.1: Average deflections and percent change for Load Case 1 36
Table 4.2: Average strains and percent change at 47.2 kips for Girder A 41
Table 4.3: Average strains and percent change at 47.2 kips for Girder B 41
Table 4.4: Average weld strains and corresponding stresses 48
Table 4.5: Average deflections and percent change for Load Case 2 53
Table 4.6: Average strains and percent change at 46.6 kips for Girder A 59
Table 4.7: Average strains and percent change at 46.6 kips for Girder B 60
Table 5.1: Elements used for pane model generation 69
Table 5.2: Deflection at mid-span of the finite element panel models 76
Table 5.3: Stress comparison due to eccentric loading 77
Table 6.1: ANSYS element types 82
Table 6.2: Deflection and strains comparison for Load Case 1 87
Table 6.3: Deflection and strains comparison for Load Case 2 88
Table 6.4: Displacement validation based on field test data 92
Table 6.5: Strain validation based on field test data 92
Table 6.6: LDF validation based on displacements 93
Table 6.7: LDF validation based on strains 93
Table 6.8: Shenley Bridge LDF based on displacements 96
Table 6.9: Shenley Bridge LDF based on strains 96
Table 6.10: Martin Bridge LDF based on displacements 96
Table 6.11: Martin Bridge LDF based on strains 97
Table C.1: FEA deflections and calculated LDF for Shenley bent “L” connection 114
Table C.2: FEA strains and calculated LDF for Shenley bent “L” connection 114
Table C.3: FEA deflections and calculated LDF for Shenley flange connection 115
Table C.4: FEA strains and calculated LDF for Shenley flange connection 115
Table C.5: FEA deflections and calculated LDF for Martin Branch bent “L” connection 116
Table C.6: FEA strains and calculated LDF for Martin Branch bent “L” connection 117
Table C.7: FEA deflections and calculated LDF for Martin Branch flange connection 118
Table C.8: FEA strains and calculated LDF for Martin Branch flange connection 119

List of Figures

Figure 1.1: Sandwich Plate System 2
Figure 1.2: Deck-to-girder connections used in SPS bridge deck applications 3
Figure 2.1: Equivalent weight systems 6
Figure 2.2: Shenley Bridge 7
Figure 2.3: Shenley Bridge deck installation 8
Figure 2.4: Cross section of Martin Brach Bridge 9
Figure 2.5: Shear connections 10
Figure 2.6: S-N relationship curve 13
Figure 2.7: FEA modeling techniques 15
Figure 2.8: Live Load Girder Distribution 18
Figure 3.1: Typical cross section of a SPS panel connection 23
Figure 3.2: Typical cross-section of the one-half scale bridge 24
Figure 3.3: Typical connections in the panel-to-girder and panel-to-panel connections 25
Figure 3.4: HL-93 Design Truck 26
Figure 3.5: Test setup with two point loads for each girder and corresponding moment 28
Figure 3.6: Cross section of Load Case 1 configuration with two spreader beams 29
Figure 3.7: Test setup with point load at mid-span of each girder and corresponding moment 30
Figure 3.8: Load Case 2 configuration with point loads at mid-span 30
Figure 3.9: Overview of typical girder instrumentation 32
Figure 3.10: Strain gauges (SG) instrumentation of each girder 32
Figure 4.1: Load versus displacement of MTS actuators at 43,000 cycles 35
Figure 4.2: Load versus Deflection of Girder A 37
Figure 4.3: Load versus Deflection of Girder B 37
Figure 4.4: Load Case 1 deflection at mid-span at 47.2 kips versus number of cycles 38
Figure 4.5: Details of the weld cracks at 43,000 cycles 39
Figure 4.6: Location of the weld cracks at 43,000 cycles 40
Figure 4.7: Strain throughout cross section depth at 0 cycles in Girder A and Girder B 42
Figure 4.8: Strains throughout cross section depth of Girder A at 0 and 43,000 cycles 43
Figure 4.9: Strains throughout cross section depth of Girder B at 0 and 43,000 cycles 44
Figure 4.10: Strains at maximum load of 47.2 kips versus number of cycles of Girder A 45

Figure 4.11: Strains at a maximum load of 47.2 kips versus number of cycles of Girder B 45
Figure 4.12: Typical LVDT setup 46
Figure 4.13: Weld cracks before and after repair 47
Figure 4.14: S-N relationship curve 49
Figure 4.15: S-N relationship curve with corresponding stress and cycles at weld failure 50
Figure 4.16: Spreader beam and bearing pad under maximum load after weld cracking 51
Figure 4.17: Load versus deflection of Girder A 53
Figure 4.18: Load versus deflection of Girder B 54
Figure 4.19: Load Case 2 deflection at mid-span versus number of cycles 54
Figure 4.20: Location of the weld cracks at 700,000 cycles 55
Figure 4.21: Weld crack details at 700,000 cycles 56
Figure 4.22: Weld crack details at 700,000 cycles 57
Figure 4.23: Strain throughout cross section depth at 0 cycles in Girder A and Girder B 58
Figure 4.24: Strains throughout cross section depth of Girder A at 700,000 cycles 61
Figure 4.25: Strains throughout cross section depth of Girder A at 700,000 cycles 62
Figure 4.26: Strains at 46.6 kips versus number of cycles of Girder A 63
Figure 4.27: Strains at 46.6 kips versus number of cycles of Girder B 63
Figure 4.28: Typical weld connection three point intersection 64
Figure 4.29: Typical crack initiation of a bearing-type connection (Kulak et al. 1987) 65
Figure 5.1: SPS connections and theoretical deck deformations 68
Figure 5.2: Model geometry of SPS panel 70
Figure 5.3: Finite element geometry of bent “L” connection 71
Figure 5.4: Test setup for finite element panel validation 72
Figure 5.5: Instrumentation layout for finite element panel validation 72
Figure 5.6: Comparison of boundary condition based on deflection response 74
Figure 5.7: Contour plot of deflection from the FEA of SPS panel section 74
Figure 5.8: Finite element geometry of welded flange connection 75
Figure 5.9: Location of element at the weld toe 77
Figure 5.10: Normalized stress comparison of both connections 79
Figure 6.1: Basic model geometry and finite element representation 84
Figure 6.2: ANSYS model of Load Case 1 86

Figure 6.3: Strain throughout cross section depth for Load Case 1 87
Figure 6.4: ANSYS model of Load Case 2 88
Figure 6.5: Strain throughout cross section depth for Load Case 1 89
Figure 6.6: Three Axle Dump Truck used for Shenley Bridge Testing (Harris 2007) 90
Figure 6.7: Loading Cases used for validation of Shenley Bridge model 90
Figure 6.8: Finite element model of Shenley Bridge 94
Figure 6.9: Finite element model of Martin Branch Bridge 95
Figure B.1: Contour plot of deck displacement for bent "L" panel 109
Figure B.2: Contour plot of deck displacement for welded flange panel 109
Figure B.3: Average transverse stress at 30 in. for bent "L" connection 110
Figure B.4: Average transverse stress at 24 in. for bent "L" connection 110
Figure B.5: Average transverse stress at 18 in. for bent "L" connection 111
Figure B.6: Average transverse stress at 12 in. for bent "L" connection 111
Figure B.7: Average transverse stress at 30 in. for welded flange connection 112
Figure B.8: Average transverse stress at 24 in. for welded flange connection 112
Figure B.9: Average transverse stress at 18 in. for welded flange connection 113
Figure B.10: Average transverse stress at 12 in. for welded flange connection 113

Chapter 1: Introduction

1.1 Introduction

Aging infrastructure has been a critical issue for several decades and has resulted in a growing need for rehabilitation and retrofit options for the deteriorating state of the national bridge inventory. In the report "Status of the Nation's Highways, Bridge, and Transit: Conditions and Performance" presented to Congress in 2004, the Federal Highway Administration (FHWA) estimated that 158,428 of the nation's 594,101 inventoried bridges (26.7 percent) were deficient. A deficient bridge is defined as both structurally deficient and functionally obsolete (FHWA, 2006).

It has been estimated that approximately 1 billion square feet of bridge deck is in need of replacement at a cost of $30 billion (FHWA, 2006). An investigation by Lachemi et al. (2007) surveyed 33 different bridge organizations and agencies in North America about current bridge rehabilitation practices. The survey provides guidance from past experience to aid in the selection of expeditious rehabilitation techniques. Inexpensive options can be implemented including enforcing load limits or simply detouring commercial traffic. These quick fixes, however; only causes more traffic congestion and air pollution as well as damage to secondary bridges (Vanderzee 2005). It is evident that there is a need for a practical time saving solution to either remediate or replace these bridges.

An innovative approach to possible construction or rehabilitation of bridge decks can be found in a new technology called the Sandwich Plate System (SPS). The technology developed and patented by Intelligent Engineering Canada Limited in conjunction with an industry partner, Elastogran GmbH, a member of BASF, has proven to be an effective alternative to traditional bridge construction or rehabilitation techniques (Harris 2007; Kennedy et al. 2005; Vincent and Ferro 2004). SPS is a composite system comprised of two steel plates bonded to a compact polyurethane elastomer core as shown in Figure 1.1. The core is injected into the airtight cavity formed by two steel faceplates and perimeter bars, the latter is not shown in Figure 1.1. This two-part liquid provides continuous support to the plates allowing shear transfer from one plate to another without the need for fatigue prone stiffeners found in traditional stiffened decks. The core also prevents local plate buckling and distortion, and eliminates the need for stiffeners. The

flexural stiffness and strength of the system is determined by the thickness of the sandwich plate elements, which can be modified depending on the application requirements of the SPS.

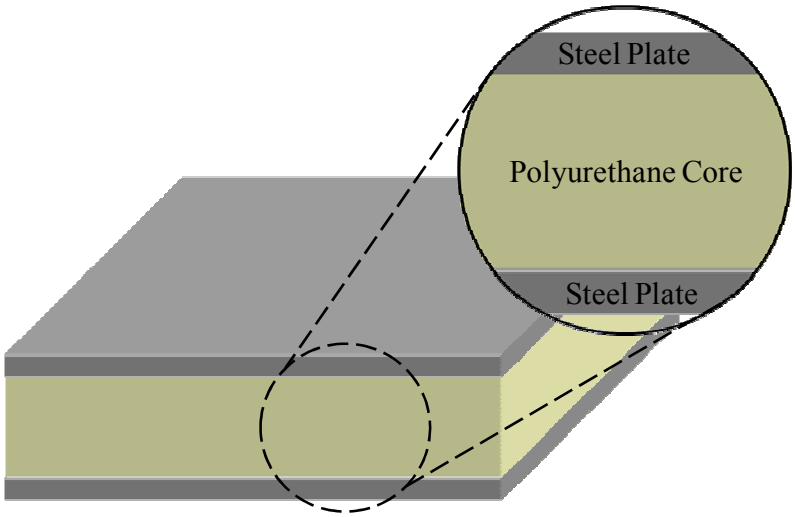

Figure 1.1: Sandwich Plate System

1.2 Objectives and Scope of Study

The use of Sandwich Plate System in bridge construction and rehabilitation is a relatively new concept. Comprehensive research has been conducted at Virginia Tech to address the usability of SPS in bridge construction and rehabilitation (Grigg 2006; Harris 2007; Martin 2005). This project is part of the ongoing investigation to assess the performance and behavior of Sandwich Plate System technology in bridge applications.

The basis of this research comes from a recently constructed SPS bridge in Quebec Province, Canada known as the Shenley Bridge and a proposed SPS bridge in Wise County, Texas known as the Martin Branch Bridge. The Shenley Bridge utilizes a bent "L" plate that is welded to the bridge deck and subsequently bolted to the supporting girders as the deck-to-girder connection, while the proposed Martin Branch Bridge connects the supporting girders directly to the deck through continuous welding of the flanges to the underside of the deck, eliminating the need for the bent "L" plate and bolted connections. The connections used in the Shenley and Martin Branch bridges are shown in Figure 1.2 (a) and (b), respectively. This research investigated the performance of the bent "L" connection and determined the effect of the different connections on the behavior of a SPS bridge system.

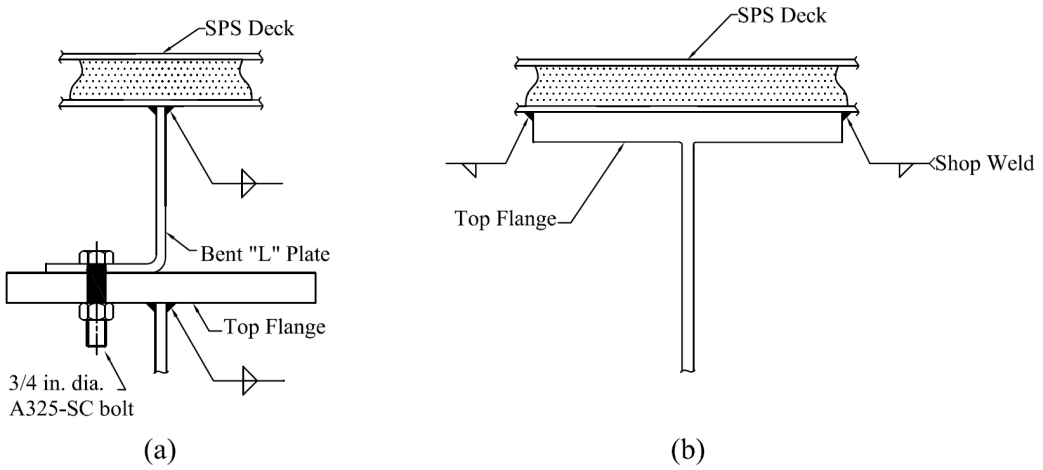

Figure 1.2: Deck-to-girder connections used in SPS bridge deck applications

This thesis focuses on two areas affecting SPS bridge technology. The first objective focuses on the performance of a specific welded and bolted connection through laboratory testing of a scaled bridge specimen. The results from the laboratory investigation were used to determine the fatigue resistance of the connection. The second objective utilizes simplistic finite element modeling to compare the behavior of the two types of connections. Stresses at the welds connecting the bent "L" and the girder flanges were used to compare local behavior of the connections, while lateral load distribution factors were evaluated to understand the affect of the connections on the global behavior of the systems.

1.2.1 Fatigue resistance testing of SPS deck-to-girder connections

Previous research at Virginia Tech has investigated the fatigue resistance of the post-injection welded joints and longitudinal weld joints between sandwich plates under cyclic fatigue loading (Grigg 2006; Martin 2005). However, the fatigue resistance of the connections between the sandwich panels and supporting girders has not been previously investigated. A testing program was conducted in the Virginia Tech Structures and Materials Research Laboratory to address the performance of a deck-to-girder connection. The connection of the deck panels to the girders consisted of a bent "L" plate welded to the bottom plate of the sandwich plate panels. This plate was secured to the girders through slip-critical bolts. The testing program addressed the primary connection of the slip-critical bolted connection as well as the welds used to connect a bent "L" plate to the panel.

To investigate the fatigue resistance of the connections, a one-half scale specimen was used. The testing procedure simulated a truck load placed on the specimen. The simulated truck load was repeated continuously to determine the fatigue life of the welded and slip-critical connections between the deck and the supporting girders. The fatigue test was designed to produce a factored stress in the composite system corresponding to the moment resulting from an AASHTO-LRFD HL-93 fatigue truck in the one-half scale bridge specimen.

1.2.2 Finite Element Modeling

Limited research and applications of SPS bridge technology make finite element modeling (FEM) of the SPS bridges essential to understanding their behavior. Research by Harris (2007) developed simplified methods of modeling SPS systems and is closely followed in this thesis for the studies involving the global behavior of the system.

Without field data from the Martin Branch Bridge, finite element modeling was necessary to investigate the affect of the new type of connection used in the proposed bridge. The finite element program ANSYS was used for all analytical analysis.

To focus on the local behavior of the connections, a SPS panel section of the laboratory bridge specimen was modeled. A three-dimensional model of a 5 ft. by 14 ft 9 in. section of the bridge deck and its deck-to-girder connections was developed using brick and shell elements. The model was validated using laboratory test data. The use of the brick elements at the deck-to-girder connection locations allowed local stresses at the welds to be evaluated as a tire patch loading was placed eccentric to the connection location.

Lateral load distribution factors were determined for different bridge configurations and used to determine the influence of connections on the global behavior of the bridge. To insure accuracy, initial models were developed of the laboratory specimen as well as the Shenley Bridge and each model was carefully validated using data from the representative testing programs. Each bridge, the Shenley Bridge and the Martin Branch Bridge were modeled with and without the bent “L” connection to determine the effect of the connection on the global behavior of each bridge system.

Chapter 2: Literature Review

2.1 SPS Technology Background

Through extensive research by Intelligent Engineering and Elastogran GmbH, SPS technology and the components of the elastomer core have been developed to create a material that can reach its full plastic capacity in flexure or compression without local buckling of the plates. To best understand the performance of the system, bond strength, flexural and compressive resistance, shear strength, and fatigue resistance need to be considered. It is important to note that there are many characteristics that affect the performance of the system; only the basic principles are discussed in this section. IE (2007), Kennedy et al. (2002), Kennedy et al. (2005), and Vincent and Ferro (2004) cover in great detail the technology and benefits of SPS.

Strong bond strength between the steel plates and the elastomer core is essential to the reliability of the system. The bond must be able to withstand a wide range of temperatures and loading configurations including static and dynamic. These bond strengths are largely affected by several factors including metal types, surface roughness, and casting conditions. Previous research suggests that a minimum of 6 MPa bond strength is required after the plates and elastomer core set (Kennedy et al. 2002). To obtain this, the faceplates are grit blasted and freed of grease, dirt or other contaminates before the elastomer is injected.

The steel-elastomer-steel construction of SPS makes the product unique in the way it handles flexure and compressive resistance. The tensile strength of the system is governed by the thickness of the faceplates, while the elastomer core provides continuous support to the faceplates preventing local bucking. This allows the flexural capacity of the system to be determined by the full plastic moment capacity of the faceplates. Although faceplate configuration is fairly standard, variations in the elastomer core design such as core material thickness can be used to optimize the structure without a significant increase in weight.

The shear strength of the system is developed through shear transfer from one plate to another through the elastomer core. This type of system is analogous to that of a standard stiffened orthotropic steel deck. Unlike stiffened orthotropic decks, there is no need for closely spaced discrete stiffeners that tend to be prone to fatigue of the steel to steel welds.

The fatigue resistance of the interface of the sandwich plates and the elastomer core is vital to the performance of the system. Weakening of the bond between the core and the faceplates due to loading over time can significantly reduce the strength and stiffness of the system. The interface of the plates and core has been exhaustively tested and found to be relatively fatigue insensitive; the faceplates have a fatigue resistance associated with category type A (IE, 2007).

The interaction of the steel faceplates and the elastomer core create a system that is comparable to traditional bridge materials. The sandwich system is considerably stronger and stiffer when compared to an equivalent weight non-sandwich alternative, as shown in Figure 2.1. The density of the steel plates is approximately 490 pounds per cubic foot (pcf) while the polyurethane core has a density of only 68.7 pcf. It can be assumed for theoretical purposes that the weight of the polyurethane core in negligible. An increase in the core thickness (h_c) forces the face plates (t_f) apart and results in an improvement in flexural stiffness and ultimately a reduction in flexural stress. This concept is most commonly seen in the analogy of an equal weight rectangular beam and an I-section, where the flanges of the I-section greatly increase the moment of inertia (Harris, 2007).

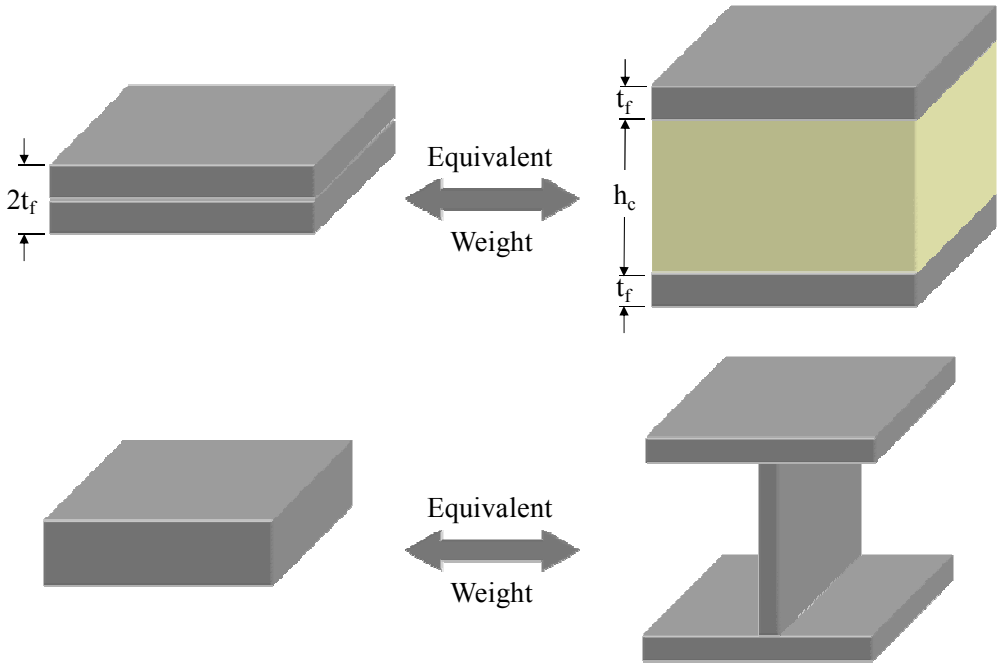

Figure 2.1: Equivalent weight systems

2.2 SPS Bridge Inventory

The use of SPS technology in bridge applications is limited. Various bridge rehabilitation projects have used SPS technology, and there are several proposed new construction projects in North America. However, to date, there is one completed highway bridge and only one under construction in North America using SPS technology. Brief descriptions of these bridges are presented.

2.2.1 Shenley Bridge

The Shenley Bridge was the first highway bridge built using a SPS deck. It was constructed in 2003 in Saint-Martin, Quebec Canada after floodwaters destroyed the existing two-lane bridge. The completed bridge is shown in Figure 2.2. The bridge deck utilizes 1/4 in. steel plates separated by a 1-1/2 in. elastomer core. The bridge has a span of 73.8 ft and a transverse width of 23.3 ft. Composite action was achieved through the connection of ten prefabricated SPS panels to three longitudinal girders with slip-critical bolts connecting the girder flanges to cold-formed angles welded to the SPS panels. Each built-up girder consisted of a top flange measuring 3/4 in. by 11-13/16 in., a web 15/32 in. by 36-7/32 in. and a bottom flange 1 in. by 13-13/16 in. The angles were 7-7/8 by 4-9/16 by 3/8 in.

The panels were also made continuous through panel-to-panel connections on the top and underside of each panel, using transverse field welds and slip-critical bolts, respectively.

Figure 2.2: Shenley Bridge

The SPS option for the Shenley Bridge was advantageous because of the avoided load limits and most importantly the minimized time out of service. The total construction process took a remarkable fourteen days with the construction of the of the superstructure including bearings, supporting girders, SPS deck, and other components only taking six days even with unfavorable weather conditions (Vincent et al. 2005). Figure 2.3 illustrates the ease of installation of a SPS panel during the construction process. A panel is simply placed on the girder system and connected by slip-critical bolts and transverse welding.

Figure 2.3: Shenley Bridge deck installation

2.2.2 Martin Branch Bridge

After being awarded funds from Innovative Bridge Research and Construction Program (IBRC) the Texas Department of Transportation (TxDOT) decided the most appropriate use of the funds would be the implementation of SPS technology in a new construction project needed to replace an outdated rural bridge. The old bridge located on CR 4191 at Martin Branch in Wise County, Texas was deficient in several areas including load carrying capacity and structural degradation. After years of experimenting with rapid construction techniques and technologies TxDOT determined the use of SPS represented a good opportunity to expedite the project. (Holt 2007).

The new SPS bridge superstructure was designed by Intelligent Engineering using applicable code requirements from AASHTO LRFD Bridge Design Specifications. The design of

bridge deck using SPS requires basic understanding of how the SPS material behaves as compared to conventional construction materials. Two basic assumptions were made about the behavior of the system. An equivalent concrete slab-girder system was used to calculate live load distributions factors and complete composite action was assumed between the deck-girder system.

At the time of this thesis the proposed Martin Branch Bridge was still under construction, so the proposed design and construction techniques are presented. The design of the new bridge has three simply-supported spans of 50 ft long and 32 ft 4 in. wide for a total span length of 150 ft. A typical span consists of two panels, 50 ft long and 16 ft 2 in. wide, supported by six longitudinal girders (W27x114) spaced 6 ft 3-1/4 in. center-to-center spacing. The girders will be transversely connected with diaphragms at each end and at mid-span utilizing C15x50 and C15x33.9 sections, respectively. Each panel consists of 5/16 in. steel faceplates separated by a 1 in. elastomer core. The supporting girders will be attached to the SPS through continuous shop welds prior to placement in the field. The two 50 ft long panels were designed to be placed longitudinally and then spliced together in the field. This panel-to-panel connection at the centerline of the bridge deck was designed to utilizing 1 in. diameter A325-SC bolts. The bolts will be spaced evenly at a 4 in. center to center spacing. After all the bolts are pretensioned, the panels will be further connected using a 7/16 in. groove weld, placed between the panels.

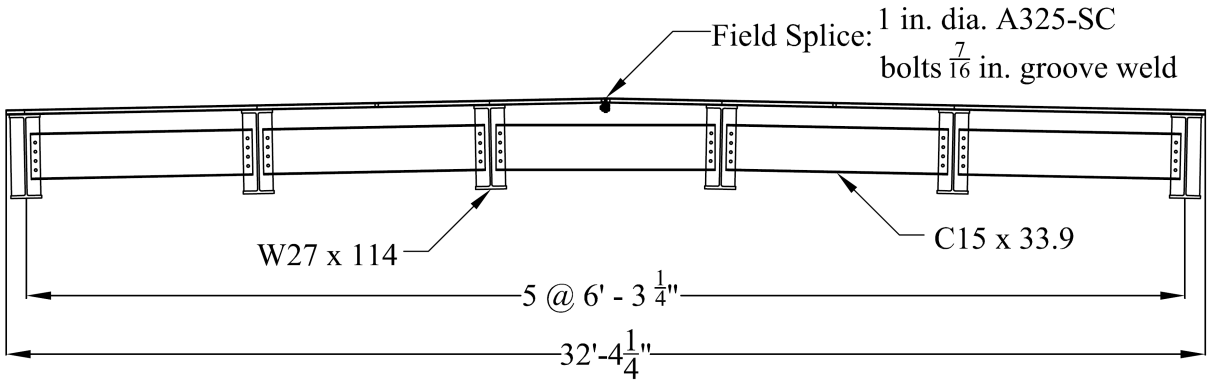

Figure 2.4: Cross section of Martin Brach Bridge

2.3 Deck-to-Girder Connections

Composite construction techniques have become essential for efficient bridge designs. Commonly, the construction technique involves a concrete deck supported by girders and connected together by shear connectors, similar to those shown in Figure 2.5 (a). The shear connectors resist the horizontal shear between the deck and the girders. Typical shear connectors, commonly called, shear studs are welded to the top flange of the supporting girder and extend into the deck. Concrete is then placed around the shear connectors and creates the composite bond between the deck and the girder. The deck and girders are assumed to act in unison since; there is essentially no slip at the deck-to-girder interface.

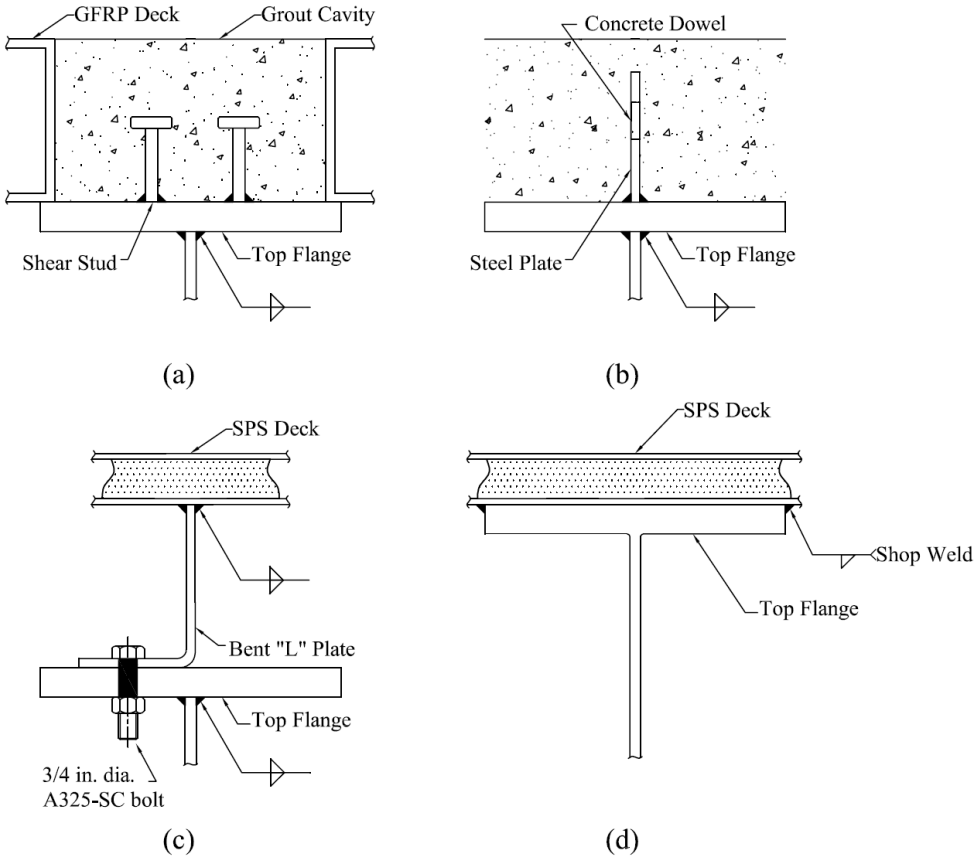

Figure 2.5: Shear connections

Composite interaction of components other than conventional concrete decks supported by steel girders has been researched. Moses et al. (2006) conducted field testing of three composite construction bridge systems using glass fiber-reinforced polymers (GFRP) supported

by steel girders and made composite by utilizing grouted cavities. The cavities provided an area where shear studs were attached to the supporting girders and subsequently grouted in place, similar to Figure 2.5 (a). Less composite action was observed in the GFRP decks when compared to conventional concrete decks, most likely due to the less stiff axial behavior of the deck. Other researchers (Higgins and Mitchell 2001) have investigated composite behavior using alternate shear connectors. The alternative connections consisted of steel plates with holes drilled along their length. The plates were welded to the top flanges of the supporting girders before placement of concrete. When concrete was placed around the plates, the cured concrete provided composite action through bearing resistance on the plate, shear strength of the "concrete dowels" and friction. This alternative connection is shown in Figure 2.5 (b). The alternative shear connection maintained composite action through service and fatigue testing.

There is a limited amount of research in alternative shear connections that do not utilize concrete as a component of the composite action. Two particular connections can be found in the Shenley Bridge and proposed Martin Branch Bridge and are shown in Figure 2.5 (c) and (d), respectively. The Shenley Bridge utilizes a bent "L" that is welded to the deck and subsequently bolted to the supporting girder, while the Martin Branch Bridge achieves composite action by welding the SPS deck directly to the supporting girder.

2.4 Fatigue in Steel Bridge Connections

Cyclic repetitive loading of a steel component can cause failure at significantly lower stresses than are required for failure under static loads. This phenomenon of fatigue is important to understand when detailing the connections in a bridge system. Zhou (2004) presents several examples of fatigue cracks from improperly detailed connections and gives successful repair recommendations. Cousins and Stallings (1998) focused on laboratory testing of different bolted diaphragm-to-girder connections, while other researchers (Xiao and Yamada 2005) used a combination of laboratory and finite element analysis to determine the fatigue performance of different intersecting attachments. The majority of the existing literature focuses on fatigue cracking in diaphragm connections or member-to-member connections, but there is a limited amount of research of the fatigue performance of deck-to-girder connections.

2.4.1 AASHTO-LRFD Specifications for Fatigue

AAHSTO-LRFD (2007) gives eight categories that are defined by the fatigue resistance of different steel components and details that are subject to load-induced fatigue cracking. To assist in defining the particular component in question, detail descriptions and situations of use are defined. Illustrative examples also allow quick and accurate determination of the component or detail. These categories can then be related to a component S/N curve, which illustrates the relationship between the stress range (S) and the fatigue life (N) to give a simple method of determining fatigue life based on the specific category. AASHTO-LRFD defines this S-N relationship as Equation (2.1). A graphical representation of the nominal fatigue resistance for categories A through E' is shown in Figure 2.6.

$$(\Delta F)_n = \left(\frac{A}{N}\right)^{\frac{1}{3}} \geq \frac{1}{2}(\Delta F)_{TH} \tag{2.1}$$

Where: $(\Delta F)_n$ = nominal fatigue resistance
A = detail category constant from Table 6.6.1.2.5-1 (ksi^3)
N = number of cycles
$(\Delta F)_{TH}$ = constant-amplitude fatigue threshold

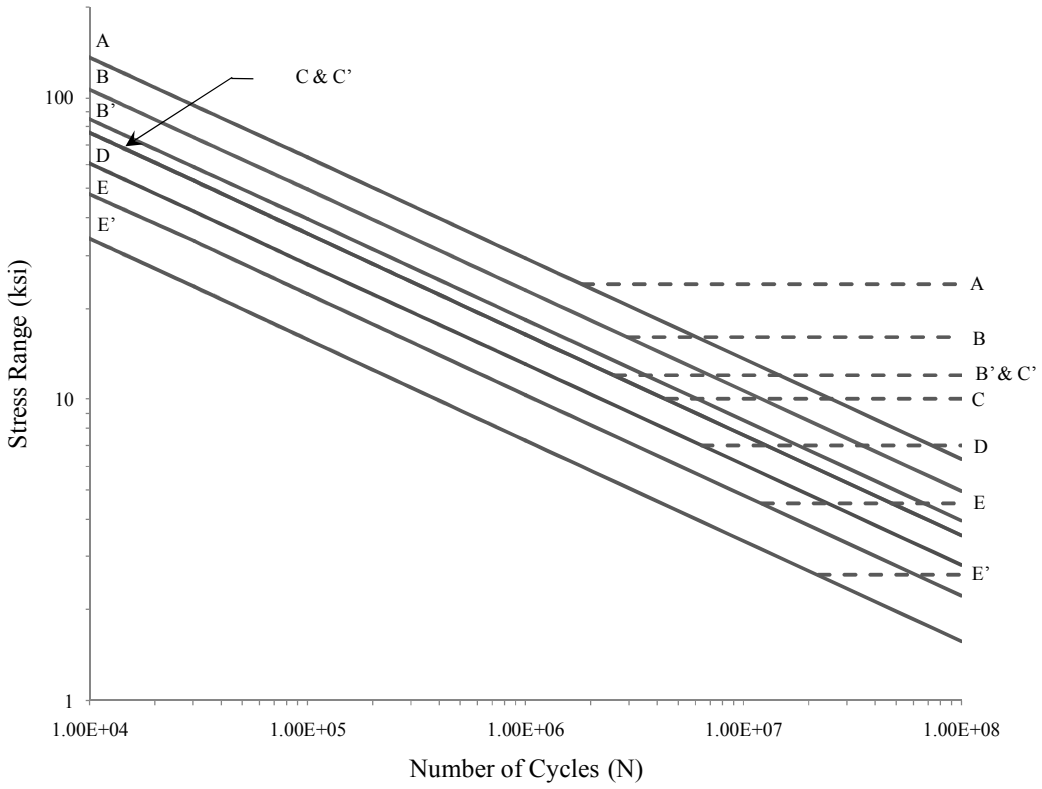

Figure 2.6: S-N relationship curve

2.5 Simplified Finite Element Modeling

In recent years, with the advancements in computer technology, the analysis of bridge structures using finite element analysis (FEA) software has become more common. Finite element analysis is a numerical approximation of a physical problem through the relationship formed by individual elements connected at points called nodes. It is important to understand that a finite element structure is a not an exact representation of the actual problem, rather a simplified model that can be used to provide results for an actual problem. It is an idealization of the geometry, material properties, loads and boundary conditions based on the understanding of the most relevant features needed to obtain the required results (Cook et al. 2001). The simplification of complex systems has proven advantageous for slab-girder bridges when compared to conventional design equations and methods (Eom and Nowak 2001; Mabsout et al. 1998; Tonias and Zhao 2007).

A simple and effective finite element model is ideal for expeditious and thorough investigations of the behavior of a bridge system, but it is imperative that the proper level of care and accuracy be applied to the model to give acceptable results. Modeling considerations such as the validity of the overall geometry, material properties, and loading and restraint conditions are essential for accurate results. Extensive literature exists for finite element modeling and most basic information can be found in any relevant textbook. This section reviews the literature related to simplistic finite element modeling of bridge structures.

2.5.1 Slab-Girder Finite Element Analysis and Element Selection

Various modeling techniques are used by researchers to best represent the behavior of slab-girder bridges. The three most common types, eccentric beam model, detailed beam model, and solid deck model, are presented. The eccentric beam considers the deck as a solid or shell element while the girder is an offset beam element connected by a rigid link and is the simplest modeling technique. The detailed beam model uses similar deck elements but adds a level of complexity by considering a combination of beam and shell elements for the girders. The slab-girder elements are again connected with rigid links. The most complex model utilizes solid elements to represent the entire structure. The use of rigid links is unnecessary in this model due to nodal connectively used to link the slab to the girder.

Many variations have been used in the formulation of the different modeling techniques as illustrated in Figure 2.7. Hays et al. (1986) developed a model using quadrilateral shell elements for the bridge deck and space frame elements for the girders. This type of model is similar to the eccentric beam model except the elements are simply connected at the center of gravity and a rigid link is not required. An true eccentric beam approach is presented by Imbsen and Nutt (1978). The model utilizes shell elements and beam elements connect by a rigid link to represent the deck and girders, respectively. Brockenbrough (1986) used a detailed beam approach and divided the beam into three parts. Each flange is modeled as a beam element and the web as a shell element. The slab utilizes shell elements connected through a rigid link to the centroidal nodes of each element. The solid deck approach is presented by Tarhini and Frederick (1992) using solid element for the deck and shell element for the girders. Figure 2.7 illustrates each of the modeling techniques.

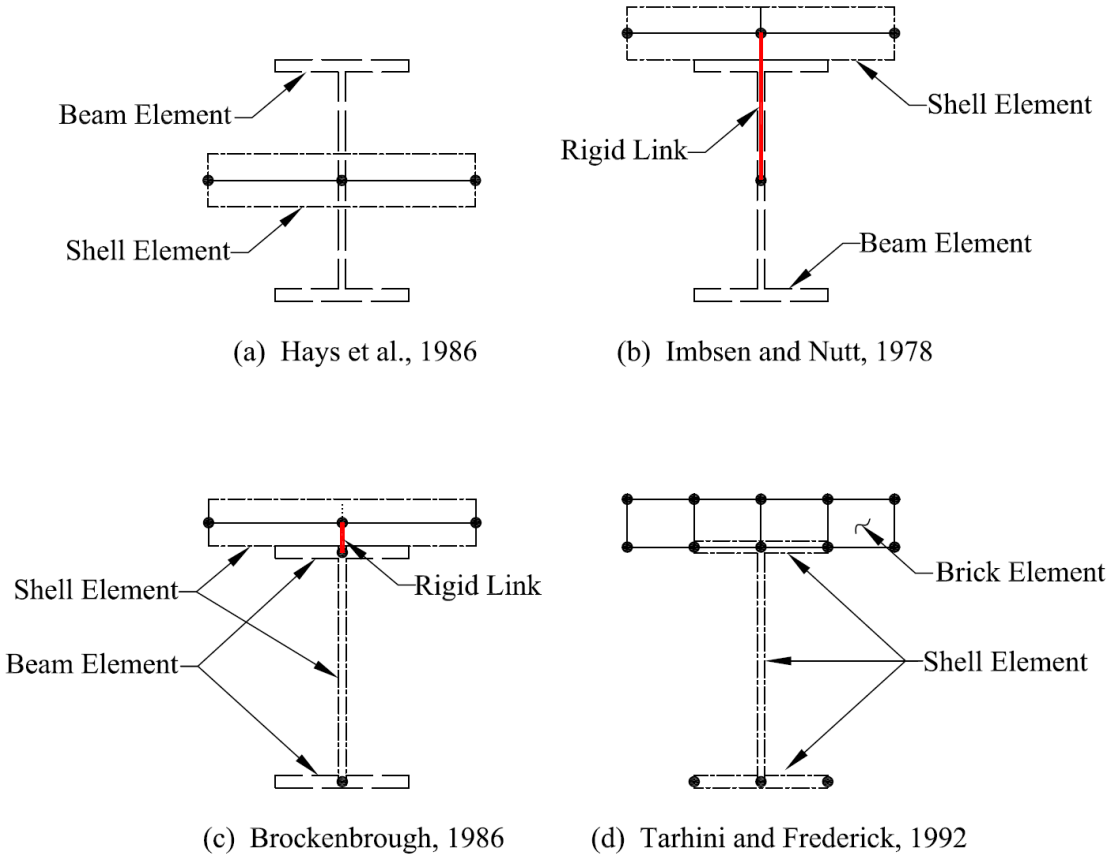

Figure 2.7: FEA modeling techniques

A study by Chung and Sotelino (2006) investigated the associated modeling errors for the eccentric beam and detailed beam models and provides guidelines for using these techniques. To study displacement incompatibilities and geometric modeling errors four basic models were compared. Each model utilized shell elements to represent the deck while varying the modeling of the girder. It was concluded that models utilizing shell element for girder modeling required high levels of mesh refinement to provide accurate results. The eccentric beam model, Figure 2.7 (b) was identified as the most economical model while still accurately predicting girder behavior.

2.5.2 Boundary Conditions

To achieve an accurate model of a structure, proper boundary or restraint conditions are essential. Theoretical idealizations have been developed to best represent different degrees of fixity. These can be a roller, pinned, or fixed support, but in reality, these conditions do not exist.

Actual structures exhibit a degree of restraint somewhere between those provided by the analytical values and careful consideration must be used to best represent a certain restraint. This is especially important when analytical values are to be compared to known results.

It is not only important to match the degree of fixity of a structure but also the location at which it acts. To accurately represent the behavior of the restraints, a model that best represents the actual bridge configuration is desired. FEA utilizes nodal degrees of freedom, meaning all boundary conditions as well as loads must be applied to the nodes. Several researchers have failed to comment on the locations of the support conditions, while others simply place the restraint at the centroid of the beam element. According to research by Bakht and Jaeger (1988) and Schulz et al. (1995) small changes in boundary conditions can have significant effects on the results of the model. This problem has been addressed by several authors. Eom and Nowak (2001) present several methods of restraints and suggest recommendations. Support conditions were applied at actual locations using either a pinned-roller or a pinned-pinned support condition. Elastic spring elements were also added to the top and bottom flanges to represent "partially frozen" supports. The FEA results were then compared to those from field testing. It was found that simple support (pinned-roller) boundary condition may provide more uniformed results. Chung and Sotelino (2006) suggest assigning boundary conditions to zero-dimensional elements located at the actual bearing location. These elements are then connected to the beam element through a rigid link.

2.5.3 Application of Loading

Similar to boundary conditions, it is essential to model the loading of a bridge to best represent actual configurations. As previously mentioned, all loads must be applied to the nodes of the elements. This can be difficult if the model is not developed so that the applied loading corresponds directly to nodal locations. Several researchers have suggested different methods for distributing loads to adjacent nodal locations. Chen (1995) uses tributary areas to distribute the loads on an element to the corresponding nodes, while Eom and Nowak (2001) use concentrated loads that are then linearly distributed to the nodes. Chung and Sotelino (2006) present a similar approach, but instead of a linearly distribution, the loads are distributed to the nodes using particular element shape functions. This method, referred to as the equivalent nodal load method

distributes applied loads by utilizing Equations (2.2) and (2.3) for distributed and concentrated forces, respectively.

$$R_e = \int N^T t \, dS \tag{2.2}$$

$$R_e = \sum_{i=1}^{K} N_i^T p_i \tag{2.3}$$

Where: N = shape function matrix
t = surface traction applied to the structure
p = point load applied to the structure

2.6 Live Load Distribution

The process of transversely distributing live load acting on a bridge deck to the supporting girders is a complicated and tedious task. Equilibrium requires that the load applied to the bridge must be equal to the summation of the loads carried by each girder, but there is not a simple correlation from load to distributed forces because of the complexity of the parameters affecting the distribution. These parameters can include but are not limited to the type and depth of deck, span length, transverse spacing of stringers and secondary members, stiffness of primary and secondary members, and the size and position of the loading (Tonias and Zhao 2007).

Ultimately, the influencing parameters affect the relative stiffness of the bridge system and the way by which the load is distributed to the girders. Assuming linear behavior of the bridge components allows the load in each girder to be proportional to its displacement (Barker and Puckett 2007). This behavior is best illustrated by comparing two slab-girder bridge systems. Figure 2.8(a) represents a relatively flexible deck system compared to the girders. It is obvious that the load is not well distributed and the girder under the load has the largest deflection while the other girder deflections are relatively small. A stiffer deck system is illustrated in Figure 2.8(b). Note the load is distributed more evenly throughout the system.

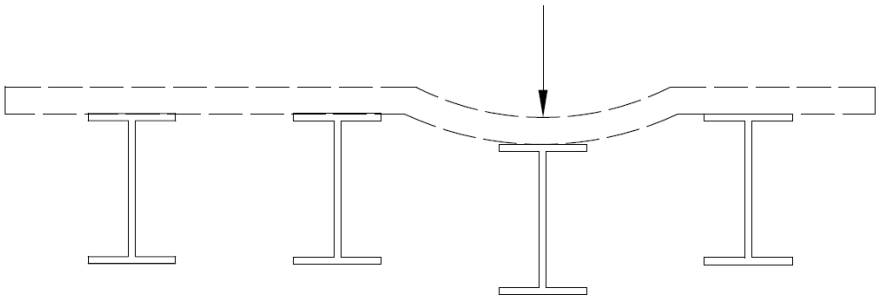

(a) Load Distribution with flexible deck components

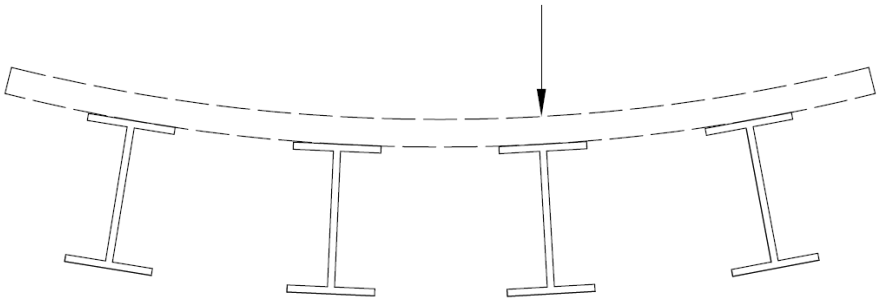

(b) Load Distribution with stiff deck components

Figure 2.8: Live Load Girder Distribution

It is well documented, that due to the complexity of load distribution, AASHTO specification design equations tend to yield overly conservative results and extensive research has addressed this issue. Kim and Nowak (1997) exhaustedly tested two simply supported steel I-girder bridges to determine load distribution. The live load testing of the bridges was performed under normal truck traffic, allowing data to be collected for approximately 900 trucks. This large amount of data was filtered and girder distribution factors compared to AASHTO methods. The measured results were consistently lower that the calculated factors. A field testing program and finite element validation of 17 steel girder bridges by Eom and Nowak (2001) investigated distribution of truck loads when compared to AASHTO specifications. It was found that measured distribution factors were lower when compared to AASHTO Standard and LRFD specifications, with the later being more consistent for longer spans with larger girder spacing. Shahawy and Huang (2001) and Yousif and Hindi (2007) also investigated girder distribution for concrete slab-girder bridges. Shahawy and Huang used observations from field testing and a parametric study of 645 slab-girder bridges, while Yousif and Hindi focused on a parametric study of 886 bridge structures. It was concluded that the AASHTO Standard and LRFD

specifications yield overly conservative load distribution results. Recent research by Harris (2007) investigated the ability to account for lateral load distribution in SPS bridges by using AASHTO-LRFD code provisions for a concrete deck supported by steel girders. Through an extensive parametric study it was found the difference between a SPS deck and a reinforced concrete deck is the stiffness parameter which was shown to have a minimal significance on the lateral load distribution. For all cases the SPS deck lateral load distribution were found to be less than the code requirements. Although possibly over conservative, the AASHTO specifications allow for simplistic and economical designs and are common practice in standard bridge design. The Standard and LRFD specification methods for determining transverse load distribution factors are presented in the following section.

2.6.1 AASHTO Standard Specifications for Load Distribution Factors (LDF)

The AASHTO Standard specification utilizes a simple approach that applies a fraction of the applied wheel line (both front and back) determined from Equation (2.2), commonly known as the S/D equation. AASHTO (2002) provides Table 3.23.1 to detail the usage of the "D" term, outlining different flooring types as well as the number of traffic lanes.

$$\mathbf{g} = \frac{\mathbf{S}}{\mathbf{D}} \tag{2.4}$$

Where: g = distribution factor
S = spacing between girders
D = differentiates between deck types and number of design traffic lanes

Research of the S/D formula found that the application of this approach was only applicable to bridges with typical geometry of approximately 6 ft girder spacing and 60 ft span length (Zokaie 2000). An extensive research project by the National Cooperative Highway Research Program (NCHRP) 12-26 initiated the development of the current AASHTO-LRFD design equations. These equations address additional parameters such as girder spacing, span length, and slab thickness.

2.6.2 AASHTO-LRFD Specifications (2007) for Load Distribution Factors (LDF)

The AASHTO-LRFD specifications have adopted equations similar to those developed based on the research from NCHRP 12-26, but additional parameters as well as limitations on the

range of applicability have been included to obtain more accurate distribution factors (Yousif and Hindi 2007). Although the LRFD specification is considered a simplistic approach to girder distribution, several parameters and variables must be applied to different bridge systems. In the interest of brevity, only the applicable equations and limitations for concrete deck supported by steel girders are presented in Table 2.1. A full explanation of variables and a complete description of all other types of bridge systems can be found in Section 4.6.2.2 of AASHTO (2007).

Table 2.1: LRFD –LDF for a concrete deck supported by steel girders

	Interior	**Applicability**	**Exterior**	**Applicability**
Moment	*One design lane loaded*			
	$g = 0.06 + \left(\frac{S}{14}\right)^{0.4}\left(\frac{S}{L}\right)^{0.3}\left(\frac{K_g}{12Lt_s^3}\right)^{0.1}$	$3.5 \le S \le 16.0$ $4.5 \le t_s \le 12.0$ $20 \le L \le 240$ $N_b \ge 4$ $10{,}000 \le K_g \le 7\times10^6$	Lever rule*	*does not include multiple presence factor
	Two or more design lanes loaded			
	$g = 0.075 + \left(\frac{S}{9.5}\right)^{0.6}\left(\frac{S}{L}\right)^{0.2}\left(\frac{K_g}{12Lt_s^3}\right)^{0.1}$	$3.5 \le S \le 16.0$ $4.5 \le t_s \le 12.0$ $20 \le L \le 240$ $N_b \ge 4$ $10{,}000 \le K_g \le 7\times10^6$	$g = e \cdot g_{interior}$ $e = 0.77 + \frac{d_e}{9.9}$	$-1.0 \le d_e \le 5.5$
Shear	*One design lane loaded*			
	$g = 0.36 + \frac{S}{25}$	$3.5 \le S \le 16.0$ $4.5 \le t_s \le 12.0$ $20 \le L \le 240$ $N_b \ge 4$	Lever rule*	*does not include multiple presence factor
	Two or more design lanes loaded			
	$g = 0.2 + \frac{S}{12} - \left(\frac{S}{35}\right)^{2.0}$	$3.5 \le S \le 16.0$ $4.5 \le t_s \le 12.0$ $20 \le L \le 240$ $N_b \ge 4$	$g = e \cdot g_{interior}$ $e = 0.6 + \frac{d_e}{10}$	$-1.0 \le d_e \le 5.5$

For exterior girders subjected to single lane loading and for bridge systems not in the specified range of applicability the lever rule can be applied to determine distribution factors. The lever rule is applied to the transverse section of a bridge system and treats the girders as supports. All interior supports are assumed to be hinged, thus creating a statically determinate system in which moments can be summed about any support to find reaction at another support. This method gives an upper bound on load distribution since no load is permitted across the interior hinged girders.

2.7 Summary

The review of the relevant literature in this chapter is aimed to focus on the important issues that still must be addressed before SPS technology can become a viable material in bridge deck systems.

An investigation and understanding of the fatigue performance of a deck-to-girder connection that does not use typical shear stud connections requiring concrete as a composite component is essential to making SPS an effective bridge deck alternative. There is a limited amount of research that investigates the specific types of connections used in SPS construction, specifically the welded bent "L" plate that is bolted to the supporting girders and the top flange welded to the SPS deck. A comparison of experimental fatigue behavior as compared to the AASHTO-LRFD fatigue design categories may provide insight into future designs of SPS bridge decks.

A testing program was conducted in the Virginia Tech Structures and Materials Research Laboratory to address the performance of a deck-to-girder connection consisting of a bent "L" plate welded to the bottom plate of the sandwich plate panels. This plate was secured to the girders through slip-critical bolts. The testing program addressed the primary connection of the slip-critical bolted connection as well as the welds used to connect a bent "L" plate to the panel.

The interaction of a relatively flexible bridge deck with different types of deck-to-girder connections may affect the local and global behavior of the SPS system. Finite element analysis is used in this study to investigate and compare the Shenley Bridge connections and the proposed Martin Branch Bridge connections. An investigation of the stresses at weld locations, and calculated global behavior such as lateral load distribution factors may provide a better understanding of this relatively new and innovative technology for bridge applications.

A finite element testing program was developed to investigate both the local and global behavior of connection used in SPS bridge deck applications. A three-dimensional model of a section of the bridge deck and its deck-to-girder connections was developed using brick and shell elements. The use of the brick elements at the deck-to-girder connection locations allowed local stresses at the welds to be evaluated as a tire patch loading was placed eccentric to the connection location. Each bridge, the Shenley Bridge and the Martin Branch Bridge were also modeled with and without the bent "L" connection to determine the effect of the connection on the global behavior of each bridge system.

Chapter 3: Laboratory Testing

3.1 General

Previous testing of the panel-to-panel connections (Martin 2005) utilized a one-half scale bridge provided by Intelligent Engineering Ltd. (IE). This bridge specimen was ideal for testing of the deck-to-girder connections. The bridge consisted of eight one-half scale sandwich plate bridge deck panels measuring 5 ft by 14 ft 9 in. in plan. Figure 3.1 shows a typical cross section of a SPS panel including the deck and panel connections. Each consisted of top and bottom plates bonded to an elastomer core with specified dimensions of 1/8 in. and 3/4 in. thick, respectively. The panels had two cross stringers that were used for connection of the panels to the girders. The stringers were bent steel plates nominally 3/16 in. by 7-7/8 in. by 14 ft 9 in. and are subsequently referred to as bent "L" plates. The one-half scale bridge was supported by two plate girders. Each girder was a built-up member with a top flange measuring 5/8 in. by 6 3/8 in., a web 1/4 in. by 21-3/8 in., and a bottom flange 1 in. by 7 in. and were spaced at 5 ft center-to-center. The girders were connected by steel angle diaphragms spaced at 10 ft. center-to-center. Each diaphragm consisted of steel angles nominally 2 in. by 2 in. by 5/16 in.

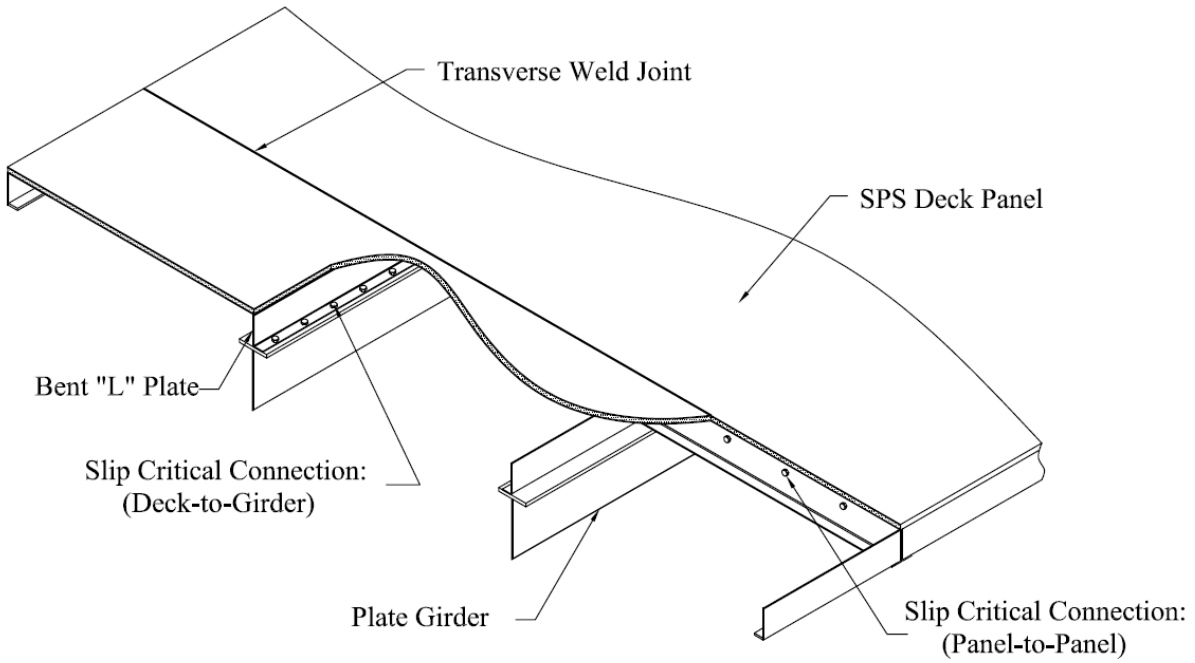

Figure 3.1: Typical cross section of a SPS panel connection

A labeling system was developed to distinguish between the two girders. Throughout this thesis all cross sectional views are taken from the same perspective with Girder A located on the left and Girder B on the right. A typical view in the longitudinal direction of the bridge shows Girder A. A cross section of the half scale specimen is shown in Figure 3.2.

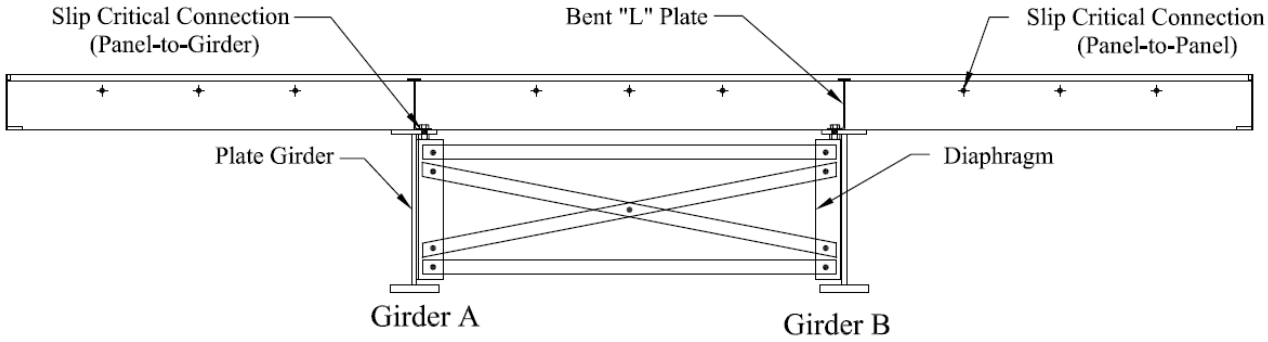

Figure 3.2: Typical cross-section of the one-half scale bridge

Two types of slip-critical connections were used in the system to ensure that the deck girder system acted compositely. Both of these connections as well as a third welded connection are shown in Figure 3.3. The connection between the deck system and girder including the welded connection and the slip-critical connection as well as the connection between deck panels are shown in details (a), (b), and (c), respectively. Due to the scope of the study only the behavior of the panel-to-girder connections were evaluated.

All connection procedures and methods were complete by Martin (2005) and a brief description is presented. The welded connection between the deck panel and the bent “L” plate was a 1/8 in. shop weld. The connections between each deck panel and the girders were designed as slip-critical using 3/4 in. diameter A325-SC bolts. The bolts were spaced evenly at a 6 in. center-to-center spacing which provided nine bolts per panel. The bolts were tightened using the turn of the nut method. Initially each bolt was tightened snug-tight with a spud wrench. Each bolt and nut was then marked with a paint marker and allowed to dry. The head of each bolt was restrained with a spud wrench while the nut was turned another one-half turn. The connections between the panels were pretensioned first, starting in the middle span and then alternating to the exterior spans to control relaxation. After the bolts connecting the panels were fully pretensioned, the bolts connecting the deck to the girder were pretensioned. After pretensioning

all bolts on a panel the previous panel was checked for bolt relaxation. This procedure was continued until all bolts had been pretensioned.

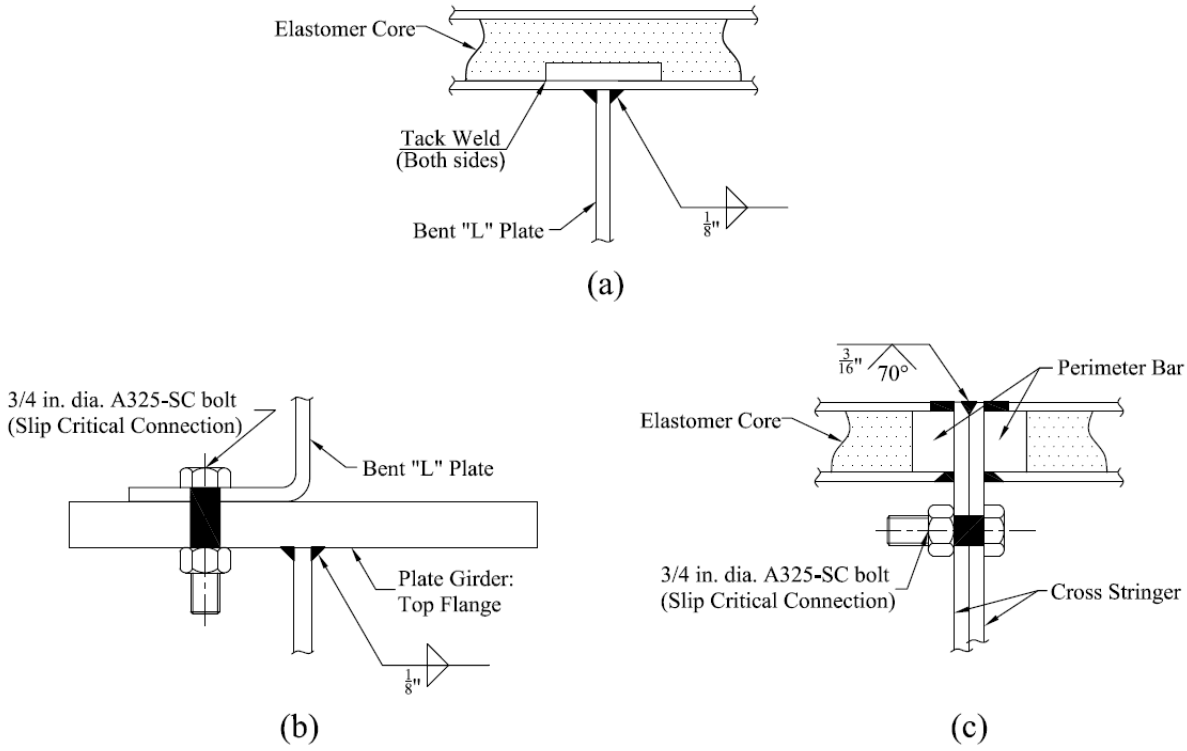

Figure 3.3: Typical connections in the panel-to-girder and panel-to-panel connections

3.2 Load Range Calculation

The loading configuration was chosen to induce the fatigue design moment for the one-half scale bridge. Although the bridge system is not a traditional slab-girder bridge, the conventional approach as outlined in Section 3.6.1.4 of AASHTO-LRFD bridge design specification was used to determine the critical loading configuration. Two design trucks are defined by AASHTO-LRFD. The design truck for the strength limit state has a front spacing of 14 ft and rear axle spacing ranging from 14 ft to 30 ft while, the design truck for fatigue has a front and rear axle spacing of 14 ft and 30 ft, respectively. Both trucks have a loading configuration of 8 kips on the front axle and 32 kips on the rear axles. The AASHTO-LRFD HL-93 truck is illustrated in Figure 3.4. To produce the maximum fatigue moment for the one-half scale bridge a ratio of the maximum moments from the HL-93 fatigue and strength trucks on a full scale 80 ft bridge was found. The 80 ft span bridge was used since the one-half scale bridge

had a span length of 40 ft. The calculated ratio was then multiplied by the ultimate moment capacity of the one-half scale bridge as calculated from yield strength moment minus dead load moment. The procedure is outlined below.

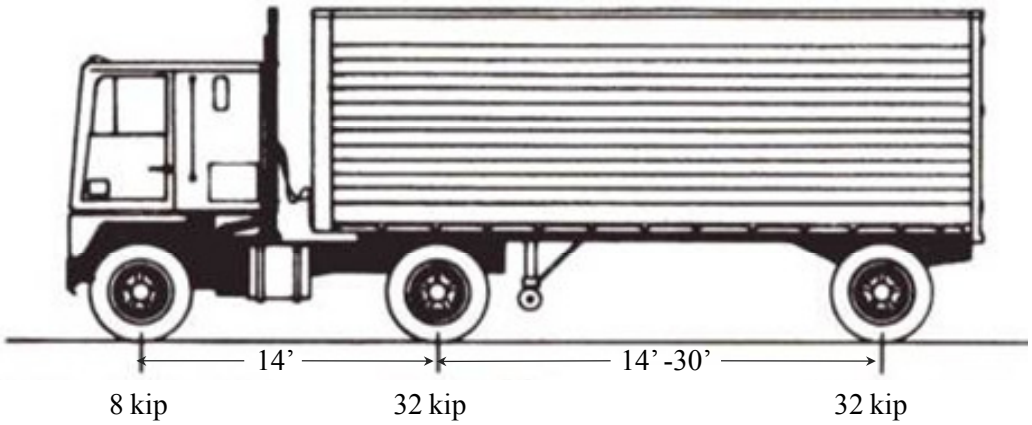

Figure 3.4: HL-93 Design Truck

The maximum moment induced from the HL-93 fatigue design truck on a full scale 80 ft bridge was found to be 1610 kips-ft. This result includes loading factors as defined by AASHTO LRFD Design Specifications. For fatigue and fracture limit states, a dynamic load allowance (IM) of 15 percent was additionally applied to the static wheel load to account for wheel load impact from moving vehicles (AASHTO-LRFD Section 3.6.2.1-1). Load combinations and load factors from AASHTO-LRFD Table 3.4.1-1 were selected to produce the maximum factored force effect. For fatigue, a factor of 0.75 was used. A fatigue resistance factor of 2.0 was applied using AASHTO-LRFD Equation 6.6.1.2.3-1 shown below as Equation (3.1), where $(\Delta F)_{TH}$ is the fatigue resistance and (ΔF) is the factored live load stress range. The 1/2 multiplier on the left side of the equation reduces the fatigue resistance, but this effect can logically be applied to the load side and is equivalent to the 2.0 multiplier (Barker and Puckett 2007). The multiplier was applied to the static wheel load to simulate the heaviest truck the bridge system would experience throughout the life cycle of the bridge.

$$\frac{1}{2}(\Delta F)_{TH} \geq (\Delta F) \tag{3.1}$$

Where: $(\Delta F)_{TH}$ = fatigue resistance
(ΔF) = factored live load stress range

The maximum moment due to the HL-93 design truck for strength, with rear axle spacing of 14 ft, was then found for the full scale 80 ft bridge. The result was then multiplied by the applicable loading factors from AASHTO-LRFD. A dynamic load allowance (IM) increase of 33% was applied and a load combination and load factor of 1.75 was used for Strength I Limit State. An additional moment from a uniformly distributed lane loading of 0.64 klf was added to the design truck moment to yield a maximum moment of 3600 kips-ft. The ratio of fatigue moment to strength moment of approximately was 0.45 (1610/3600).

The dimensions and properties of the one-half scale bridge were then used to find the applied moment that would cause first yield of the girder. The dead weight moment was then subtracted from the result to give a maximum allowable moment for the one-half scale bridge of 1040 kips-ft. This moment was in turn multiplied by the ratio of fatigue to strength, as given above, to give a fatigue moment for the one-half scale bridge. This moment was 466 kips-ft. The complete load calculation is shown in Section A.1: Load calculation example.

3.3 Testing Setup

3.3.1 Overview

This section provides a description of the test setup including loading configurations, instrumentation, and testing procedure. Load Case 1 resulted in an unanticipated weld failure. Load Case 2 is a modification of the loading arrangement. The loading arrangements are presented in the following sections.

3.3.2 Load Case 1 Setup

The load configuration developed for Load Case 1 and the corresponding moment diagram of the bridge specimen is shown in Figure 3.5. To achieve the required moment, the one-half scale bridge was placed on two W21x 132 support beams, spaced 40 ft apart to simulate a simple span bridge. Neoprene pads measuring 2 in. by 9 in. by 18in. were used to support each end of the girders. A load frame with two MTS hydraulic actuators mounted directly over the

girders was setup at the mid-span the bridge. The two actuators applied a load of 51.8 kips at each actuator to a W10x88 spreader beam. Bearing pads measuring 2 in. by 9 in. by 18in. were used to distribute the load 2 ft from the mid-span of the bridge. This configuration was chosen for two reasons; to move the point of loading away from the panel-to-panel connection at mid-span, and to increase the shear in the bolted connections. A cross section of testing configuration for Load Case 1 is shown in Figure 3.6.

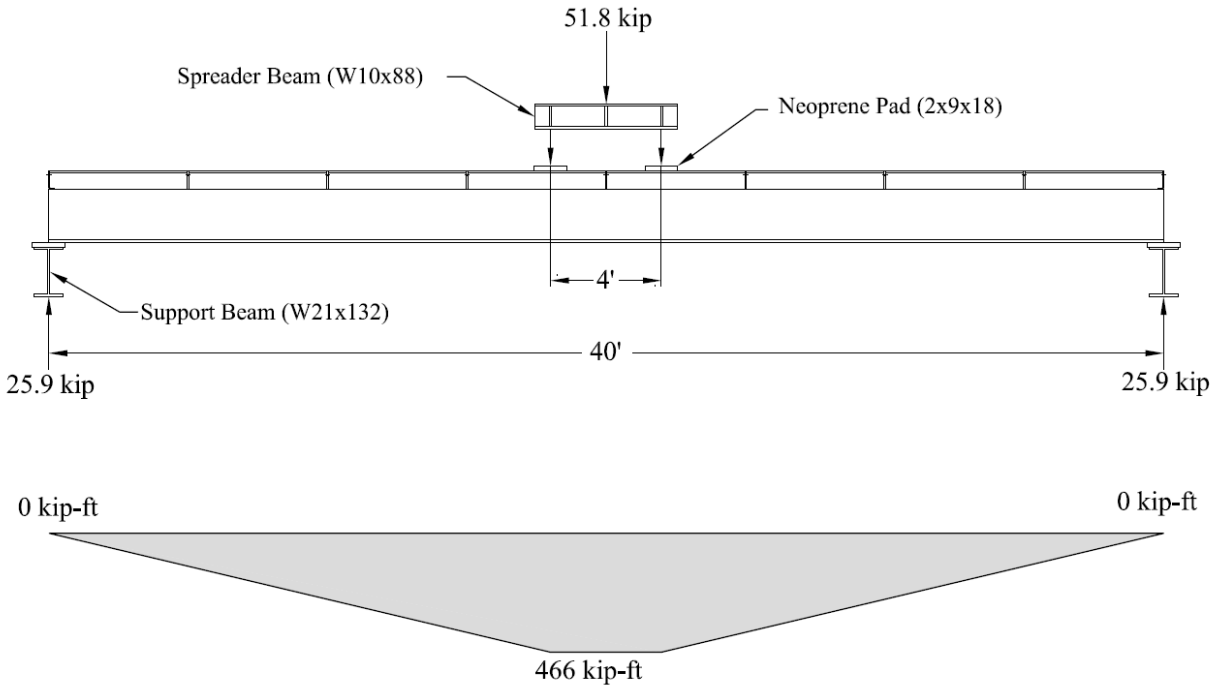

Figure 3.5: Test setup with two point loads for each girder and corresponding moment

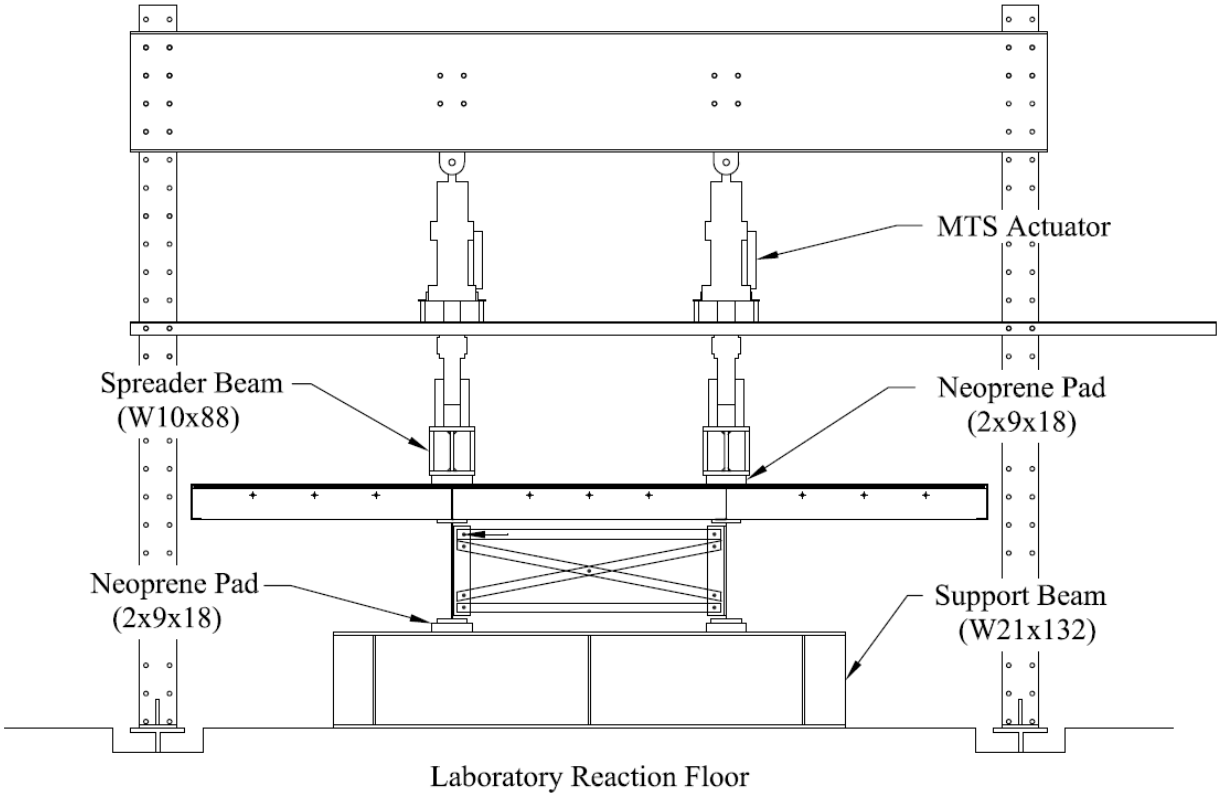

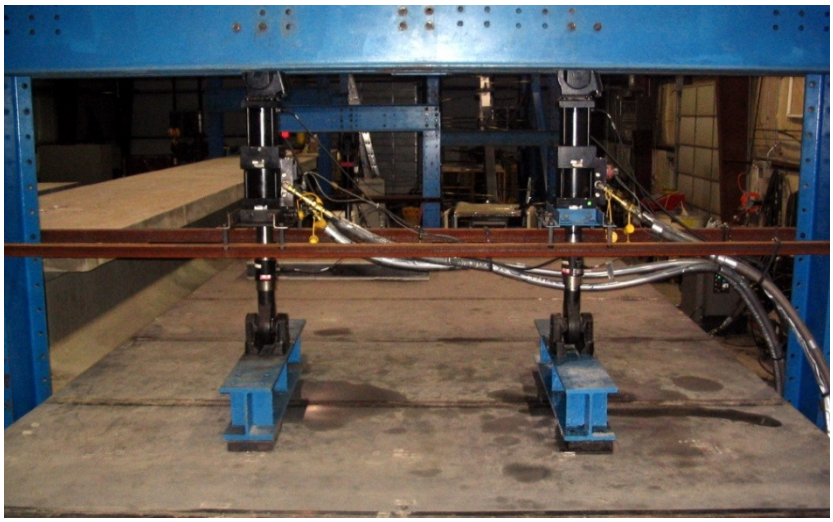

Figure 3.6: Cross section of Load Case 1 configuration with two spreader beams

3.3.3 Load Case 2

After unanticipated weld failures from the first test were repaired, the second test setup was developed. For Load Case 2, the loading was changed from two point loads to a one point

load at mid-span of each girder. The required loading range, to produce the maximum moment of 466 kip-ft, was reduced to 46.6 kips per actuator. The loading configuration and the moment diagram for Load Case 2 are shown in Figure 3.7. Figure 3.8 shows the test setup with the point loads at mid-span of the girder. Again, the girders were supported by bearing pads.

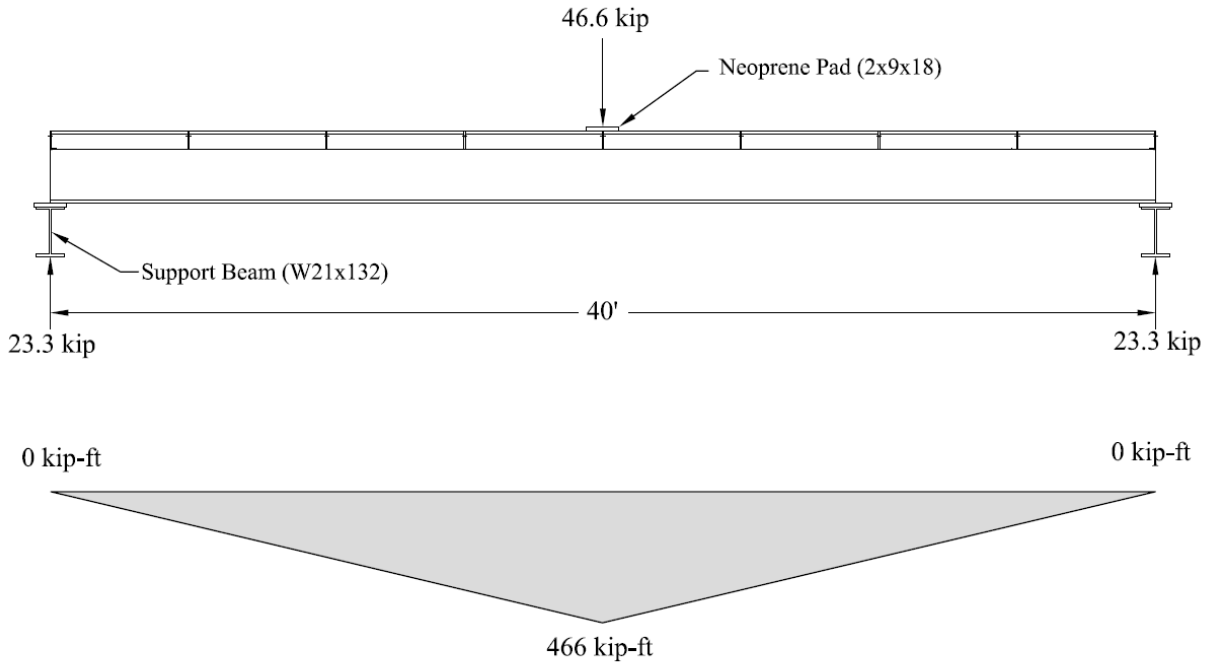

Figure 3.7: Test setup with point load at mid-span of each girder and corresponding moment

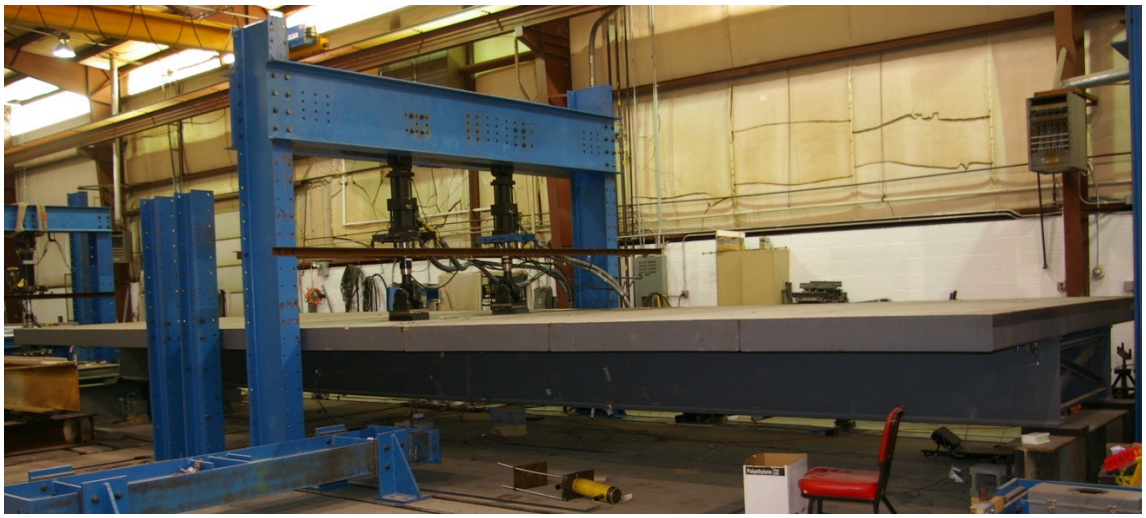

Figure 3.8: Load Case 2 configuration with point loads at mid-span

3.3.4 Instrumentation

Instrumentation was identical for the two test setups. Two MTS 407 controllers were setup in a master-slave combination to allow the loading to be directed by one source. Both MTS actuators were equipped with a linear variable displacement transformer (LVDT) and a load cell to measure deflection and load, respectively. To measure the behavior of the bridge specimen, external instrumentation was required. Six Celesco PT101 cable extension transducers (CET) were used to measure total deflection of the bridge specimen throughout the test. Each transducer had a full stroke range of 10 in. and an accuracy of 0.15 in. (Celesco 2007) The CETs were used to measure vertical deflection of the entire system located as shown in Figure 3.9 for Girder A; locations for Girder B being similar. Four Trans-Tek LVDTs were mounted at the ends of each girder to measure any slip of the deck relative to the girder located as shown in Figure 3.9. The transformers had a stroke of 0.10 in. with a 0.001 in. calibrated accuracy (AASHTO Trans-Tek 2007).Thirty-four quarter bridge 120 ohm strain gauges were strategically placed to monitor strain levels throughout the cross section of the bridge specimen. Figures 3.9 and 3.10 show the configuration and numbering used. The labeling of each gauge depended on the gauge type, its number, and a girder designation. For example, the strain gauge (SG) located at mid-span on the bottom of Girder A is referred to as SG15A. A series of strain gauges was placed on the cross section at the center of the panel adjacent to mid-span of the bridge. This location and layout was chosen to measure strains throughout the cross-section and to monitor composite action between the deck and the girder without the influence of possible local effects due to the mid-span connection. Location of the cross-sectional strain gauges is shown in Figure 3.10.

Notice in Figure 3.10 that the strain gauges in each girder are not symmetric. Girder A has gauges on the outside while Girder B gauges are located on the inside of the web and bottom flange. This layout was chosen after several preliminary tests determined that small initial deformations tended to cause unexpected tension and compression strains in opposite sides of the member. To assist in data acquisition it was decided to setup the strain gauges to give similar strain values for both girders.

Data acquisition for all sensors, including the MTS instrumentation was obtained using a Campbell Scientific CR9000 multiprocessor system (Campbell Scientific 2007). All gauges were wired into the system and data was collected in real time during the testing procedure.

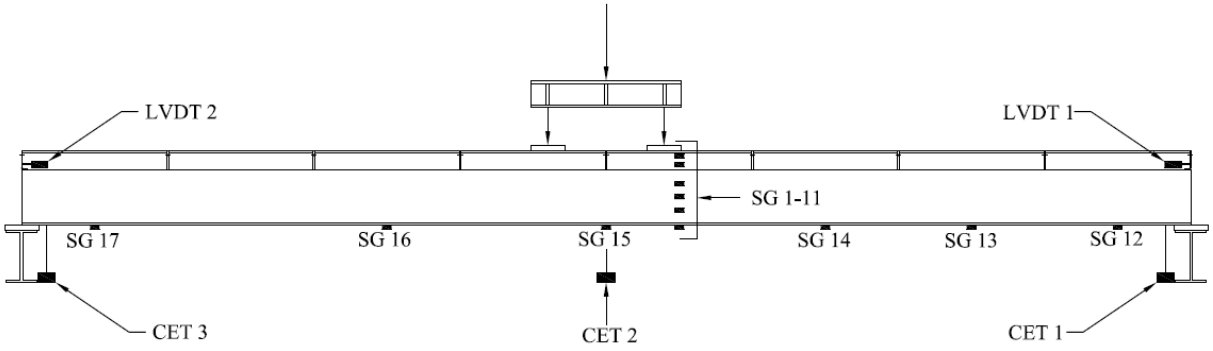

Figure 3.9: Overview of typical girder instrumentation

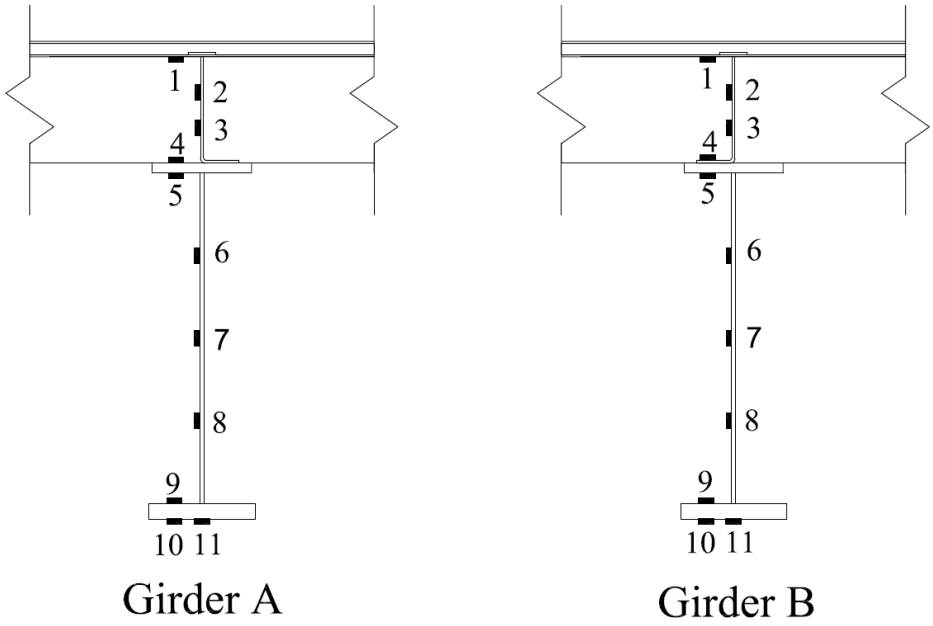

Figure 3.10: Strain gauges (SG) instrumentation of each girder

3.3.5 Testing

Before cyclic loading was started, a thorough inspection of the bridge was conducted and five static tests were performed to establish the pretest behavior of the specimen. A static test was defined as a slowly applied load starting from zero and reaching the maximum desired fatigue load of 51.8 kips per actuator for Load Case 1 and 46.6 kips per actuator for Load Case 2. The actuators diplaced at a rate of 0.03 in. per minute, which corresponds to approximately 36.6 kips per minute. This rate was chosen to aid in data acquisition and was used in all subsequent

static tests. At regular intervals the cyclic tests was stopped and static tests were performed. Five repetitions were conducted at each interval.

The cyclic loading range was determined based on the calculated point load for each setup as previously described. To prevent unexpected damage due to a sudden loss of stiffness in the system, deflection limits were used. To define the deflection range the upper and lower limits of the girder displacements were set based on the corresponding loads applied for each load case. A load range of 2.0 kips to 53.8 kips for Load Case 1 and 2.0 kips to 48.6 kips for Load Case 2 was used. This resulted in a load range of 51.8 kips and 46.6 kips for the respective test setups (see Sections 3.3.2 and 3.3.3 for load range calculation methodology).

After all initial setup tests were performed; cyclic loading on the specimen began. The cyclic loading rate was set at 0.5 hertz. The testing procedure was continuous with the exception of the static tests. During cyclic loading of Load Case 1, static tests were conducted at a logarithmic interval of 10, at each step. Due to the unexpected failure during the first test setup, it was decided to take additional measurements every 10,000 cycles for the first 100,000 cycles for Load Case 2.

Chapter 4: Laboratory Fatigue Test Results

4.1 Load Case 1 Results

This section contains the test results from the Load Case 1. After 10,000 cycles, the bridge specimen showed no obvious loss in stiffness or any signs of slip. During the testing between 10,000 and 43,697 cycles, a creaking noise was noticed and the testing was stopped. The bridge was inspected and three substantial cracks, two in Girder A and one in Girder B were found in the welds that connect the bent "L" plates to the deck panel. All three cracks occurred under the point of load application and propagated along the weld into adjacent plates. A detailed explanation of the weld failures follows in Sections 4.1.2 and 4.4.2 and detailed drawings are shown in Figure 4.5.

Although, the exact number of cycles that caused cracking in the welds is unknown, it is assumed that crack initiation occurred at 43,000 cycles, which was the last recorded cycle before the test was stopped and final static tests were made.

The unexpected weld failures changed the stiffness of the system and ultimately affected measured vertical displacements during the final static testing. To investigate the effect on the loading of the specimen, a plot of vertical displacements from the MTS actuators versus the applied load after 43,000 cycles is shown in Figure 4.1. Notice that both actuators had the same displacement, but MTS actuator B only applied 47.2 kips. The maximum load of 51.8 kips was not reached due to the stroke control settings of the MTS actuators (see Section 3.3.2 for load setup methodology). The initial vertical displacements were compared and found to be the same. The weld failures at 43,000 cycles, subsequently caused the MTS actuator B to only apply 47.2 kips load, therefore the results in the following section will be compared at a maximum loading of 47.2 kips not the intended loading of 51.8 kips

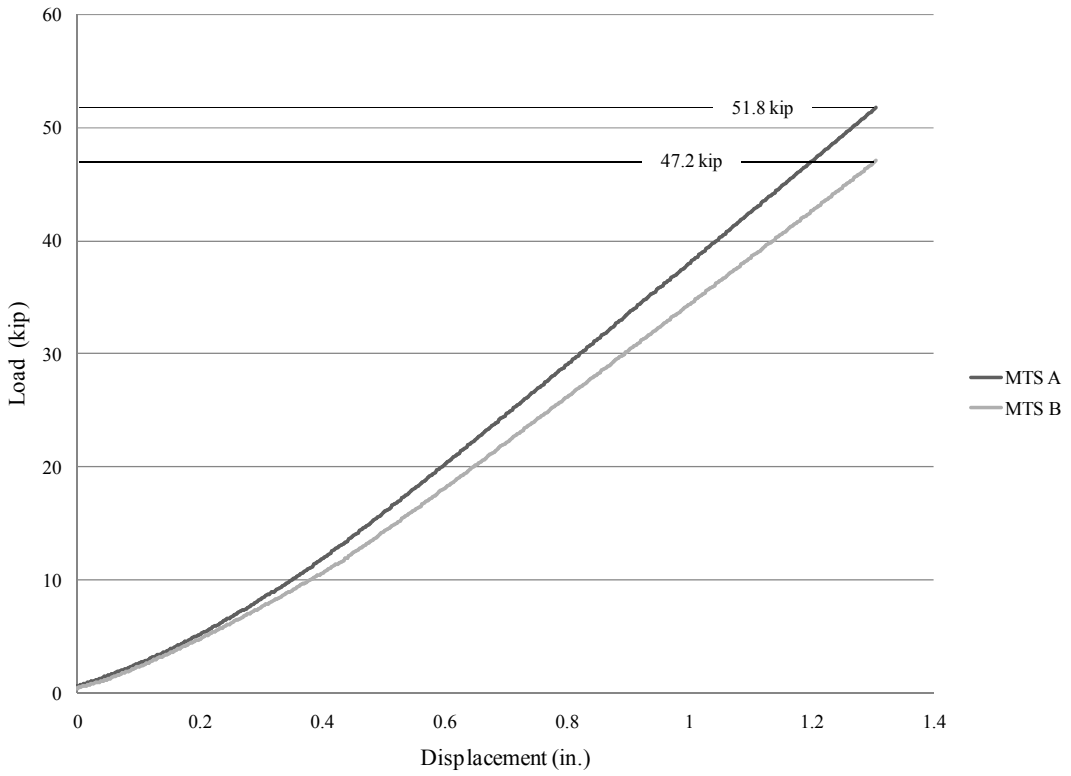

Figure 4.1: Load versus displacement of MTS actuators at 43,000 cycles

The following sections contain the results of Load Case 1. The deflections of the specimen were investigated to find possible changes in stiffness due to connection slip or weld failure. The weld failures are discussed and the strain gauge data was used to substantiate the findings. Slip of the girder relative to the panel was also investigated.

4.1.1 Vertical Deflection Results

The displacements measured by the CETs were used to calculate the mid-span deflection of the system. Table 2.1 shows the average displacements found from each static test as well as the average mid-span displacements of each girder. The two CET located at the bearing locations of the girders were used to measure any deflection due to the neoprene pads. These deflections were then averaged and subtracted from the mid-span deflection to find the total mid-span deflection. The average deflection over the testing period of the specimen under the 47.2 kips loading was 0.68 in. in both girders. The average mid-span percent change over the testing was minimal, with a maximum of 1.0 percent change.

Table 4.1: Average deflections and percent change for Load Case 1

Cycles		CET 1A	CET 2A	CET 3A	Mid-span A	CET 1B	CET 2B	CET 3B	Mid-span B
1	Deflection (in)	0.10	0.78	0.10	0.68	0.11	0.79	0.10	0.69
	% Change	0.0%	0.0%	0.0%	0.0%	0.0%	0.0%	0.0%	0.0%
10	Deflection (in)	0.10	0.78	0.10	0.68	0.11	0.78	0.10	0.68
	% Change	-1.7%	0.1%	-1.6%	0.4%	2.5%	1.1%	1.1%	1.0%
100	Deflection (in)	0.10	0.77	0.10	0.68	0.11	0.79	0.10	0.68
	% Change	-0.5%	0.7%	-0.5%	0.9%	-0.7%	0.3%	-1.0%	0.4%
1000	Deflection (in)	0.10	0.78	0.10	0.68	0.11	0.79	0.10	0.68
	% Change	-1.8%	0.1%	-2.0%	0.4%	-1.9%	0.2%	-1.8%	0.5%
10000	Deflection (in)	0.09	0.77	0.11	0.67	0.11	0.80	0.12	0.69
	% Change	7.9%	0.7%	-10.9%	1.0%	1.3%	-0.8%	-14.1%	0.0%
43679	Deflection (in)	0.10	0.79	0.11	0.68	0.10	0.80	0.13	0.68
	% Change	-6.8%	-1.0%	-12.0%	0.2%	3.7%	-0.8%	-22.2%	0.5%

Load versus deflection plots of each girder were used to investigate the effect of the weld failures on the deflection of the composite system. It is important to note that the maximum load was 47.2 kips for reasons previously discussed. It is obvious from Figure 4.2 and 4.3 that the weld failures did not significantly change the deflections as evident by the linear behavior of the static tests at 0 and 43,000 cycles. This implies that the stiffness of the system was not affected by the localized weld failures and that slip at the connections was unlikely.

To investigate this further, a plot of deflection at 47.2 kips versus the number of cycles is shown in Figure 4.4. Notice that the displacements are relatively the same throughout the testing in both girders. Thus it further concluded that the weld failures or slip at the connections did not cause a significant change in stiffness of the composite system.

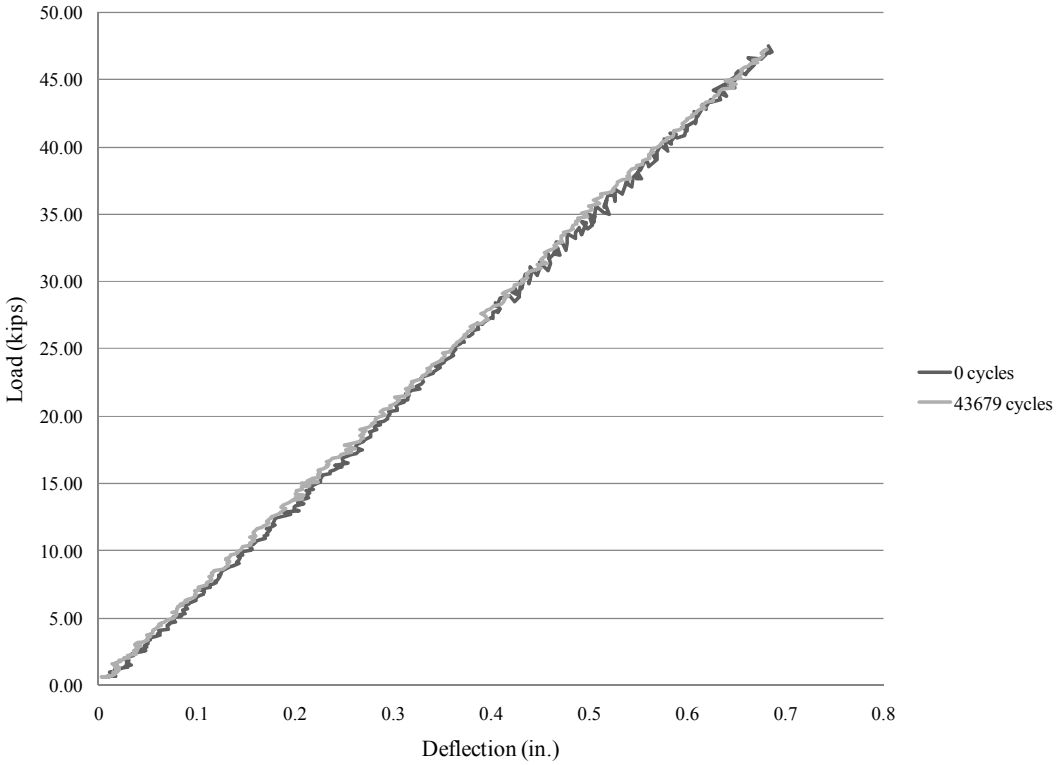

Figure 4.2: Load versus Deflection of Girder A

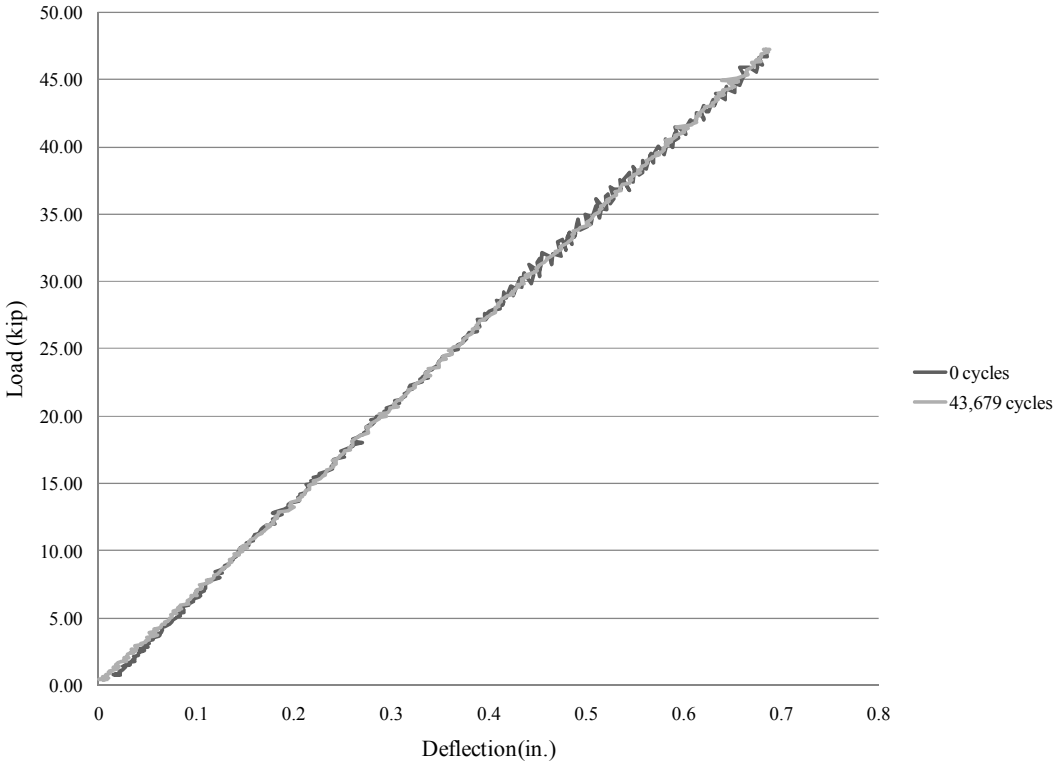

Figure 4.3: Load versus Deflection of Girder B

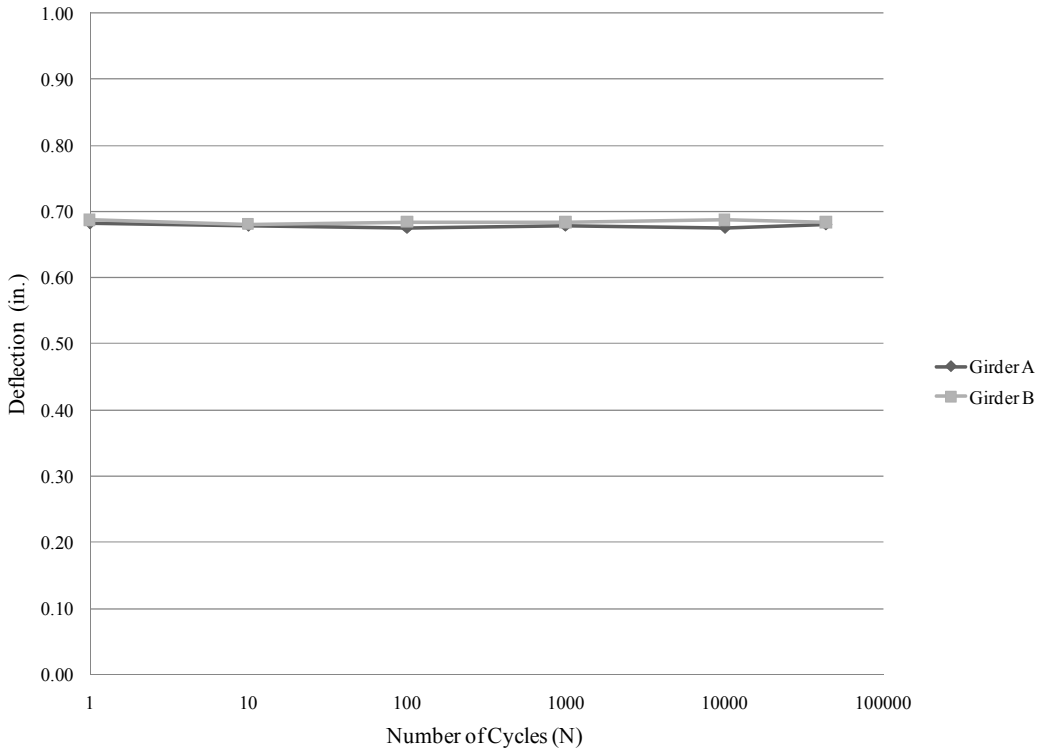

Figure 4.4: Load Case 1 deflection at mid-span at 47.2 kips versus number of cycles

4.1.2 Weld Failures

The measured lengths and locations of the cracks are shown in cross sectional views in Figure 4.5. The plan view of the bridge shown in Figure 4.6 illustrates the approximate locations of the cracks, as well as the labeling system used to identify the failure locations. The weld failure on the left side of Girder A is referred to as A1. The failures were localized to the point of load application and no other cracks or damage was found. It is important to note that the welds only cracked on the outside weld connection. It is also important, from a failure analysis approach that only three of the four load application points failed. This will be further explained in Section 4.2.

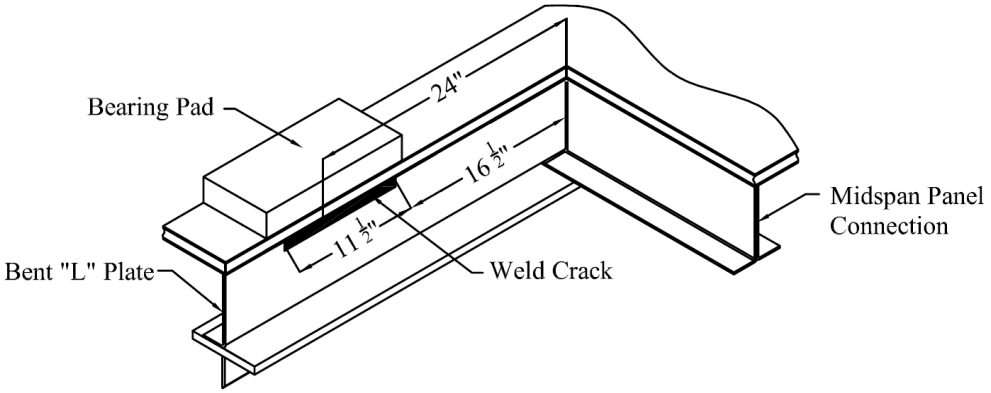

Weld Crack A-1

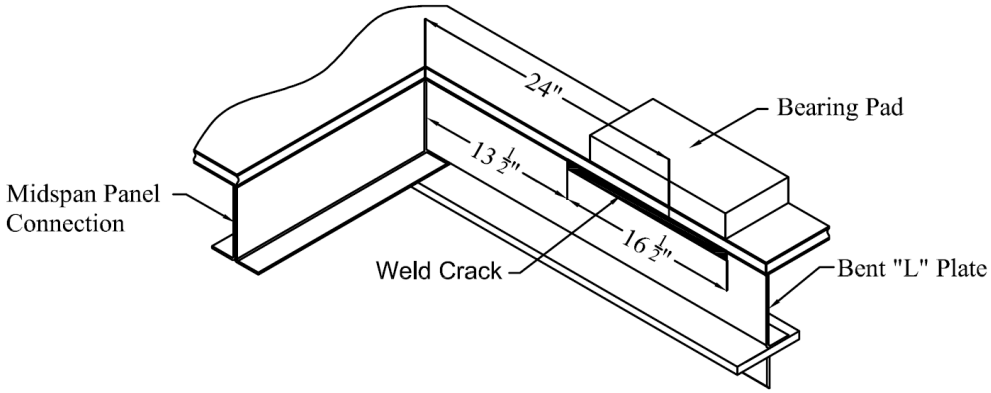

Weld Crack A-2

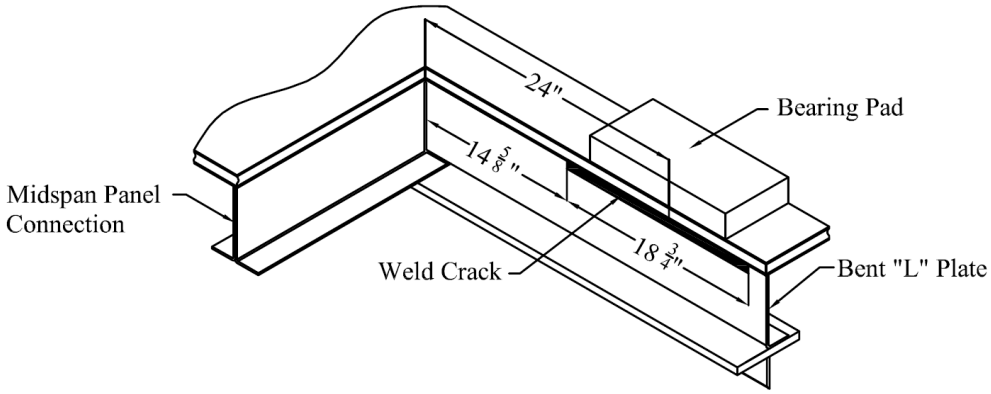

Weld Crack B-1

Figure 4.5: Details of the weld cracks at 43,000 cycles

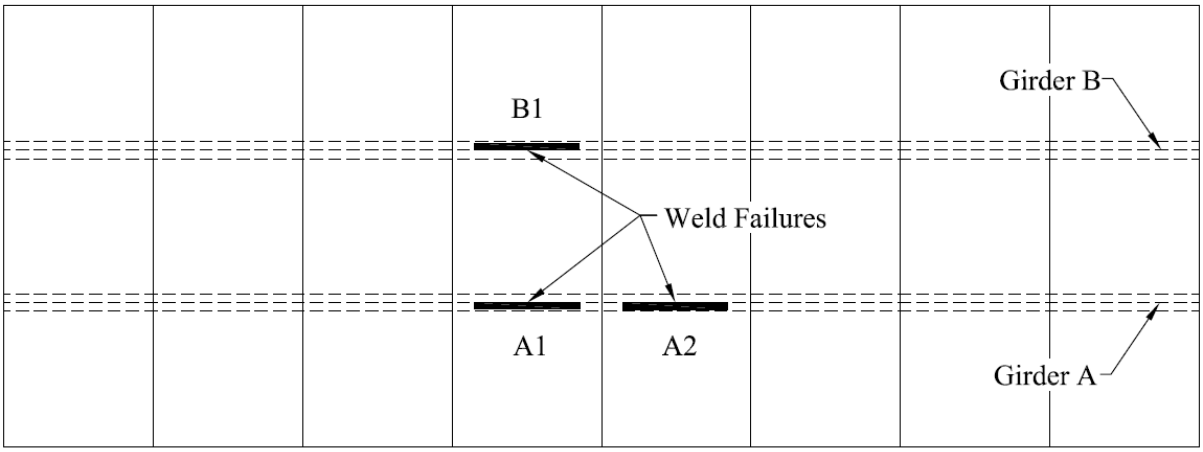

Figure 4.6: Location of the weld cracks at 43,000 cycles

4.1.3 Strain Gauge Results

The eleven strain gauges located through the depth of the cross section of each girder were used to substantiate the finding from the vertical deflection results. To determine if a change in stiffness occurred or if the effect was local to the failures, the location of the composite section neutral axis of the specimen was monitored a each static test. Tables 4.2 and 4.3 show the average strains at the maximum loading of 47.2 kips per actuator for each static test on Girder A and Girder B, respectively. The table also contains the percent change in stiffness compared to the initial static test. Any significant change in strain would suggest a loss in composite action and possibly slip in the bolted connection. The sign convention for strain in this study is tension positive and compression negative. The most significant change in strain was in gauge SG1A during the static test at 43,697 cycles. There was an increase of approximately 122% strain from the initial strain measured in the 0 cycle test, and is likely due to the localized failure at the location. It is interesting to note all other strain gauges had similar results throughout the testing procedure.

Table 4.2: Average strains and percent change at 47.2 kips for Girder A

Cycles		SG1A	SG2A	SG3A	SG4A	SG5A	SG6A	SG7A	SG8A	SG9A	SG10A	SG11A
1	Strain	-187.2	-150.3	56.6	-20.8	-61.8	252.9	452.9	615.3	558.7	622.4	714.8
	% Change	0.0%	0.0%	0.0%	0.0%	0.0%	0.0%	0.0%	0.0%	0.0%	0.0%	0.0%
10	Strain	-186.0	-148.0	57.0	-19.0	-57.5	254.2	457.2	614.9	564.0	622.0	719.1
	% Change	-0.7%	-1.5%	0.8%	-8.8%	-7.1%	0.5%	0.9%	-0.1%	1.0%	-0.1%	0.6%
100	Strain	-183.3	-147.7	58.6	-16.3	-58.7	252.4	452.9	613.5	559.4	624.4	713.2
	% Change	-2.1%	-1.7%	3.5%	-21.7%	-5.1%	-0.2%	0.0%	-0.3%	0.1%	0.3%	-0.2%
1000	Strain	-182.6	-148.8	58.1	-17.2	-60.5	252.2	452.7	614.3	561.9	622.7	718.0
	% Change	-2.5%	-0.9%	2.6%	-17.2%	-2.2%	-0.3%	-0.1%	-0.2%	0.6%	0.0%	0.4%
10000	Strain	-170.3	-151.6	57.0	-20.4	-59.3	253.3	451.6	619.9	566.8	626.2	719.5
	% Change	-9.0%	0.9%	0.7%	-2.0%	-4.0%	0.1%	-0.3%	0.7%	1.5%	0.6%	0.7%
43679	Strain	-415.3	-179.0	46.5	-11.1	-55.6	256.9	458.4	619.5	566.5	627.4	723.3
	% Change	121.8%	19.1%	-17.9%	-46.5%	-10.2%	1.6%	1.2%	0.7%	1.4%	0.8%	1.2%

Table 4.3: Average strains and percent change at 47.2 kips for Girder B

Cycles		SG1B	SG2B	SG3B	SG4B	SG5B	SG6B	SG7B	SG8B	SG9B	SG10B	SG11B
1	Strain	-231.9	-199.8	-164.0	40.2	-30.1	231.7	442.2	605.6	636.4	666.2	676.6
	% Change	0.0%	0.0%	0.0%	0.0%	0.0%	0.0%	0.0%	0.0%	0.0%	0.0%	0.0%
10	Strain	-231.3	-197.0	-162.9	44.9	-25.8	229.4	442.0	601.8	637.1	663.5	676.3
	% Change	-0.3%	-1.4%	-0.7%	11.5%	-14.4%	-1.0%	-0.1%	-0.6%	0.1%	-0.4%	-0.1%
100	Strain	-231.1	-196.0	-159.9	45.0	-25.2	231.1	439.8	602.8	638.0	665.9	675.4
	% Change	-0.3%	-1.9%	-2.5%	11.8%	-16.3%	-0.3%	-0.6%	-0.5%	0.3%	0.0%	-0.2%
1000	Strain	-230.4	-193.5	-161.1	46.3	-26.2	227.1	438.4	597.4	641.5	663.3	679.7
	% Change	-0.7%	-3.2%	-1.8%	15.1%	-13.1%	-2.0%	-0.9%	-1.3%	0.8%	-0.4%	0.5%
10000	Strain	-221.9	-184.7	-149.0	48.1	-29.0	227.3	438.9	602.1	639.6	668.0	681.0
	% Change	-4.3%	-7.6%	-9.2%	19.5%	-3.6%	-1.9%	-0.8%	-0.6%	0.5%	0.3%	0.6%
43679	Strain	-361.2	-205.8	-158.8	38.2	-34.7	212.4	422.6	588.7	627.2	655.4	675.5
	% Change	55.8%	3.0%	-3.2%	-5.2%	15.3%	-8.4%	-4.4%	-2.8%	-1.5%	-1.6%	-0.2%

The measured strains from the first static test (0 cycles) are shown in Figure 4.7. The change in strain at the connection between gauges SG4 and SG5 is small but noticeable. This area was observed closely throughout the test to determine if the change in strains propagated. It is also interesting to note the significant deviation in strains on the bottom flange of the girders. This change was most likely due to a rotation in the flange, but due to the scope of this study, no further investigation occurred and the initial results were accepted.

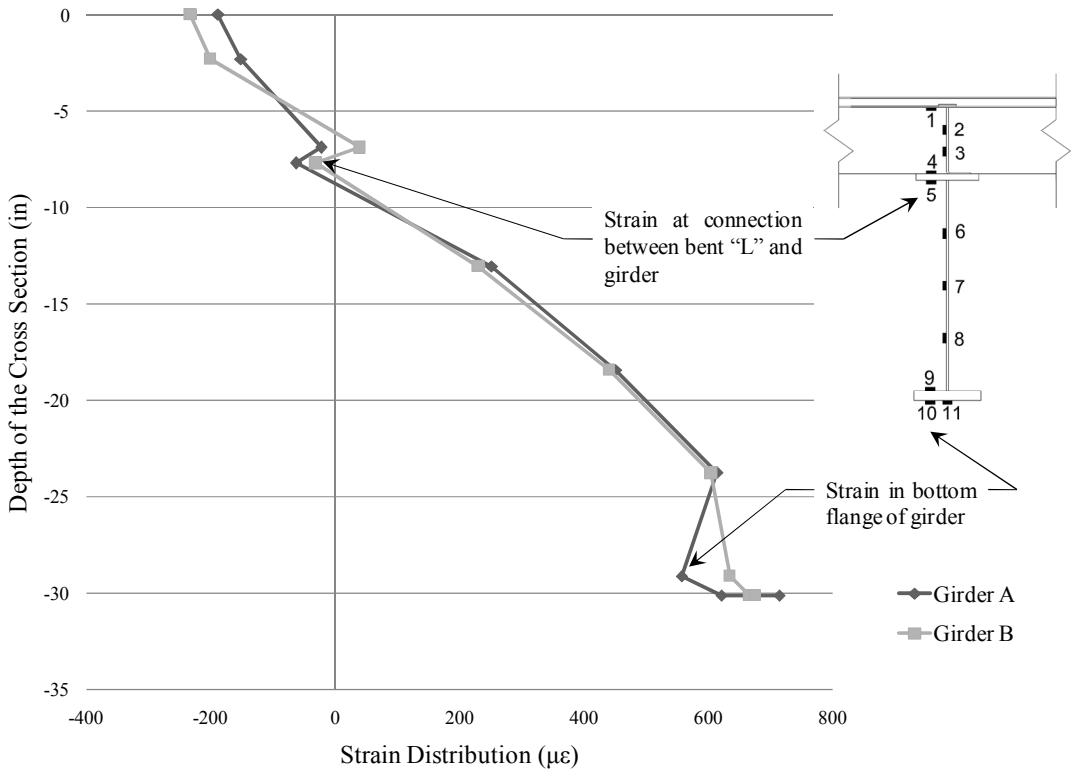

Figure 4.7: Strain throughout cross section depth at 0 cycles in Girder A and Girder B

After cyclic testing began, strains were compared at each logarithmic static test. No noticeable strain changes occurred through the first 10,000 cycles. At 43,000 cycles the strains were compared to the initial strains at 0 cycles; no significant change in strain was found in the cross-sections of the girders expect at the panel where the welds broke. Figures 4.8 and 4.9 compare the strains at 0 cycles and at 43,000 cycles of Girders A and B, respectively. The strains in the gauges adjacent to the cracked weld increased approximately 114 percent and 42 percent for Girders A and B, respectively, but the strains throughout the rest of the cross section are unchanged. Notice at the location of the composite neutral axis, the changes in strains are

relatively insignificant and there is no noticeable shift. It is also important to note that the strains at the slip-critical connections between gauges SG4 and SG5 did not significantly change, and slip at the connection was unlikely.

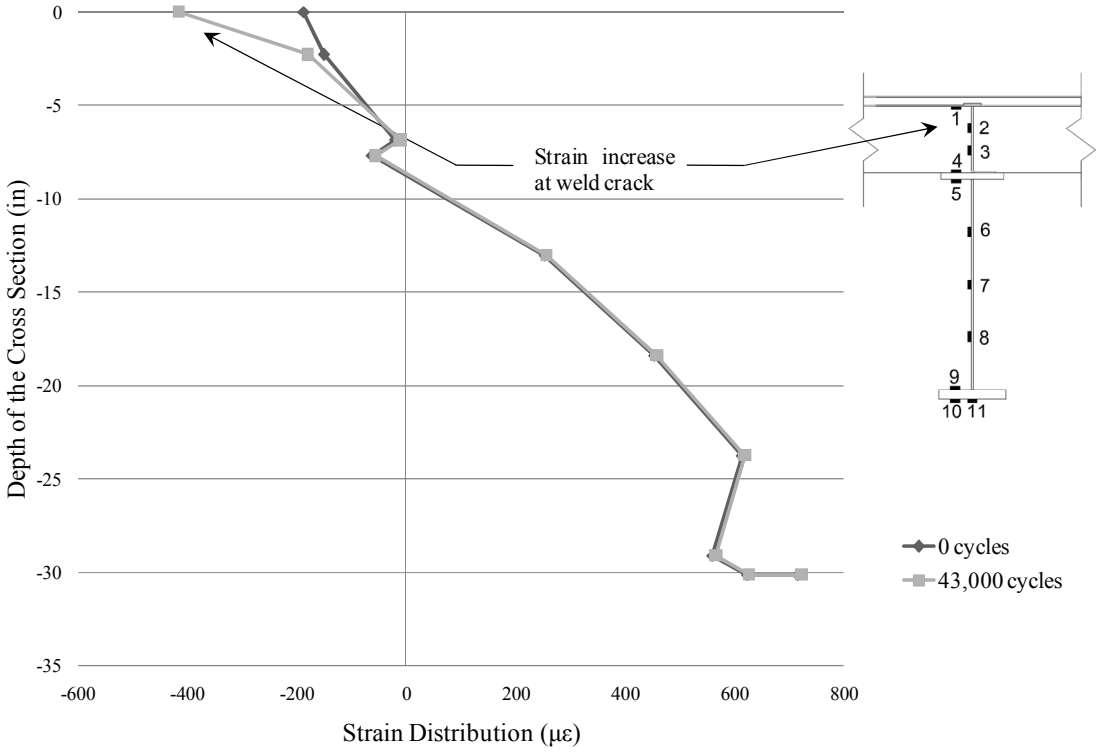

Figure 4.8: Strains throughout cross section depth of Girder A at 0 and 43,000 cycles

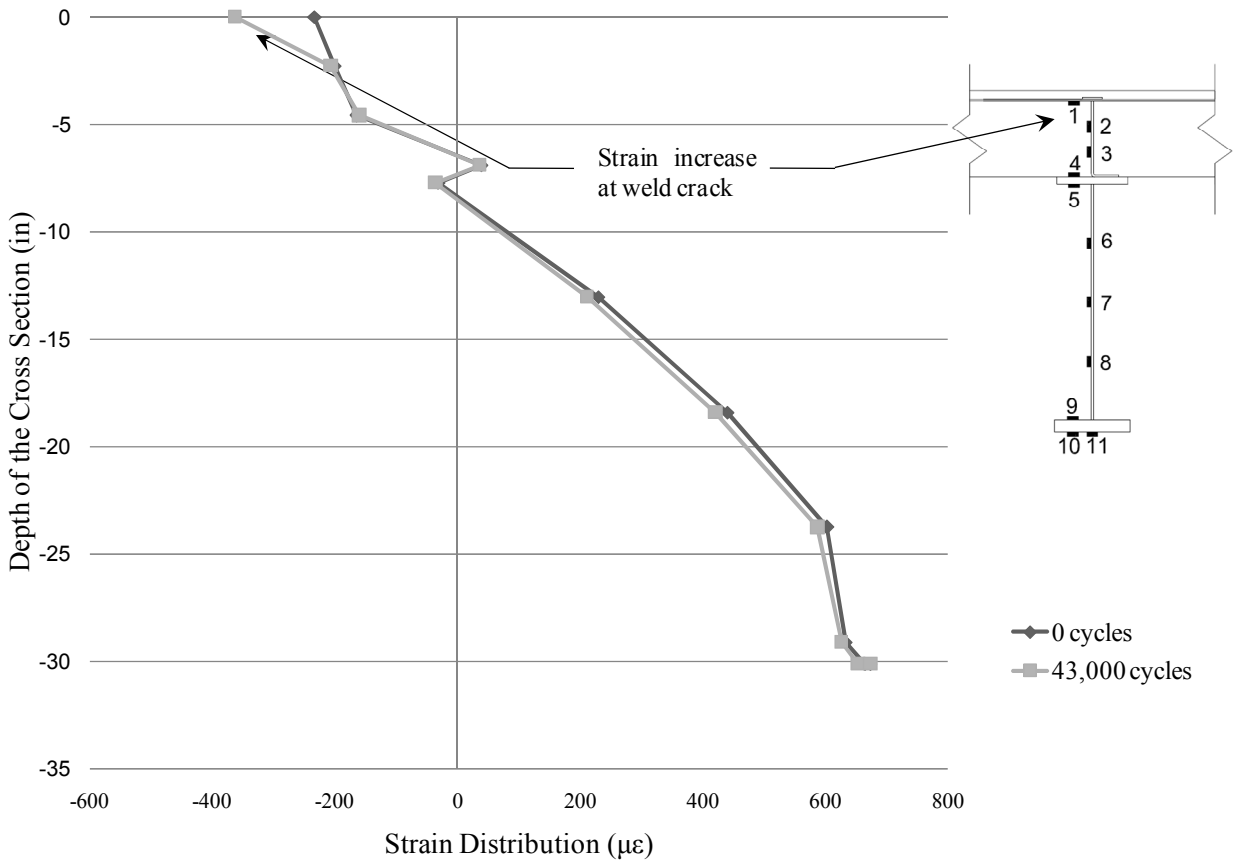

Figure 4.9: Strains throughout cross section depth of Girder B at 0 and 43,000 cycles

A change in strain over the number of cycles was also investigated to ensure no unusual strains occurred during testing. Figures 4.10 and 4.11 illustrate the change in strain of each gauge throughout the entire test of Girders A and B, respectively. They are based on a logarithmic scale, and follow the same sequence that was used for static testing. It is obvious that the only significant change in strain during the testing was local at the weld failures adjacent to SG1 at 43,000 cycles. Again, notice the strains from SG4 and SG5, at the slip-critical connection, do not significantly change throughout the testing.

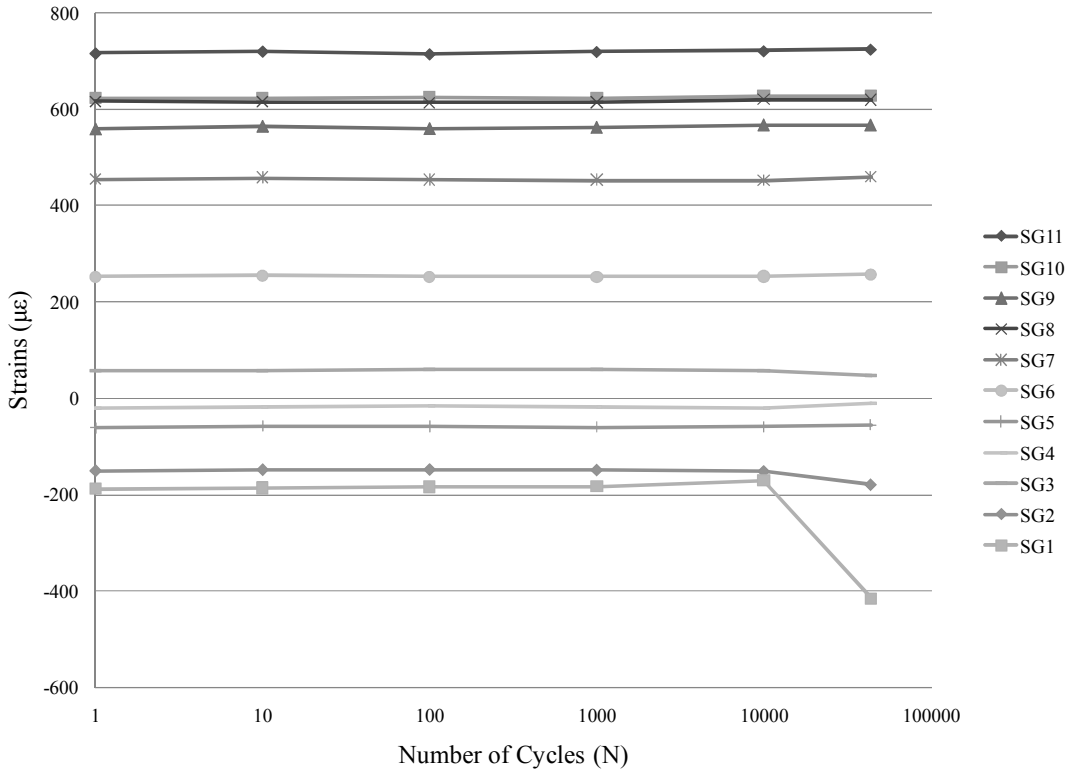

Figure 4.10: Strains at maximum load of 47.2 kips versus number of cycles of Girder A

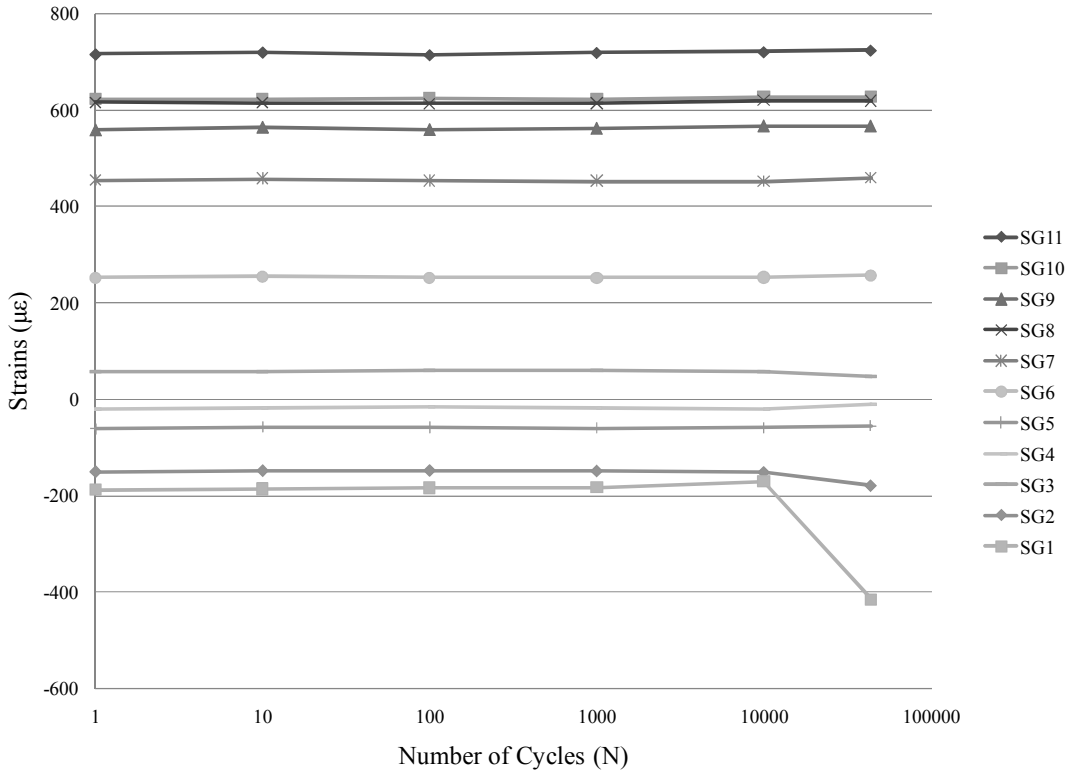

Figure 4.11: Strains at a maximum load of 47.2 kips versus number of cycles of Girder B

By investigating the changes in strains throughout the cross section of each girder during the testing of the specimen, it is obvious that the effects of the weld failures at 43,000 cycles were localized near the weld cracks. The composite neutral axis was not significantly affected and there was no evidence of slip at the connections.

4.1.4 Slip Displacement Results

LVDTs were placed at both ends of each girder. They were secured to the girder and measured slip between the deck panel relative to the girder. A typical LVDT installation is shown in Figure 4.12. The LVDTs were monitored closely throughout the test. Even with a calibrated accuracy of 0.001 in., the LVDTs did not measure any slip relative to the girder and the end deck panel.

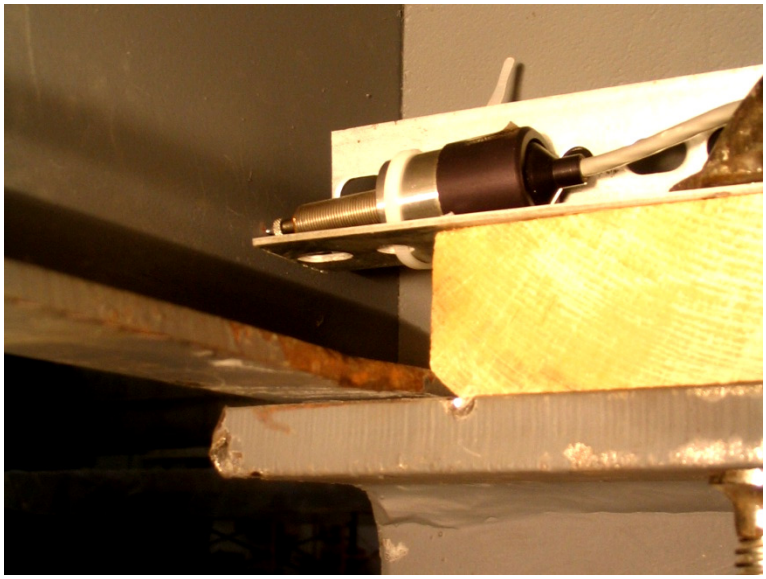

Figure 4.12: Typical LVDT setup

4.2 Repair of Cracked Welds

To continue the test and to investigate the failures, it was determined that the cracked welds could be repaired, strengthening the bridge to its approximate original stiffness. To repair the failures, the cracks were ground down and the majority of the old welds were removed. The deck was then leveled using hydraulic jacks and the cracks were re-welded. Figure 4.13 shows a typical cracked joint before and after welding.

(a) Before repair

(b) After repair

Figure 4.13: Weld cracks before and after repair

4.3 Analysis of Load Case 1 Results

After the repair of the weld failures two more strain gauges were mounted to the underside of the panel adjacent to the lone uncracked weld. The strain gauges were aligned perpendicular to the weld to allow the measurement of transverse strains and stresses. The use of the original strain gauge (SG1B) along with the additional two transverse gauges allowed strains to be measured biaxially. The bridge was loaded and corresponding strains in the longitudinal and transverse directions were measured at the maximum loading range of 51.8 kips. The

corresponding average strains and stresses from three static tests, using a modulus of elasticity of 29,000 ksi are shown in Table 4.4.

Table 4.4: Average weld strains and corresponding stresses

	Average Max Strain (με)	Average Max Stress (ksi)
Longitudinal	-250	-7.25
Transverse	-1110	-32.3

An attempt was made to match the detail category of the weld to the fatigue resistance as defined by the AASHTO-LRFD specification (AASHTO 2007). Eight predefined detail categories (A through E) are provided in the specification for different component details and situations that are susceptible to load-induced fatigue cracking. For built-up members that are connected by continuous fillet welds parallel to the direction of applied stress, the detail category is defined as "B." Eccentrics due to the loading configuration in the test may have induced transverse loading into the weld, and, if so, the category changes to "E" when the component is defined as a transversely loaded fillet welded attachment with welds parallel to the direction of primary stress.

The calculated stresses, and number of cycles were then applied to a component S-N curve, which illustrates the relationship between the stress range (S) and the fatigue life (N) to ensure the weld corresponded to the category definitions. AASHTO-LRFD defines this S-N relationship in Equation 6.6.1.2.3-1 of Section 6.6.1.2.5, as:

$$(\Delta F)_n = \left(\frac{A}{N}\right)^{\frac{1}{3}} \geq \frac{1}{2}(\Delta F)_{TH} \tag{4.1}$$

Where: $(\Delta F)_n$ = nominal fatigue resistance
A = detail category constant from Table 6.6.1.2.5-1 (ksi^3)
N = number of cycles
$(\Delta F)_{TH}$ = constant-amplitude fatigue threshold

The equation is best represented on a log-log scale schematic and shown in Figure 4.14. Each category is defined by a separate curve which represents the corresponding anticipated finite life for that category. If the stress range is below the line the component is considered safe, but if the stress is higher, the component will most likely crack. The dashed horizontal line represents the constant-amplitude fatigue threshold and defines the infinite-life of the component.

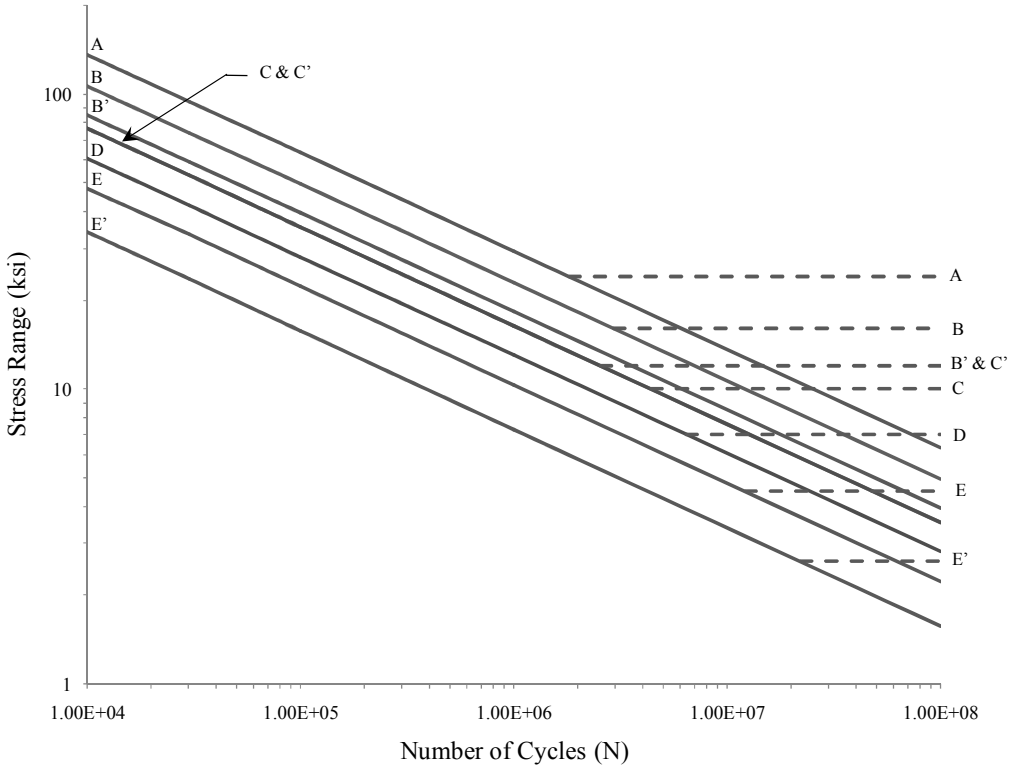

Figure 4.14: S-N relationship curve

Knowing the approximate stress range in both longitudinal and transverse directions as shown in Table 4.4, as well as the assumed number of cycles (43,000) at which the cracks initiated, allowed the category of the weld to be determined. The intersection of the stress and number of cycles are plotted on the S-N curve as shown in Figure 4.15. Note the intersection of the transverse strains above the Category E threshold. This corresponds closely to the general condition of the detail category "E". By using the stress of 32.3 ksi from Table 4.4 and a detail category of "E," an approximately number of cycles to failure can be found to be 33,000 cycles.

It is important to note that crack initiation could have started before the test was stopped at 43,000 cycles.

Notice that the intersection of the longitudinal strain is well below the horizontal dotted line of category "B." According to AASHTO, when the design stress range is less than one-half of the constant-amplitude fatigue threshold, the detail will theoretically provide infinite life. This applies in this case where the constant amplitude threshold for category "B" is 16.0 ksi.

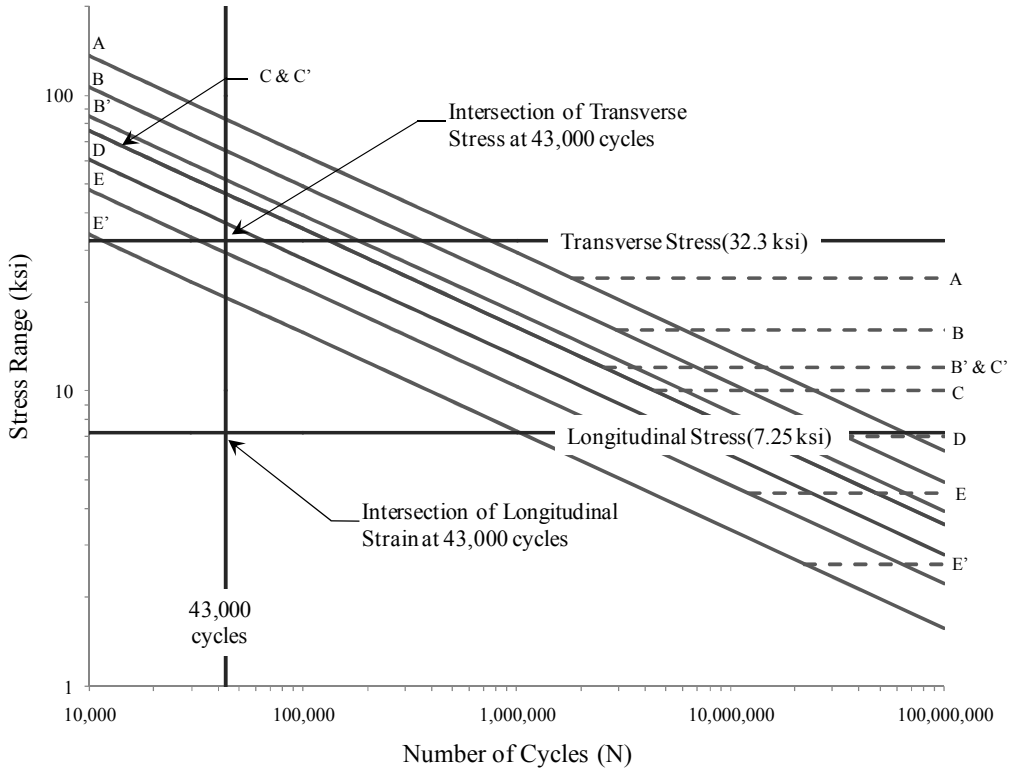

Figure 4.15: S-N relationship curve with corresponding stress and cycles at weld failure

According to the definitions as well as the measured stresses, the weld was considered to be categories "B" and "E" in the longitudinal and transverse directions, respectively. An intersection of the transverse stress of 32.3 ksi and the category "E" curve results in an failure at approximately 30,000 cycles, but the reason for the high stresses in the transverse direction is not clear. It is most likely due to an eccentricity of the loading setup due to the spreader beam and the bearing pads. The bearing pad measuring 9 in. wide could have induced some eccentricity due to the distribution of loads. Figure 4.16 shows the spreader beam and the bearing pad under the maximum loading after the welds cracked. It is interesting to note the angle of the spreader

beam relative to the panel section after the weld cracking. From this vantage, it is obvious that an eccentricity occurred at the weld connection. Further investigation of the weld stresses due to transverse loading is presented in Chapter 5.

Figure 4.16: Spreader beam and bearing pad under maximum load after weld cracking

4.3.1 Load Case 1 Summary

Load Case 1 resulted in weld failures at the connection of the bent "L" plate to the deck panel between 30,000 and 43,000 cycles. Investigation of the cracked welds showed that only the outside weld under three of the four load points failed. By using the lone uncracked weld, approximate strains were measured and stresses were calculated. The stresses were then compared to the S-N curve for fatigue resistance, as defined by AASHTO-LRFD. Through classification of the weld category as "B" in the longitudinal direction and "E" in the transverse direction it was concluded that the failures were due to high stresses from loading in the transverse direction of the welds. It was also determined through investigations of the vertical deflection, strain gauge, and slip displacement data that the weld failures caused significant changes local to the failures but did not influence the overall stiffness of the composite system. There was also no evidence that slip occurred in the slip-critical connection at the panel-to-girder connections.

4.4 Load Case 2 Results

This section contains the test results from Load Case 2. It is important to note that the bridge specimen had an initial 43,000 cycles from Load Case 1, but to aid in data acquisition and documentation, Load Case 2 starts at 0 cycles. Thus the total accumulated cycles on the bridge specimen is 43,000 cycles plus the number of cycles form Load Case 2. Strains and deflections were carefully monitored throughout the testing to ensure that more damage did not initiate from the repaired welds or any other signs of cracking occurred. At 700,000 cycles a creaking noise was noticed and the testing was stopped. The bridge was inspected and substantial cracks were found in the welds that connect the bent "L" plate to the deck panel at mid-span and also in the bent "L" plate. These cracks are described in detail in Section 4.4.2 and detailed drawings are shown in Figures 4.21 and 4.22. All four cracks initiated at mid-span, under the point of load application and propagated along the weld and into the plate.

The results from Load Case 2 were investigated to find possible change in stiffness due to connection slip or weld failures. Vertical deflection results were substantiated by strain gauge findings and an analysis of the results is presented.

4.4.1 Vertical Deflection Results

The data from the six CETs is presented in Table 4.5, which shows the average displacements from each static test as well as the corresponding average mid-span deflection. The two CET located at the bearing locations of the girders were used to measure any deflection due to the neoprene pads. These deflections were then averaged and subtracted from the mid-span deflection to find the total mid-span deflection.

Load versus deflection plots of each girder were used to investigate the effect of the weld failures on the deflection of the composite system as shown in Figure 4.17 and 4.18. A change in deflection can be seen in Girder A at 700,000 cycles, suggesting a loss in stiffness. There is no noticeable change in deflection in Girder B. This suggests that the weld failures or possibly a slip at the connection caused a loss in the stiffness of the composite system. To investigate this further, a plot of deflection versus the number of cycles in shown in Figure 4.19. The deflection readings were variable after 100,000 cycles with a maximum of 6.0 percent change in Girder B at 500,000 cycles. This suggests that the there were variations in deflection readings throughout the testing program and the deflection differences may not be an indicator or slip.

Table 4.5: Average deflections and percent change for Load Case 2

Cycles		CET 1A	CET 2A	CET 3A	Mid-span	CET 1B	CET 2B	CET 3B	Mid-span
1	Deflection (in)	0.09	0.81	0.11	0.71	0.10	0.78	0.11	0.67
	% Change	0.0%	0.0%	0.0%	0.0%	0.0%	0.0%	0.0%	0.0%
10	Deflection (in)	0.09	0.81	0.10	0.71	0.10	0.78	0.11	0.67
	% Change	1.1%	0.0%	3.7%	-0.4%	2.1%	0.3%	-0.6%	0.2%
100	Deflection (in)	0.09	0.81	0.10	0.71	0.10	0.78	0.11	0.67
	% Change	2.6%	0.1%	4.6%	-0.4%	1.2%	0.1%	0.6%	0.0%
1000	Deflection (in)	0.09	0.80	0.11	0.70	0.11	0.77	0.10	0.66
	% Change	1.4%	0.4%	-7.4%	1.0%	-4.5%	1.1%	10.3%	0.8%
10000	Deflection (in)	0.10	0.82	0.10	0.73	0.12	0.77	0.10	0.67
	% Change	-4.3%	-2.1%	3.2%	-2.6%	-14.9%	0.6%	13.6%	0.3%
100000	Deflection (in)	0.08	0.82	0.10	0.73	0.11	0.78	0.10	0.68
	% Change	11.5%	-2.2%	4.9%	-3.6%	-8.4%	-0.6%	15.5%	-1.3%
200000	Deflection (in)	0.09	0.80	0.10	0.70	0.10	0.77	0.10	0.67
	% Change	4.0%	1.0%	4.7%	0.6%	4.4%	0.6%	11.0%	-0.6%
300000	Deflection (in)	0.06	0.80	0.12	0.71	0.08	0.76	0.10	0.67
	% Change	33.6%	1.2%	-12.5%	0.1%	20.6%	2.4%	12.6%	0.1%
400000	Deflection (in)	0.06	0.80	0.12	0.70	0.08	0.79	0.10	0.70
	% Change	32.0%	1.2%	-18.7%	0.6%	24.5%	-1.3%	13.0%	-4.5%
500000	Deflection (in)	0.07	0.82	0.11	0.73	0.09	0.81	0.10	0.71
	% Change	23.3%	-2.3%	-4.9%	-3.8%	13.6%	-3.5%	10.5%	-6.0%
600000	Deflection (in)	0.06	0.81	0.10	0.73	0.08	0.77	0.10	0.67
	% Change	30.6%	-1.0%	3.3%	-3.4%	20.8%	1.0%	15.3%	-0.1%
700000	Deflection (in)	0.06	0.82	0.10	0.74	0.08	0.76	0.10	0.67
	% Change	30.9%	-2.1%	2.4%	-4.6%	22.3%	2.1%	13.4%	-0.4%

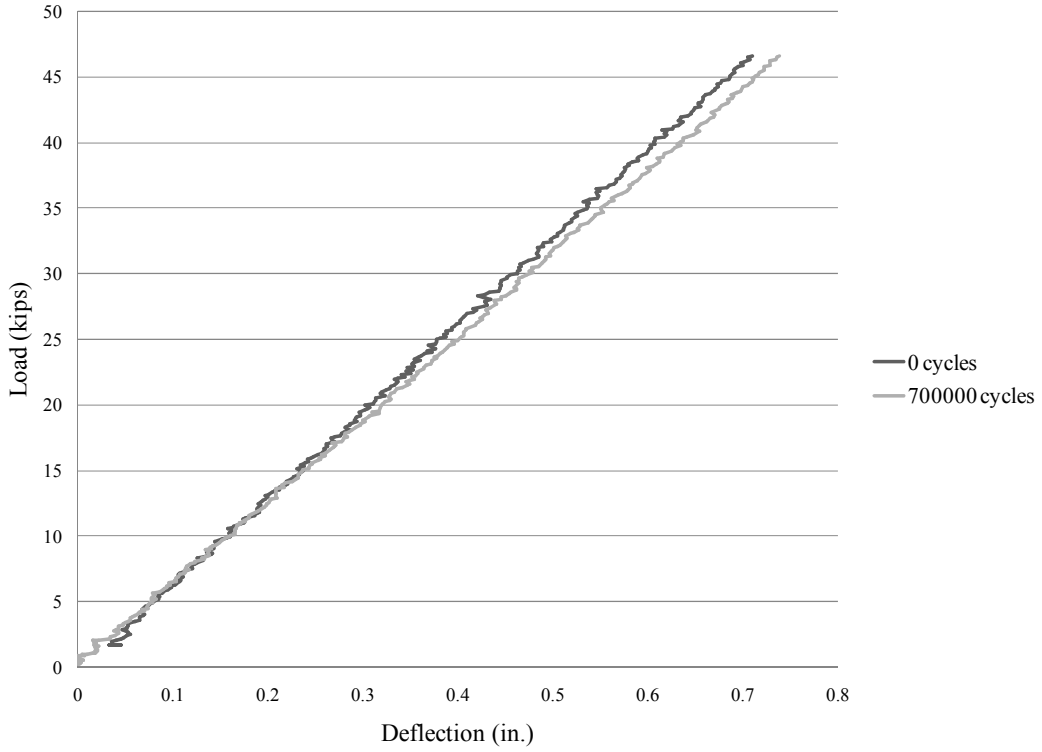

Figure 4.17: Load versus deflection of Girder A

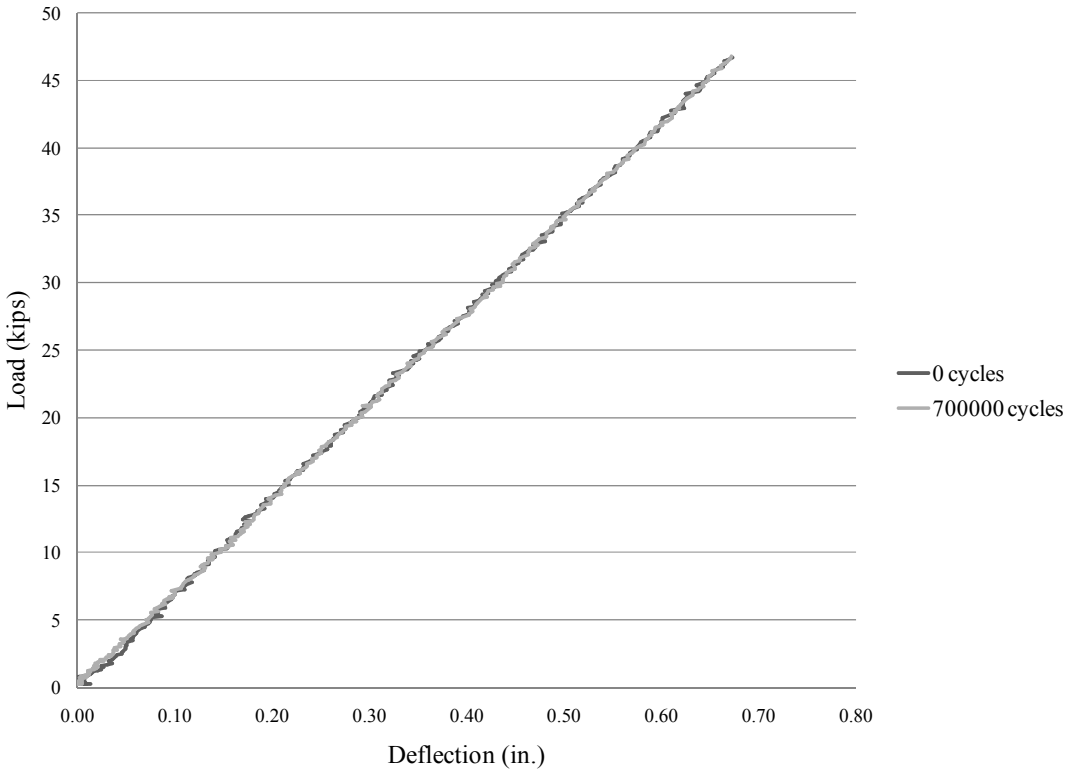

Figure 4.18: Load versus deflection of Girder B

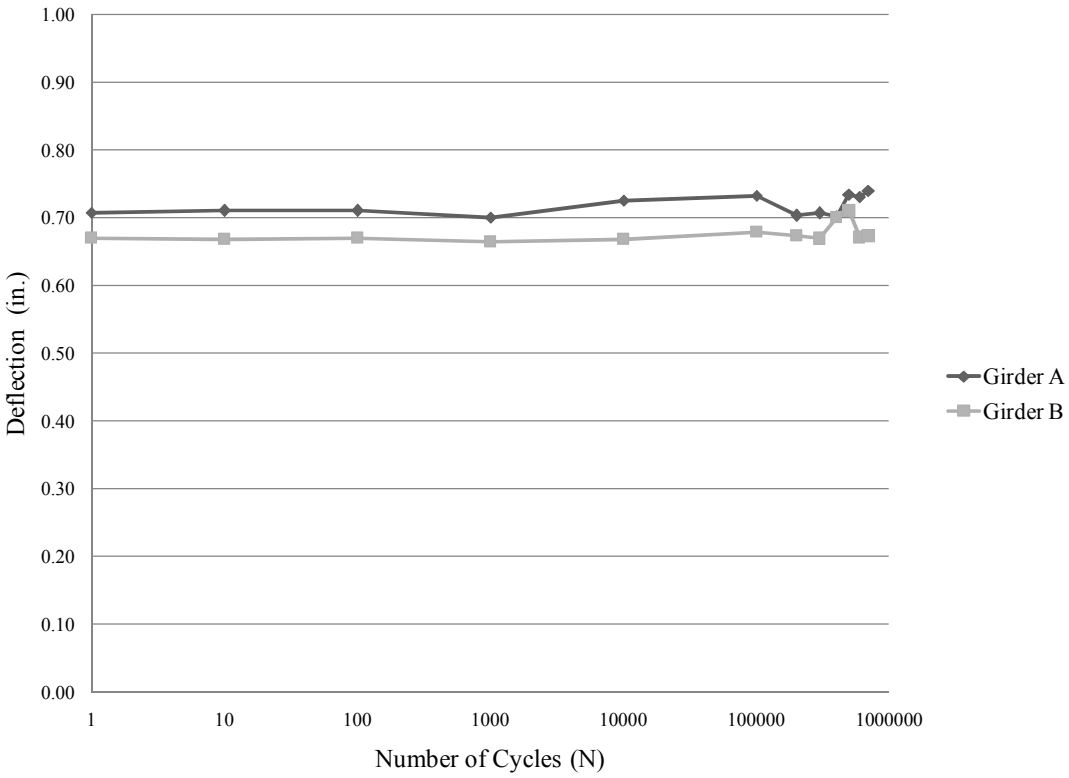

Figure 4.19: Load Case 2 deflection at mid-span versus number of cycles

4.4.2 Weld Failures

The following section contains the documented weld failures from Load Case 2. Figure 4.20 shows the approximate locations of the cracks, as well as the labeling system used for the failures. The weld failure on the left side of Girder A is referred to as A1. The failures were localized to the point of loading and no other cracks or damage was found. It was determined that the cracks initiated at the three point intersection of the welds and propagated down the weld of the bent "L" plate and continued into the plate. The measured lengths and locations of the cracks in Girder A and Girder B are shown in cross sectional views in Figures 4.21 and 4.22, respectively.

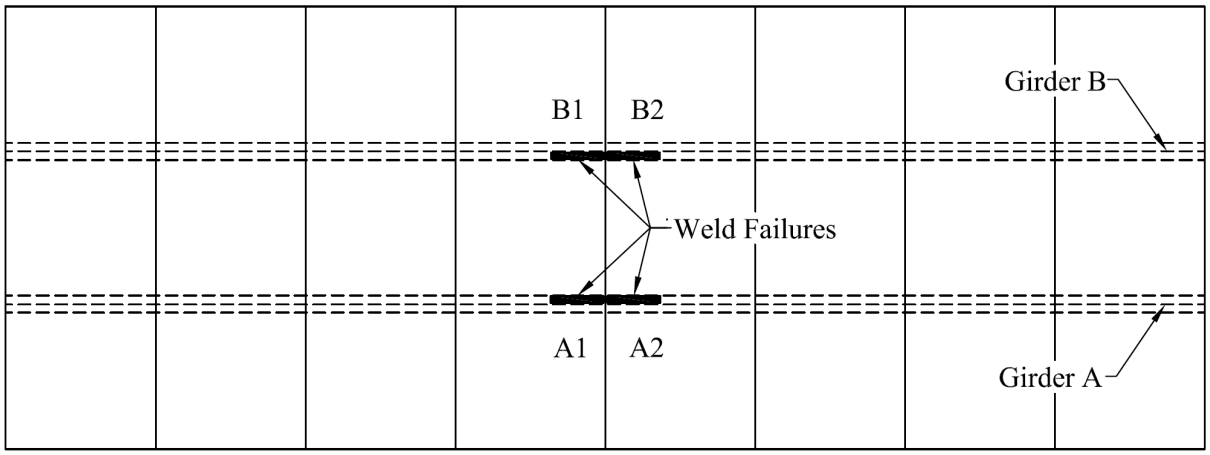

Figure 4.20: Location of the weld cracks at 700,000 cycles

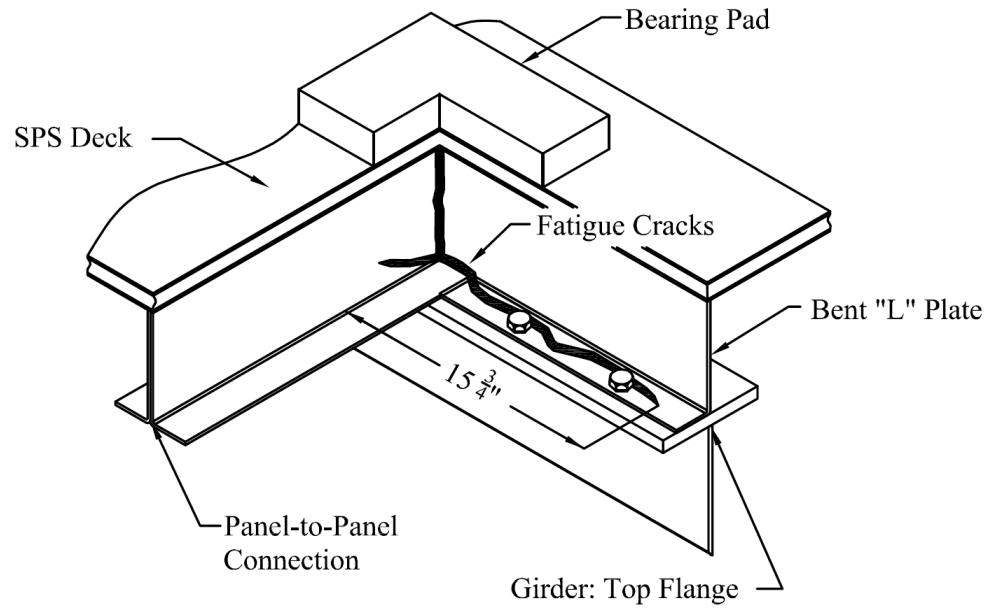

Weld Crack A-1

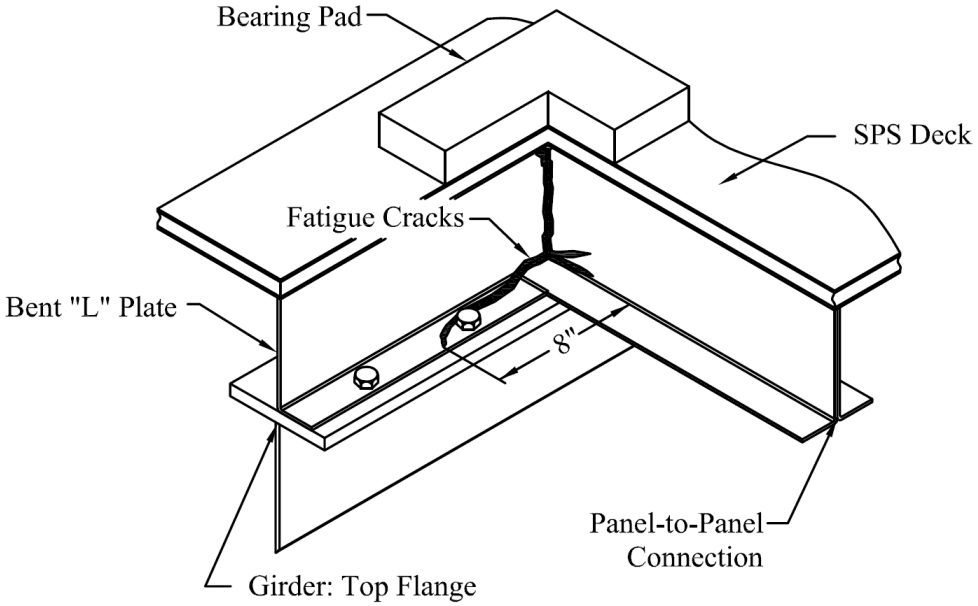

Weld Crack A-2

Figure 4.21: Weld crack details at 700,000 cycles

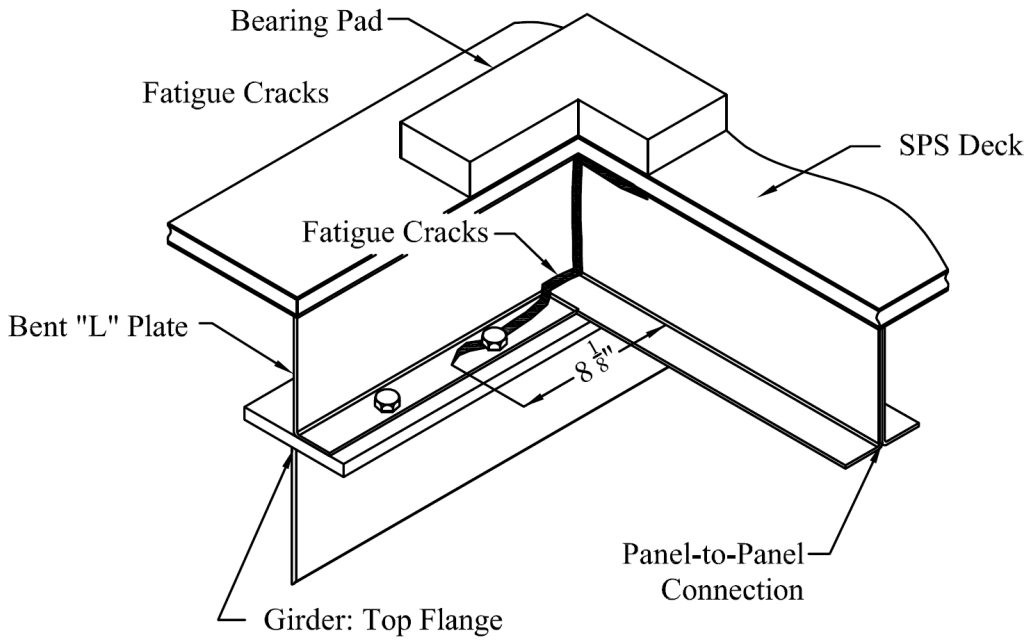

Weld Crack B-1

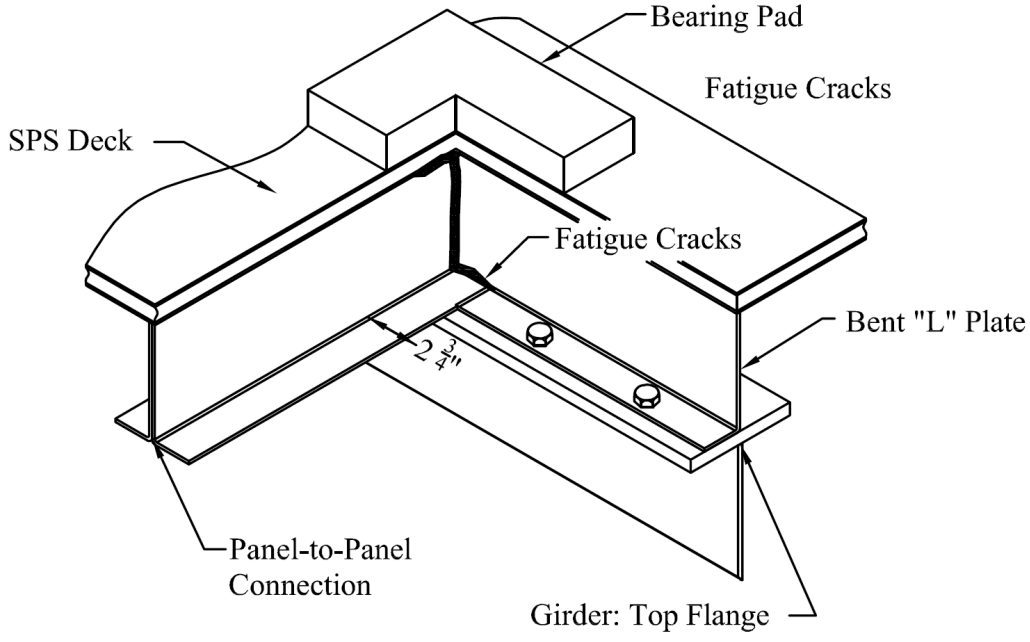

Weld Crack B-1

Figure 4.22: Weld crack details at 700,000 cycles

4.4.3 Strain Gauge Results

The following section contains the data from the eleven strain gauges located through the depth of the cross section of each girder. The strains were used to determine if any slip occurred, or if the location of the composite section neutral axis of the specimen changed during testing. Tables 4.6 and 4.7 show the average strains at the maximum loading of 46.6 kips during each static test and the corresponding change in strain when compared to the initial static test readings.

Any significant change in strain would suggest a loss in composite action or possibly slip in the bolted connection. The initial strains from the static tests prior to cyclic loading of both Girder A and Girder B are plotted in Figure 4.23. The strains are similar throughout both cross-sections with the exception of the strains at the bottom plate of the SPS panels and also at the bottom flange of the girders. These gauges deviate from the linear pattern of the strain and are most likely due to out-of-plane movement of the cross section. It is also interesting to note the small jump in strain at the connection of the bent "L" to the girder. These gauges were monitored closely throughout the test.

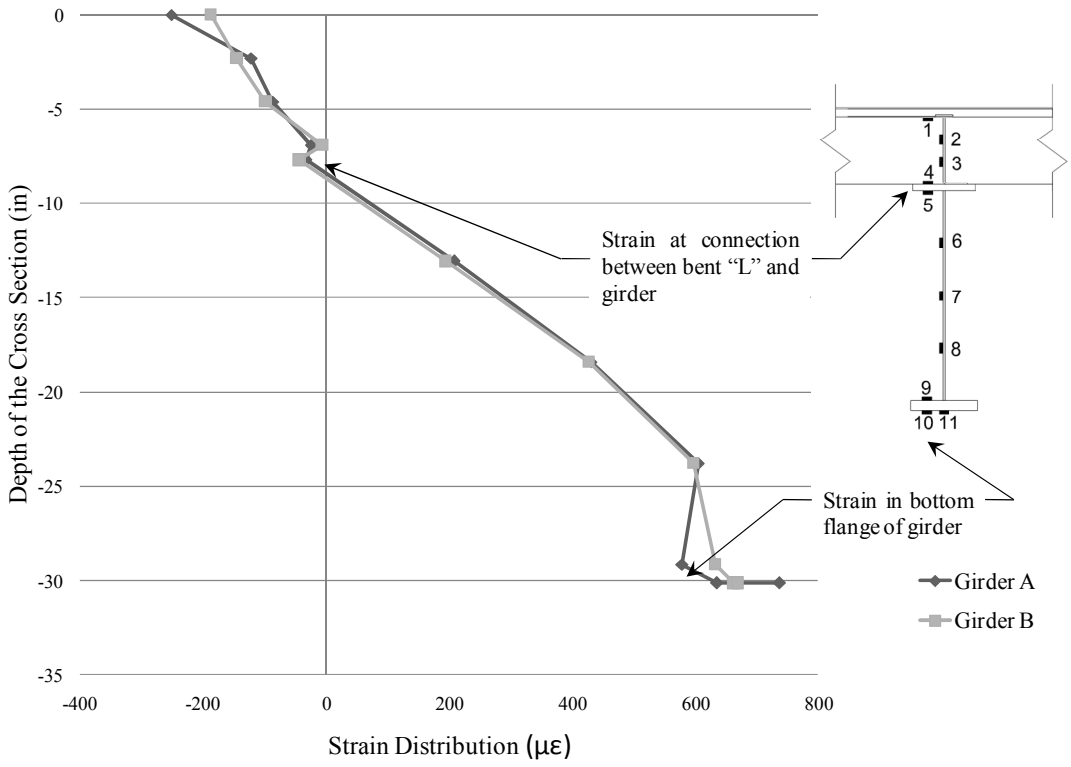

Figure 4.23: Strain throughout cross section depth at 0 cycles in Girder A and Girder B

Table 4.6: Average strains and percent change at 46.6 kips for Girder A

Cycles		SG1A	SG2A	SG3A	SG4A	SG5A	SG6A	SG7A	SG8A	SG9A	SG10A	SG11A
1	Strain	-250.9	-121.5	-86.0	-24.1	-32.7	208.4	430.7	605.4	578.7	635.6	737.0
	% Change	0.0%	0.0%	0.0%	0.0%	0.0%	0.0%	0.0%	0.0%	0.0%	0.0%	0.0%
10	Strain	-250.2	-121.7	-86.0	-22.8	-31.2	207.3	431.8	607.0	579.8	637.9	739.1
	% Change	-0.3%	0.1%	0.0%	-5.4%	-4.4%	-0.6%	0.2%	0.3%	0.2%	0.4%	0.3%
100	Strain	-250.2	-120.0	-86.5	-22.4	-32.7	209.5	431.5	607.0	580.9	636.1	739.9
	% Change	-0.3%	-1.3%	0.6%	-7.3%	0.2%	0.5%	0.2%	0.3%	0.4%	0.1%	0.4%
1000	Strain	-248.4	-120.5	-84.0	-22.0	-29.6	207.4	430.4	605.7	579.1	638.3	737.4
	% Change	-1.0%	-0.8%	-2.3%	-8.9%	-9.5%	-0.5%	-0.1%	0.0%	0.1%	0.4%	0.1%
10000	Strain	-248.1	-123.8	-86.6	-26.8	-35.0	207.8	428.9	610.6	579.2	640.6	739.1
	% Change	-1.1%	1.9%	0.6%	11.1%	7.2%	-0.3%	-0.4%	0.8%	0.1%	0.8%	0.3%
100000	Strain	-238.6	-122.6	-88.4	-25.0	-35.9	205.2	432.2	609.4	584.1	642.4	742.8
	% Change	-4.9%	0.8%	2.8%	3.5%	9.9%	-1.6%	0.3%	0.7%	0.9%	1.1%	0.8%
200000	Strain	-233.2	-115.7	-90.4	-21.0	-36.0	200.4	423.2	595.3	568.4	622.1	723.0
	% Change	-7.1%	-4.8%	5.1%	-13.1%	10.1%	-3.9%	-1.7%	-1.7%	-1.8%	-2.1%	-1.9%
300000	Strain	-241.1	-111.8	-85.8	-27.5	-39.6	204.5	431.0	603.1	577.4	631.2	734.2
	% Change	-3.9%	-8.0%	-0.2%	14.0%	21.1%	-1.9%	0.1%	-0.4%	-0.2%	-0.7%	-0.4%
400000	Strain	-222.7	-105.3	-87.2	-35.0	-44.6	197.6	428.0	598.9	576.5	633.3	736.4
	% Change	-11.3%	-13.4%	1.4%	44.9%	36.6%	-5.2%	-0.6%	-1.1%	-0.4%	-0.4%	-0.1%
500000	Strain	-211.2	-110.5	-89.7	-42.8	-51.5	192.8	424.8	606.9	583.5	641.3	709.0
	% Change	-15.8%	-9.0%	4.3%	77.1%	57.7%	-7.5%	-1.4%	0.2%	0.8%	0.9%	-3.8%
600000	Strain	-211.3	-117.8	-94.5	-55.3	-67.8	190.6	431.1	626.2	602.2	669.4	702.3
	% Change	-15.8%	-3.1%	9.9%	128.9%	107.6%	-8.5%	0.1%	3.4%	4.1%	5.3%	-4.7%
700000	Strain	-199.5	-121.3	-104.8	-65.4	-82.9	177.5	425.1	624.5	607.0	672.9	711.7
	% Change	-20.5%	-0.2%	21.9%	170.6%	153.7%	-14.9%	-1.3%	3.2%	4.9%	5.9%	-3.4%

Table 4.7: Average strains and percent change at 46.6 kips for Girder B

Cycles		SG1B	SG2B	SG3B	SG4B	SG5B	SG6B	SG7B	SG8B	SG9B	SG10B	SG11B
1	Strain	-187.0	-144.5	-97.6	-6.0	-43.0	195.0	427.3	596.9	632.6	663.1	669.1
	% Change	0.0%	0.0%	0.0%	0.0%	0.0%	0.0%	0.0%	0.0%	0.0%	0.0%	0.0%
10	Strain	-188.2	-142.5	-98.5	-4.9	-41.9	195.0	428.8	597.4	634.4	662.1	667.9
	% Change	0.6%	-1.4%	0.9%	-18.7%	-2.4%	0.0%	0.3%	0.1%	0.3%	-0.1%	-0.2%
100	Strain	-184.6	-143.2	-96.7	-4.0	-41.7	196.9	425.7	599.0	632.0	662.6	669.1
	% Change	-1.3%	-0.9%	-0.9%	-34.1%	-3.0%	1.0%	-0.4%	0.4%	-0.1%	-0.1%	0.0%
1000	Strain	-185.7	-141.1	-98.1	-4.4	-42.4	194.7	424.8	598.4	631.2	664.3	670.2
	% Change	-0.7%	-2.4%	0.5%	-27.4%	-1.4%	-0.2%	-0.6%	0.3%	-0.2%	0.2%	0.2%
10000	Strain	-191.4	-150.2	-104.3	-15.7	-51.2	187.4	417.5	593.4	625.4	656.5	665.6
	% Change	2.4%	3.9%	6.9%	161.3%	19.2%	-3.9%	-2.3%	-0.6%	-1.1%	-1.0%	-0.5%
100000	Strain	-194.5	-152.6	-111.3	-9.4	-45.1	191.7	423.3	590.9	625.8	652.3	663.2
	% Change	4.0%	5.6%	14.0%	56.4%	4.9%	-1.7%	-0.9%	-1.0%	-1.1%	-1.6%	-0.9%
200000	Strain	-181.8	-141.0	-103.4	-9.2	-43.7	189.1	412.5	579.0	609.9	640.3	646.4
	% Change	-2.7%	-2.4%	6.0%	52.2%	1.8%	-3.0%	-3.5%	-3.0%	-3.6%	-3.4%	-3.4%
300000	Strain	-181.3	-139.7	-104.3	-12.3	-47.2	184.1	403.5	571.7	605.8	629.1	640.5
	% Change	-3.0%	-3.4%	6.9%	104.0%	9.9%	-5.6%	-5.6%	-4.2%	-4.2%	-5.1%	-4.3%
400000	Strain	-180.1	-142.8	-112.5	-20.4	-52.7	181.9	402.6	571.5	602.3	630.0	641.5
	% Change	-3.7%	-1.2%	15.3%	238.2%	22.6%	-6.7%	-5.8%	-4.2%	-4.8%	-5.0%	-4.1%
500000	Strain	-176.8	-141.2	-118.6	-27.1	-57.9	175.2	403.2	570.9	603.7	632.3	644.5
	% Change	-5.4%	-2.3%	21.5%	350.2%	34.8%	-10.2%	-5.6%	-4.4%	-4.6%	-4.6%	-3.7%
600000	Strain	-172.2	-134.5	-109.9	-28.3	-56.8	173.0	401.8	568.0	600.2	633.5	640.7
	% Change	-7.9%	-7.0%	12.6%	370.0%	32.1%	-11.3%	-6.0%	-4.8%	-5.1%	-4.5%	-4.2%
700000	Strain	-162.9	-134.9	-113.8	-35.8	-65.1	170.3	394.8	562.8	599.5	629.8	639.4
	% Change	-12.9%	-6.6%	16.5%	493.1%	51.5%	-12.6%	-7.6%	-5.7%	-5.2%	-5.0%	-4.4%

Noticeable changes are evident in the strains at 0 cycles and 700,000 cycles. Figure 4.24 compares the initial and final strains of Girder A while Figure 4.25 compares the strains in Girder B. The composite neutral axis dropped in both girders, which is most evident in Figure 4.25. This suggests a loss of stiffness in the composite section mostly likely due to the weld failures or possible slip at the connection.

Further investigation of the strains at the connection between SG4 and SG5 showed that slip was unlikely. The shift in the neutral axis changed the strains from the static test at 0 cycles, and inflated percent change at the connection. From Table 4.7 the percent change of SG4 was 493 percent at 700,000 cycles. This is reasonable considering how close the strains are to zero. When a local value is close to zero a reasonably small change from iteration to iteration can result in a large percent change. The strains did not change significantly relative to each other and it was determined that slip at the connection was unlikely.

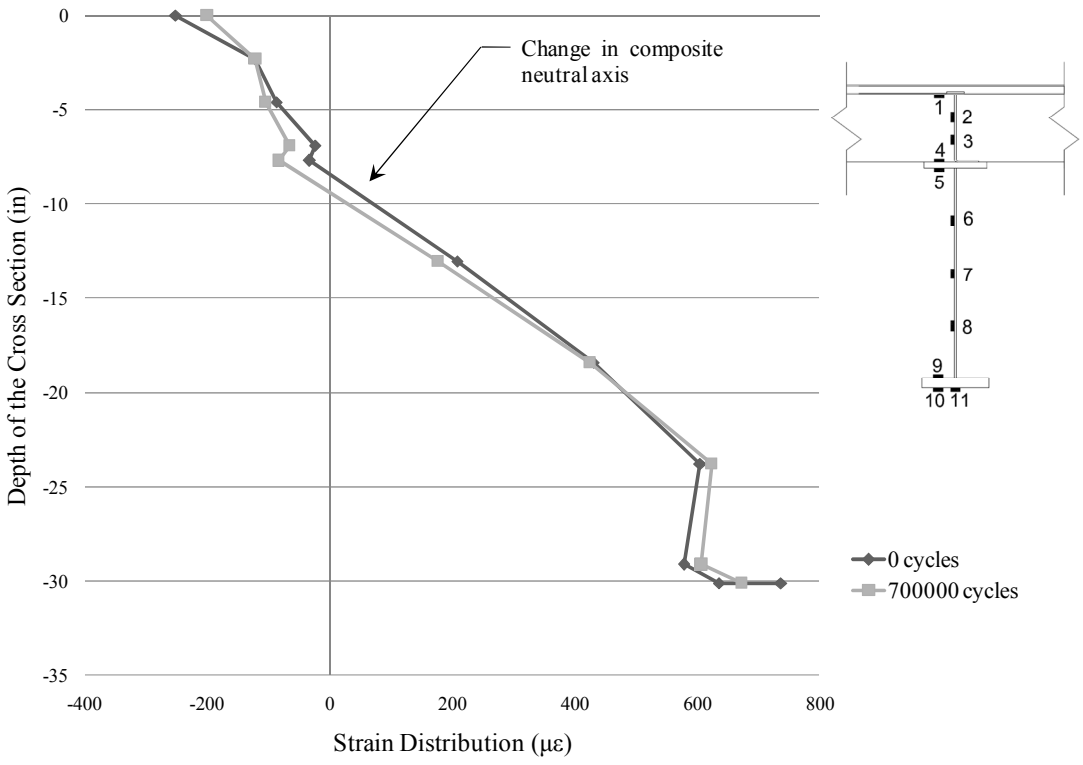

Figure 4.24: Strains throughout cross section depth of Girder A at 700,000 cycles

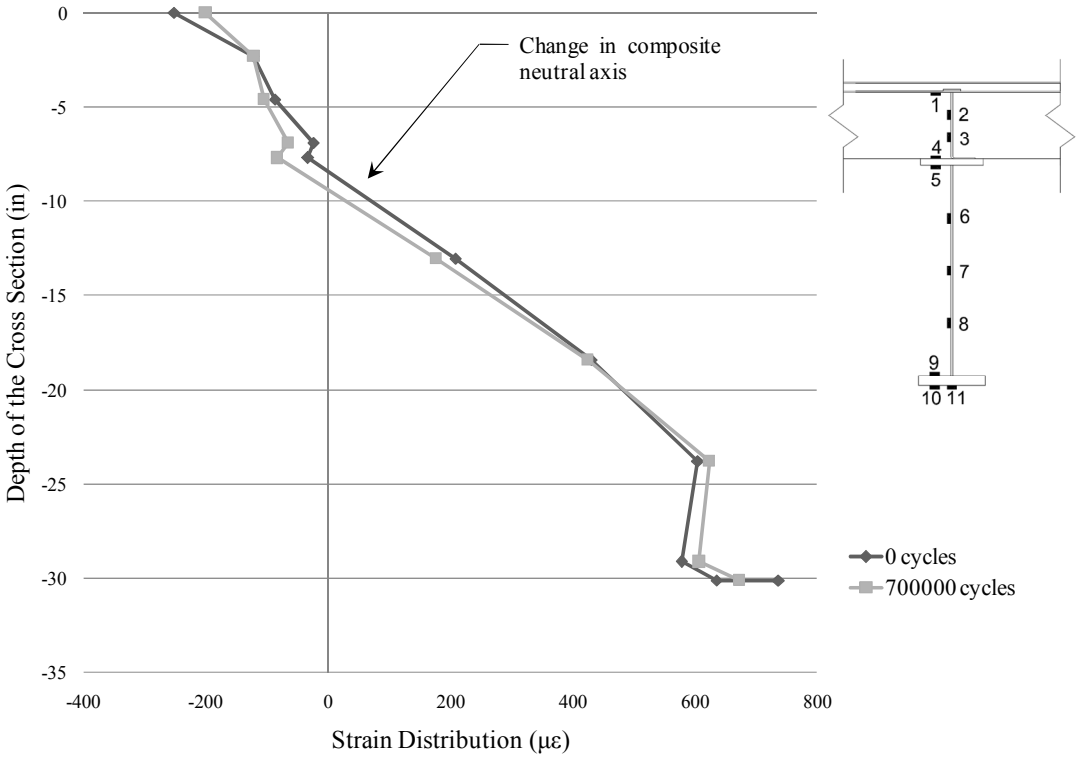

Figure 4.25: Strains throughout cross section depth of Girder A at 700,000 cycles

A change in strain over the number of cycles was investigated to determine any unusual strains change occurring during testing. No noticeable strain changes occurred through 100,000 cycles. After 100,000 cycles the strains began to vary in both Girder A and Girder B as shown in Figures 4.26 and 4.27, respectively.

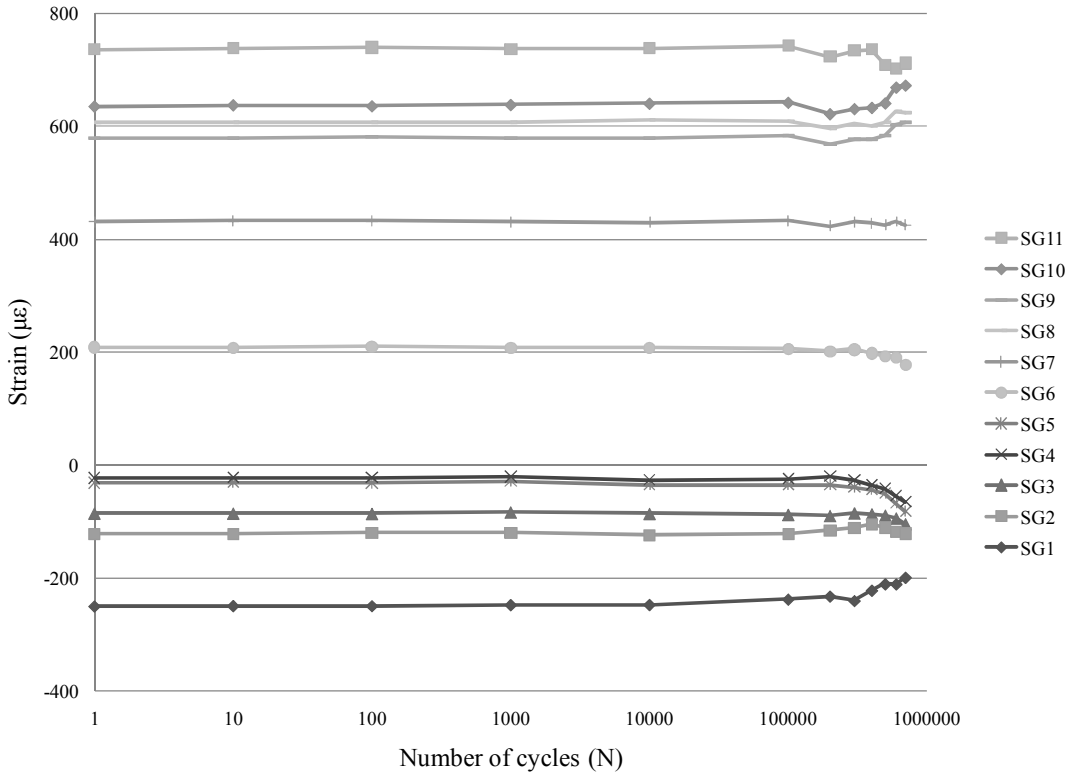

Figure 4.26: Strains at 46.6 kips versus number of cycles of Girder A

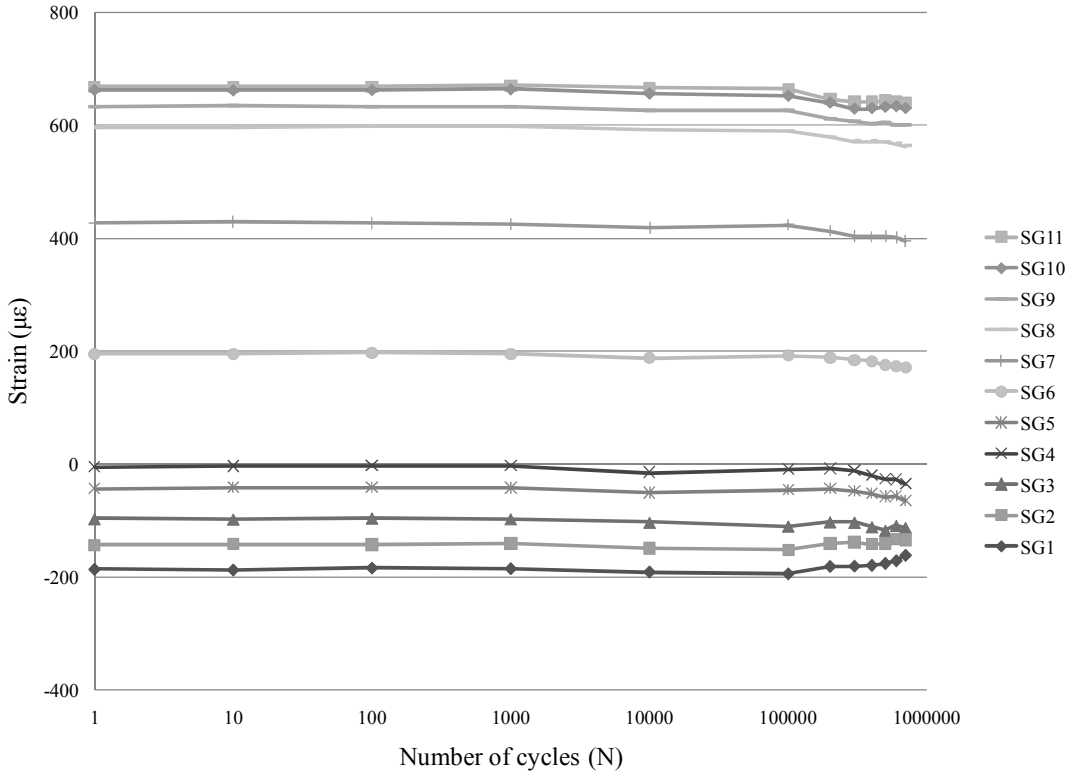

Figure 4.27: Strains at 46.6 kips versus number of cycles of Girder B

4.4.4 Slip Displacement Results

As in Load Case 1 four LVDTs were closely monitored throughout the testing procedure. There was no recorded slip relative to the end panel and the girder at any point during the test.

4.5 Analysis of Load Case 2 Results

The weld failures were investigated to find the approximate point of initiation and direction of propagation. The data was used to determine if slip occurred in the slip-critical connection and caused weld cracking or if an underlying cause was present.

All four weld cracks had a common feature; the cracks were at the intersection of the bent "L" plate, panel connection, and the deck. This intersection and approximate stress field directions indicated by the arrows are shown in Figure 4.28. As the specimen was loaded, the steel was loaded in all three orthogonal directions simultaneously. This intersection significantly increased the probability of fatigue cracking in the welds which suggest that the weld cracks most likely initiated from the intersection.

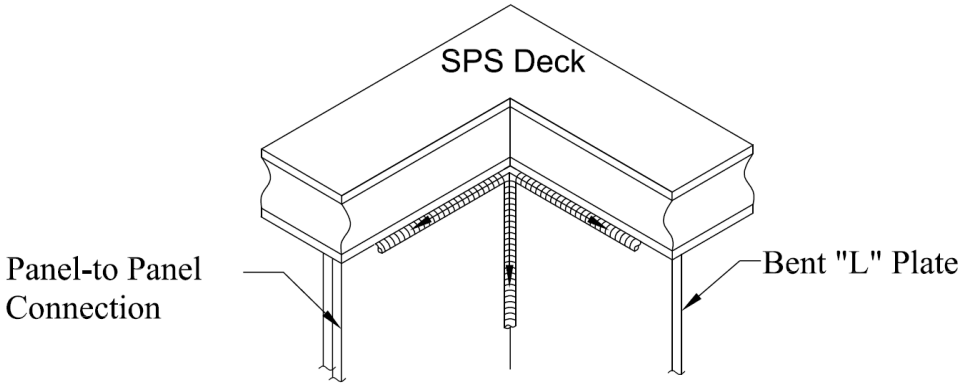

Figure 4.28: Typical weld connection three point intersection

Assuming the weld cracking initiated at the three point intersection, the cracks would have propagated along the existing welds. The details of the weld cracks show that the welds extended down the welded panel and bent "L" plate. The cracks then propagated into the bent "L" plate splitting the bolted section. The cracks extended through the plate and into the bolt holes. This is most likely due to bending of the bent "L" plate in the transverse direction and possibly to eccentric loading from the patch load. It is interesting to note that no cracks were found in the transverse direction of the plate perpendicular to the direction of the bolt holes. If slip occurred in the slip-critical connection, the connection would be considered a bearing-type

connection. If the bearing connection caused crack initiation, the cracks would have developed perpendicular to the bolt hole alignment through the bolted section where the edge of the bolt hole becomes the point of crack initiation as shown in Figure 4.29 (Kulak et al. 1987). It is obvious that the cracks did not develop in the transverse direction and the cracking in the bent "L" plate most likely was not due to a bearing failure and ultimately slip failure

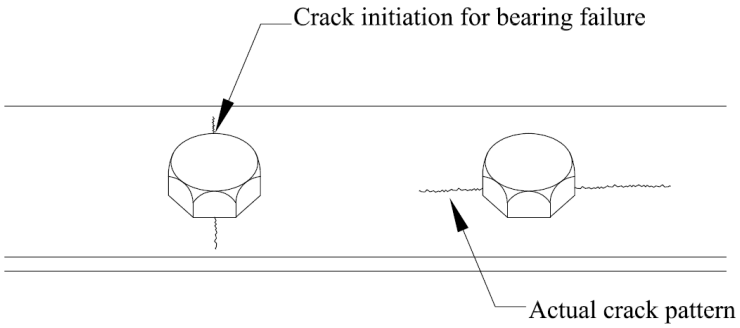

Figure 4.29: Typical crack initiation of a bearing-type connection (Kulak et al. 1987)

4.5.1 Load Case 2 Summary

Load Case 2 resulted in weld failures at the three point intersection of the bent "L" plate to the deck panel at approximately 750,000 cycles. These weld failures changed the stiffness of the system and an increase in deflection under the same load was recorded after weld failures. It was determined that the welds most likely initiated from the three point intersection of the welds at mid-span. Further investigation of the weld cracks show that a bearing failure is unlikely and suggesting that no slip of the bolted connection occurred.

4.6 Laboratory Fatigue Testing Summary

A one-half scale SPS bridge utilizing the bent "L" connection was tested to determine the fatigue resistance connection, especially the welded joint and the slip-critical connections. A testing program was developed for the project. The laboratory bridge was loaded cyclically, with a simulated fatigue truck load, to determine the fatigue life of the connection between the deck and the supporting girders.

Several types of readings, including strain gauges throughout the girder cross-sections, average deflections, and displacement relative to the girder and the deck panels, were used to collect data through the testing procedure. The data was used to determine if there was a loss in

composite action of the system or if any measured slip occurred at the connection. Two test setups were required for the testing of the specimen due to an unanticipated weld failure that occurred during the first test setup. Descriptions of the findings from the results of each load case are given. In summary,

- The testing was stopped at 43,000 cycles due unexpected weld failures. The welds failed due to transverse loading on the connection most likely due to eccentricities in the spreader beam setup.
    - The fillet weld connecting the bent "L" to the SPS deck was classified using the ASSHTO-LRFD Specification as a weld category "E" when load was applied in the transverse direction.
- Testing continued after repairing the cracked welds and changing the loading configuration until 743,000 cycles when more weld cracks were found. The cracks were located at the intersection of the panel-to-panel connection and the bent "L"
    - This type of weld detailing significantly decreased the fatigue resistance of the system and subsequently was the limiting state of the fatigue test.

Chapter 5: Local Behavior Investigation

5.1 Introduction

Laboratory fatigue testing of a one-half scale SPS bridge utilizing a deck-to-girder connection consisting of a bent "L" plate that was welded to the bridge deck and subsequently bolted to the supporting girders was presented in the previous chapter. The results indicated that high stresses, at the fillet welds, due to transverse loading may limit the fatigue performance of the bridge system. This type of deck-to-girder connection was used in the Shenley Bridge, but a new type of connection has been proposed for the Martin Branch Bridge. The new deck-to-girder connection used in the proposed Martin Branch Bridge connects the supporting girder directly to the deck through continuous welding of the flanges to the underside of the deck and eliminates the need for the bent "L" and bolted connections. This type of connection will subsequently be referred to as the welded flange or flange connection. A comparison of deck deformations and stresses at the welds due to eccentric loading for each connection detail was the basis for the investigation of the local behavior of the deck-to-girder connections.

The two types of connections investigated in this research are illustrated in Figure 5.1. The corresponding theoretical deck deformations are also shown. The bent "L" connection shown in Figure 5.1 (a) has a small surface area in contact with the deck and would be expected to act similar to a pinned connection, preventing vertical translation but allowing rotation at the connection. The small surface area and possible bending of the bent "L" may contribute to increased deck deformations and high transverse stresses at the fillet weld. The welded flange connection is shown in Figure 5.1(b). The increase in surface area between the flange and the deck would be expected to decrease the deformation of the deck and cause lower transverse stresses at the weld. The scope of the current research limits the investigation of the localized stress to a simple magnitude comparison and the investigation did not consider different flange widths or modifications to the SPS properties.

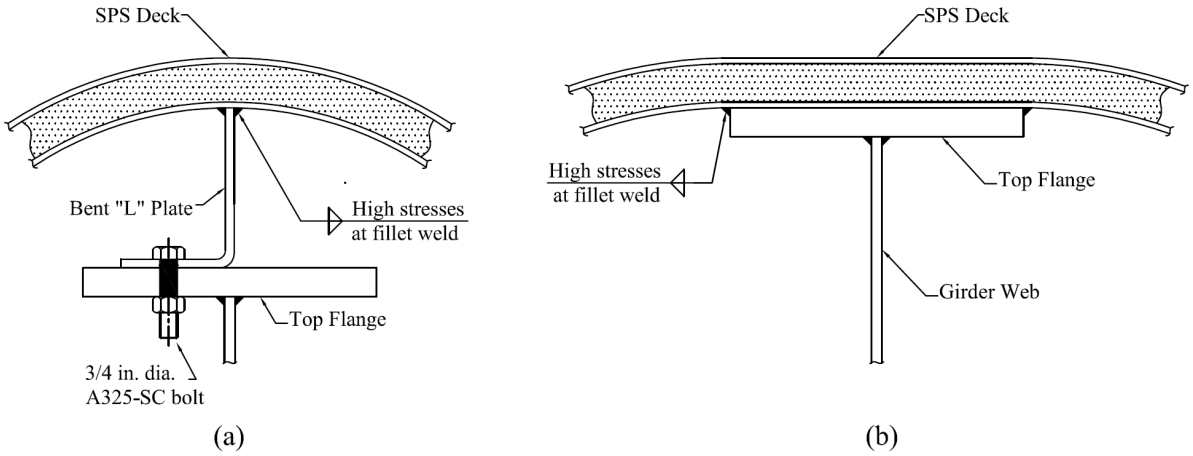

Figure 5.1: SPS connections and theoretical deck deformations

Without laboratory specimens to test and compare the different connection details, finite element modeling was used to study the connections. The FEA program, ANSYS was used to develop a model that could represent the connections, specifically the welded areas at the bent "L" and the flange. Because the scope of the research focused only on the connection influence on deck deflection and stresses at the weld, it was determined that the finite element models would be limited to the geometry of one panel of the laboratory bridge. Other influence factors such as girder spacing, and deck thickness were not investigated. An initial model of one panel of the laboratory bridge utilizing the bent "L" connection was developed and validated from laboratory results. After the initial model was validated, a second model was developed that represented the flange connections. The deflections and stresses were compared for both models.

5.2 Finite Element Model

The finite element model developed for this research represented the different connection types as accurately as possible. The use of three dimensional brick elements allowed the geometry of the connections to be easily duplicated. Ideally, the entire finite element model would have been represented by utilizing solid brick elements with 20 nodes and 60 degrees of freedom (DOF). This would allow for an accurate representation of bending in the solid elements but at a significant computational cost. Due to limitations of the finite element program used for this research, which only allowed a limited amount of nodal modeling, a simplified model was

required. Two elements were selected for the model generation and are presented in Table 5.1. The geometry localized to the weld locations was modeled using the Solid 185 elements while, the remainder of the deck utilized shell elements. The Solid 185 elements allowed accurate geometrical representation of the actual connection, and the Shell 99 elements were able to predict behavior over a wide range of aspect ratios as well as being capable of modeling the sandwich structure of the SPS by defining layers to represent the steel plates and the polyurethane core. It should be noted that the combination of the Solid 185 and Shell 99 elements caused inconsistencies at the element connection. The solid elements have a linear relationship that does not match the quadratic shape function of the shell elements. Also, the elements do not share the same set of degrees of freedom, and no rotational DOF was transferred between the solid and shell elements. These limitations due to the finite element program influenced the results at the solid-shell interface, but because data at the location of this interface was not relevant to this research, the inaccuracies of the model were considered acceptable.

Table 5.1: Elements used for pane model generation

Element	Description	Capabilities
Solid 185	8 node element with 3 DOFs per node	3-D solid modeling of structural shapes
Shell 99	8 node element with 6 DOFs per node	Linear layered structural shell capable of modeling sandwich structures

The model geometry was developed to accurately represent the actual connection details while maintaining a limited amount of nodes. This was achieved by modeling the SPS deck with two element types as previously described. The overall deck geometry matched the laboratory bridge panel and measured 5 ft in the longitudinal direction and 14 ft 9 in. in the transverse direction with center-to-center girder spacing of 5 ft. The welds and the surrounding geometry including the steel and polyurethane layers of the SPS deck were modeled with the solid brick elements that were modified to represent the respective material properties and were connected through coincident nodes. The geometry was also simplified by only modeling the bent “L” plate that measured 7 in. from the SPS deck to the supporting girder. Boundary conditions limiting all translational and rotational DOF were applied at this location to represent the restraint of the bent “L” to girder connection provided by the slip-critical bolt connection. By restraining the vertical

translation of the bent "L" connection only the relative deflection of the SPS deck was measured, however, this was well within the scope of this research as only a comparison of the panel deflection and stresses were compared. A similar geometrical configuration was used for the welded flange connection, and only 7 in. of the web was modeled, allowing the same distance for flexural rotation to occur in both connection models. Figure 5.2 illustrates the geometry of the SPS panel section. Figure 5.3 shows a detailed section of the finite element geometry of the bent "L connection. The element mesh is more refined closer to the welded area and gradually gets larger until the shell elements represent the SPS deck.

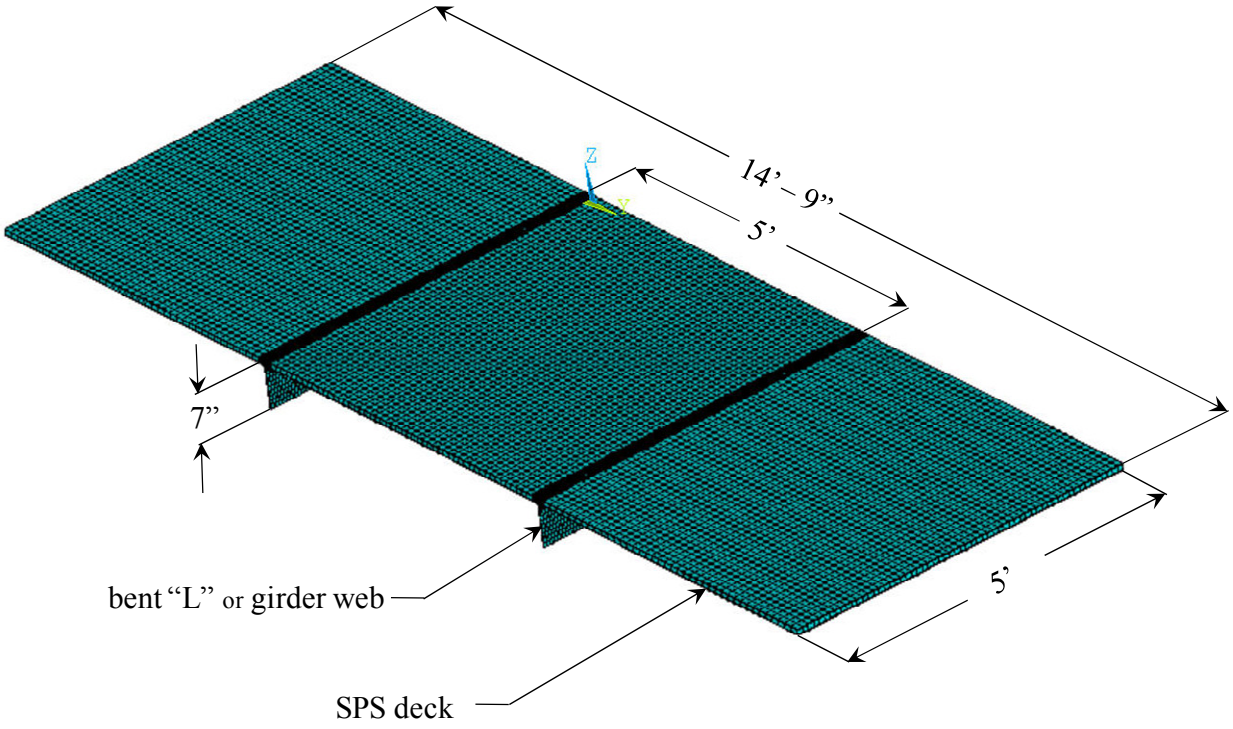

Figure 5.2: Model geometry of SPS panel

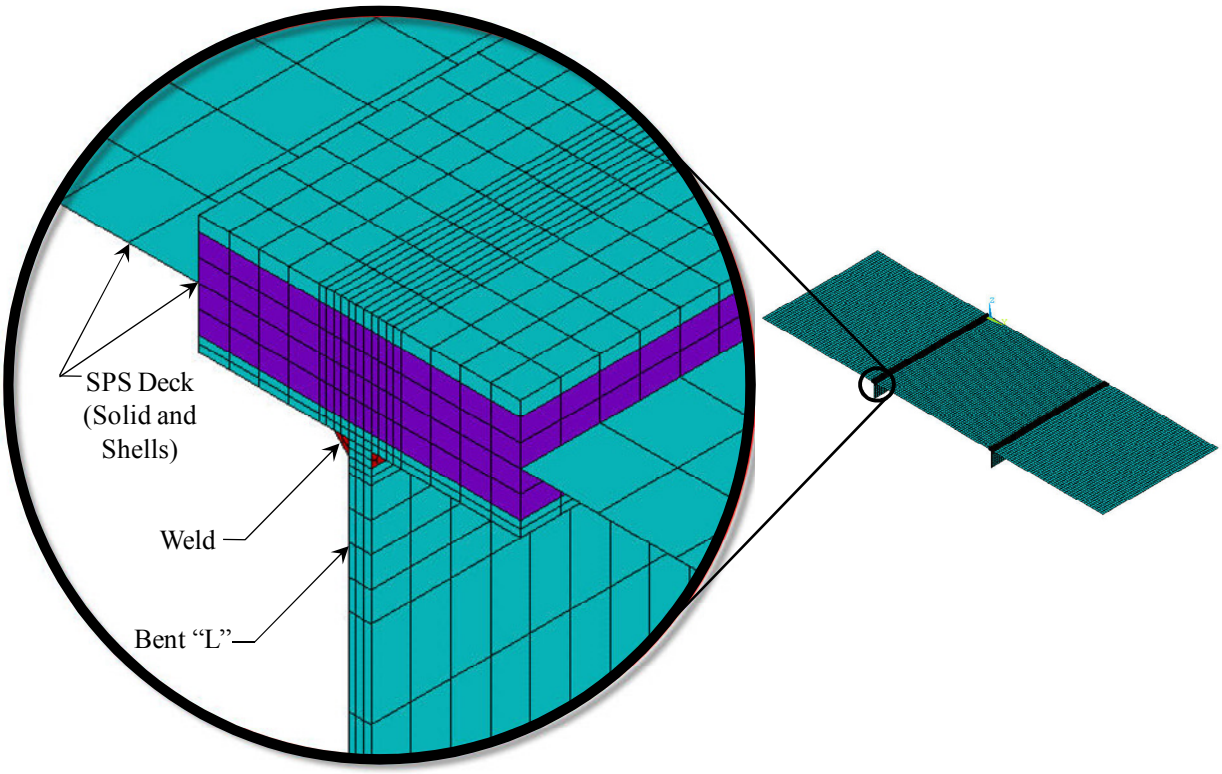

Figure 5.3: Finite element geometry of bent "L" connection

5.2.1 Validation of Initial Model

An experimental testing program was developed to determine the validity of the finite element model. The one-half scale laboratory bridge was loaded 7ft-6in. in the longitudinal direction from mid-span of the bridge at the middle of a SPS panel. This location allowed modeling of the panel with symmetric loading at the middle and also provided distance from the previous weld failures that occurred during the laboratory fatigue testing as discussed in Chapter 3. The bridge was instrumented with seven cable-extension transducers (CET) to measure displacement of the girders as well as the deck. Four CETs were placed at the support locations to measure any displacement due to end condition displacements of the bridge, two were place at the middle of the panel under each girder, and the last CET was placed directly under the loading position to measure the deck displacement. The relative displacement of the deck was calculated by subtracting the girder displacements from the measured deck displacement. Strain gauges

were also placed on the bridge specimen and used to ensure the loading did not yield the steel. The test setup and instrumentation layout is shown in Figures 5.3 and 5.4, respectively.

Figure 5.4: Test setup for finite element panel validation

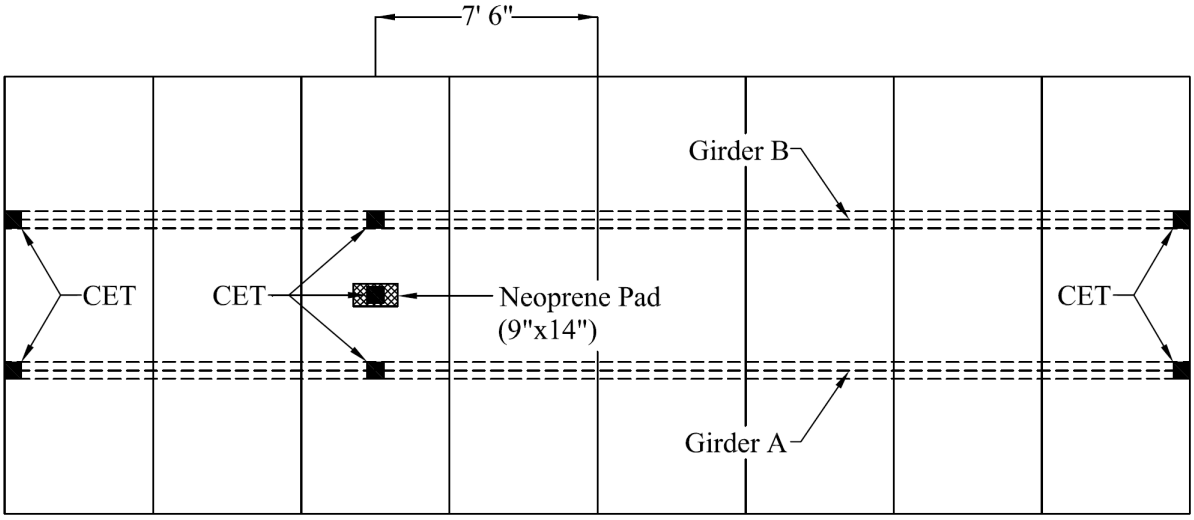

Figure 5.5: Instrumentation layout for finite element panel validation

Three tests were performed on the laboratory panel section. The load for each test was slowly applied using a hydraulic ram that distributed the load through a rectangular neoprene patch measuring 9 in. by 14 in. until the measured strains approached the yield strain of

approximately 1,724 με based on Grade 50 ksi steel. This load corresponded to approximately 23.9 kips, but for simplicity of modeling and comparison, the measurements used for validation corresponded to 20 kips.

The finite element panel model was loaded with an equivalent 20 kip load distributed over an area of 9 in. by 14 in. The method of equivalent nodal loading was used to apply the load to the shell elements representing the SPS deck. This method distributes a series of distributed loads acting on the element to the node through the use of element shape functions. For the Shell 99 elements, a quadratic shape function was utilized. This method allowed the patch load to be applied at any location of the finite element panel.

It is difficult to assess the actual boundary conditions that occur in a SPS bridge specimen. Modeling only one panel section of a bridge required the use of theoretical restraints such as a pinned or fixed connections to represent the behavior of a single panel as it would act within the complete bridge system. The end condition of the bent "L" was restrained against all translation and rotation and was considered a fixed connection. This restraint was chosen to idealize the fixity from the rest of the girder, and to allow bending of the bent "L" based on its material and sectional properties. Both simply supported and fixed end conditions were applied to the panel-to-panel connection and the deflection response of the laboratory specimen was compared and shown in Figure 5.6. The maximum deflection measured at the center of the panel from the three laboratory test were averaged and an approximate displacement of -0.51 in. was found. The fixed end condition from the finite element model produced a displacement of -0.38 in., which corresponds to approximately a 25 percent difference as compared to the laboratory test. The simple support model produced a displacement of 0.66 in. and corresponds to approximately a 29 percent difference. This comparison suggests that the actual boundary conditions in the bridge are bounded between theoretical simply supported and fixed end conditions and a limited amount of rotation exists between the panel connections. The results from this study validated the finite element panel behavior and were consider acceptable for comparison of the influence of the connections. The simple support condition was chosen to represent the panel-to-panel connection and to allow rotation at the location. A contour plot of the FEA representation of the vertical deflections due to the 20 kip load at the middle of the panel modeled with fixed restraints at the bent "L" and simple supports at the panel-to-panel connection is shown in Figure 5.7. The contour plot allows for a visual check of the finite

element results as well as a theoretical representation of the displaced shaped of the panel. The smooth uninterrupted contours suggest that there is no interelement discontinuity in the panel mesh.

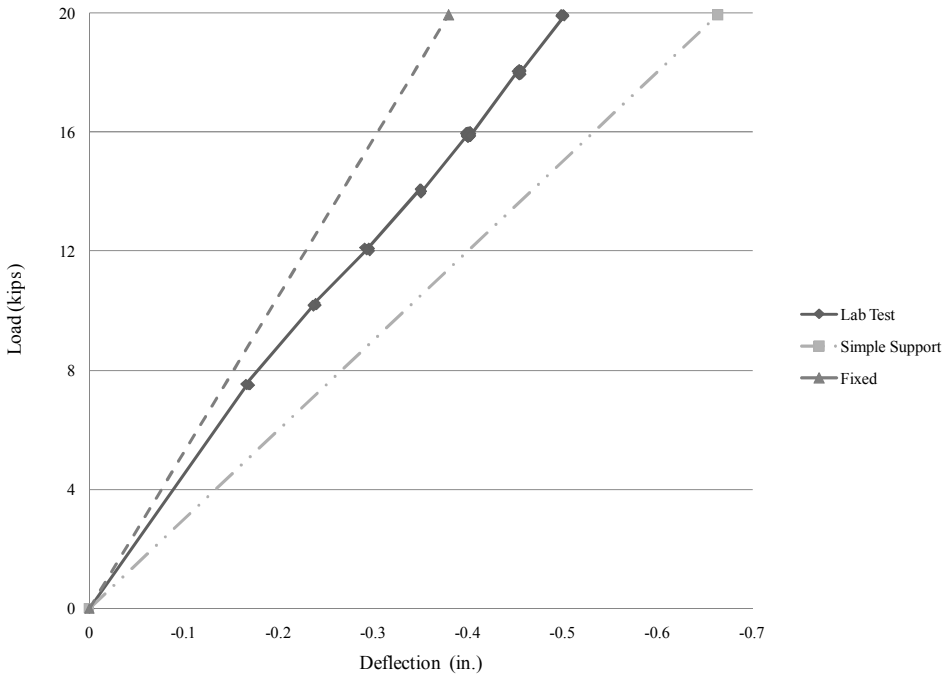

Figure 5.6: Comparison of boundary condition based on deflection response

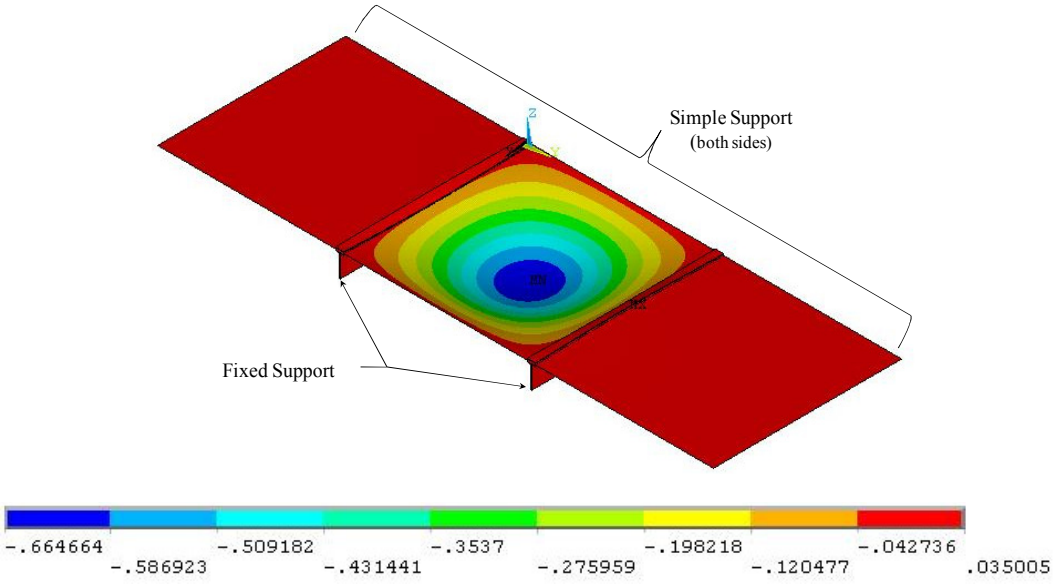

Figure 5.7: Contour plot of deflection from the FEA of SPS panel section

5.3 Connection Comparisons

After validation of the initial panel model utilizing the bent "L" connection, a panel utilizing the flange connection was developed using the same modeling techniques. The SPS deck was modeled with the same geometry measuring 5 ft by 14 ft-9in. with center-to-center girder spacing of 5ft. The welds connecting the flange to the deck, and the girder web to the flange, as well as the surrounding geometry were modeled with solid brick elements. Again, to simplify the model, only 7 in. of the flange web was modeled. Boundary conditions limiting all translational and rotational DOF were applied at this location to represent the restraint of web to the remaining girder. By limiting the web distance to the same 7 in. depth as the bent "L" connection model, similar restraint conditions were assumed between the two models. Figure 5.8 illustrates the finite element geometry of the welded flange connection.

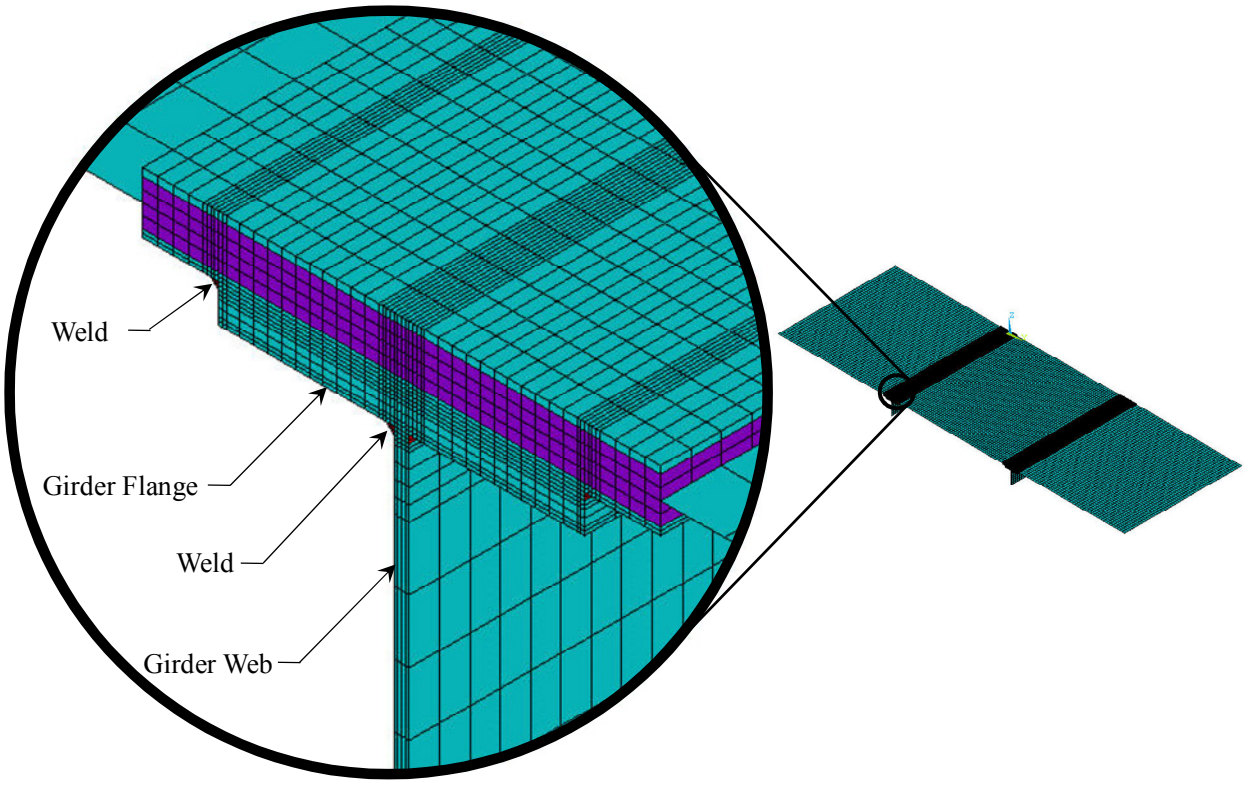

Figure 5.8: Finite element geometry of welded flange connection

5.3.1 Deflection Comparison

The same patch loading configuration as used in the laboratory validation setup was used to determine relative deck deflection between the two finite element models. A 20 kip load distributed over a path area measuring 9 in. by 14 in. was placed at the mid-span of the specimen. The deflections at the mid-span of each panel section were compared to determine if the connection type changed the stiffness of the system. A summary of the results is shown Table 5.2. The finite element representation of each panel section with its corresponding deflection is shown in Appendix B.1. The flange connection provided a small increase in stiffness of approximately nine percent. Although the change in deflection was small, it appears that the welded flange connection changes the rigidity of the panel end condition at the girder connection and the overall stiffness of the SPS deck.

Table 5.2: Deflection at mid-span of the finite element panel models

Connection	Deflection (in.)
Bent "L"	0.664
Flange	0.605

5.3.2 Stress Comparison

Calculation of stresses at a definite location using finite element models is a complicated task. Computed stresses are usually most accurate within an element at the Gauss quadrature points, not at the nodal locations. Typical finite element software extrapolates the stresses from the quadrature points to the nodal locations. Nodal stresses between adjacent elements are simply the average of the extrapolated stresses. Element stresses are also an interpolation of the stresses throughout the cross-section of the element but are not averaged to create interelement continuity (Cook et al. 2001). For this research, a comparison of the stresses near the weld-toe interface was desired. The nodal interface at the weld location was not analyzed; instead, the stresses as calculated by the finite element software were compared for the element adjacent to the weld location at the mid-span of the panel as represented in Figure 5.9. To produce accurate results the highest level of refinement was used at the weld toe interface without exceeding the nodal limitation imposed by the software.

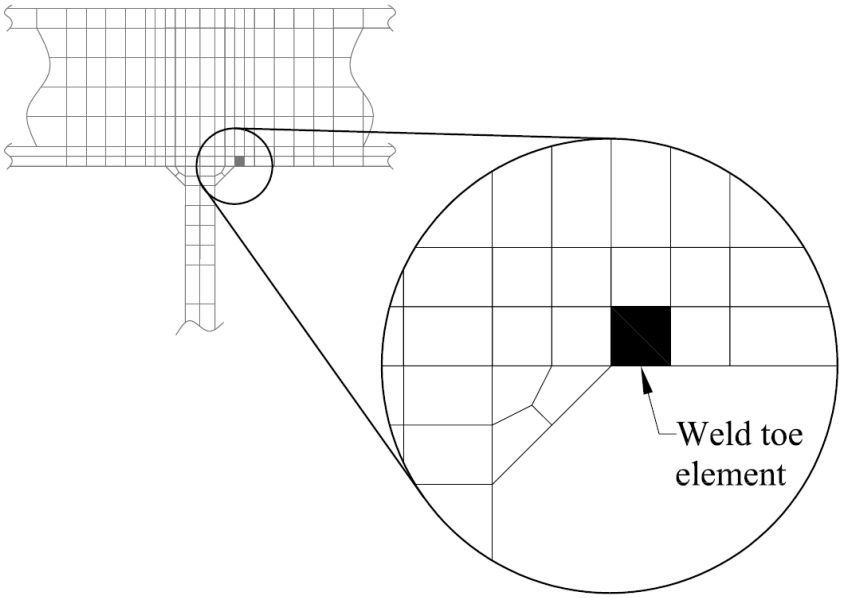

Figure 5.9: Location of element at the weld toe

Each panel model was loaded utilizing the patch loading. The centerline of the patch was placed at 6 in. intervals starting at 12 in. from the girder line to 30 in. at the middle of panel section. The element adjacent to the weld at mid-span of the panel is shown in Figure 5.9 was analyzed for transverse stresses. The maximum stress at the bottom of the element was used for comparison. Appendix B shows all elements and corresponding calculated stress. Table 5.3 compares the stresses calculated by ANSYS at the bottom of the weld toe element for each type of connection at the different loading locations.

Table 5.3: Stress comparison due to eccentric loading

Eccentricities (in.)	12	18	24	30
Bent "L" Transverse Stress (ksi)	-123.7	-92.1	-69.2	-50.3
Flange Transverse Stress (ksi)	-80.5	-57.6	-42.1	-30.2
% Difference	-34.9%	-37.5%	-39.1%	-40.0%

It is important to note that the finite element analysis utilized to calculated the stresses only considered the linear elastic material properties of the SPS deck and the connection details. This linear behavior of the model does not allow yielding of the section and can provide misleading results, such as the high stresses of -123.7 ksi at 12 in. eccentricity when utilizing the bent "L" connection. This high stress would have resulted in yielding of the steel section.

To account for this behavior, the data was normalized to the minimum stress calculated for the bent "L" connection at the 30 in. eccentricity. By normalizing the data, a relative comparison of the stress due to the eccentricities as well as the change in stress due to the flange connection as it compares to the bent "L" flange loaded at mid-span can be illustrated as shown in Figure 5.10. The values given by the normalized graph are essentially a multiplier that can be used for calculating stresses at the weld toe due to loading eccentricities for linear elastic behavior of the panel section. Note that the connection utilizing the bent "L" has a multiplier equal to 1.0 at the 30 in. eccentricity, while the flange connection has a corresponding multiplier of 0.6 at the same location. There is a 40 percent decrease in the stresses at the weld toe based on the type of connection used. The stresses increased as the load approached the deck-to-girder connection location and resulted in an approximate increase of 2.46 and 2.67 for the bent "L" and flange connection, respectively. The flange connection resulted in an average of 38 percent decrease in stress at the weld toe location as compared to the bent "L" connection.

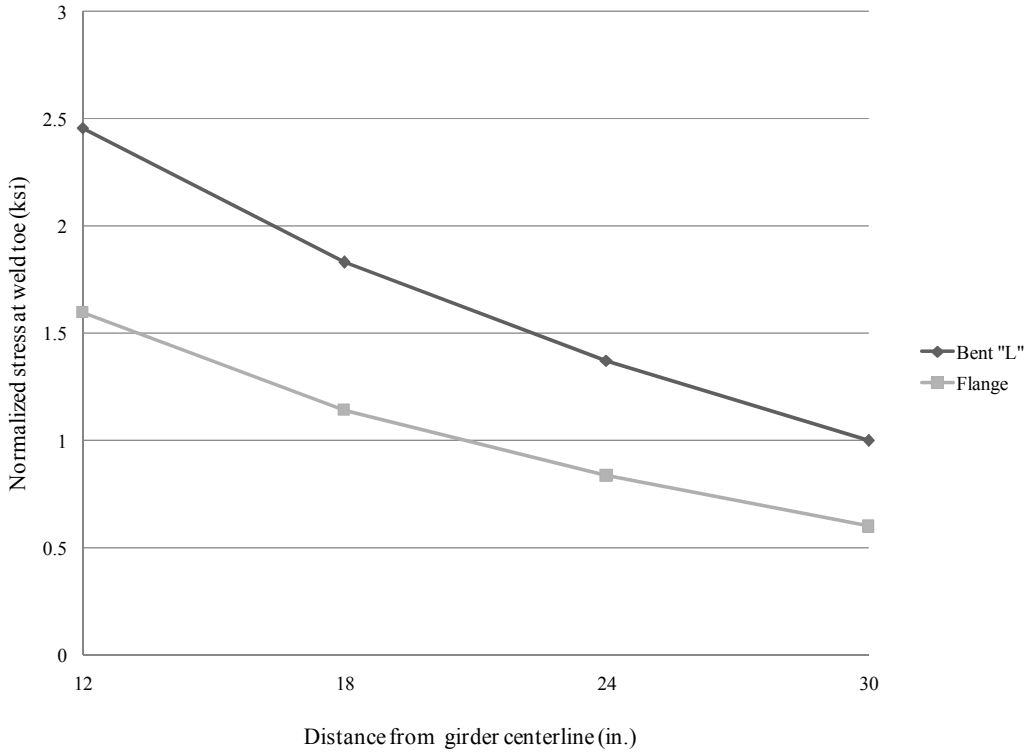

Figure 5.10: Normalized stress comparison of both connections

5.4 Summary

Initial laboratory testing of a one-half scale bridge indicated that high stresses at the fillet welds, used in the deck-to-girder connection, due to transverse loading of the weld may limit the fatigue performance of the bridge. A testing program was developed to compare the influences of the two types of deck-to-girder connections on mid-span deck deflection and the stresses at the weld connection. Finite element analysis was used to model panel sections of a SPS bridge deck utilizing both the bent "L" connection and the welded flange connection. The data from deflection test and average element stresses were compared.

A patch load was applied to each panel model to determine the influence of the different connection details on the deflection response of the SPS panel. It was determined that the welded flange connection provides more rigidity at the deck-to-girder connection and resulted in less deflection when compared to the bent "L" connection.

The influence on transverse stress based on the two connection types was investigated by comparing average element stresses at the weld toe location when loaded at several loading configurations eccentric to the connection. The comparison of stresses at the location of the weld toe between the two connection types showed a significant decrease in stresses when the flange connection is used. The welded flange connection resulted in an average of 38 percent decrease of stresses at the weld toe location. This comparison suggests that the welded flange connection would increase the fatigue life of the structure based on lower stresses due to eccentric loading at the fillet weld locations.

Chapter 6: Global Behavior Investigation

6.1 Introduction

This chapter presents an investigation of the global behavior of a SPS bridge deck considering two types of deck-to-girder connections. Transverse lateral load distribution factors were used to compare the load sharing abilities and overall behavior of the bridge system depending on the connection used. Previous research in SPS global behavior has indicated that the parameters with the greatest influence on transverse load distribution are girder spacing and flexural plate rigidity, while other factors such as span length and longitudinal stiffness have a lesser effect (Harris 2007). The influence of deck stiffness of an SPS deck as compared to a reinforced concrete deck would be expected to significantly influence lateral load distribution behavior. Harris considered different plate designs, changing plate and core thickness to influence flexural plate rigidity, and conservatively assumed that the plates were simply supported on each side. The current research was aimed to investigate the change in flexural stiffness of SPS decks based on different end conditions, by investigating different types of connection used in the deck-to-girder interface. As previously discussed in Chapter 4, the bent "L" and flange connections influence the deck stiffness, with the later resulting in less deck deflection.

Finite element modeling was essential for modeling bridges with the same geometric properties that only differed at the deck-to-girder connections. To ensure accuracy an extensive validation program was developed. The laboratory bridge was modeled and loaded to represent the load cases discussed in Chapter 3. The Shenley Bridge was then modeled and loaded to validate field testing data from previous research. After validation of the finite element models, the Shenley and Martin Branch bridges were then modeled with the bent "L" connection and with the welded flange connection. The influence of these connections was compared to determine if a change in the flexural stiffness of the system based on connections affected the global behavior of the transverse load distribution. Extensive research by Harris (2007) investigated different element types, loading configuration, and levels of finite element model complexity on SPS bridge systems. The research extended from basic modeling of the Shenley Bridge to parametric studies of the lateral distribution factors for typical SPS bridge deck

systems. Different element types and configurations were investigated and validated by Harris, and have been adopted for use in the current research.

6.2 Development of Initial Models

The finite element software program ANSYS was used to create the finite element models. Limiting the analytical investigation to the global behavior of the bridge deck system allowed the use the primary components of influences. Several components affect the overall bridge system, but it has been found that the most influential of these include the deck, the girders, and the diaphragms (Harris 2007). To model these components, three basic elements were used as described in Table 6.1.

Table 6.1: ANSYS element types

Element	Description	Capabilities
Shell 99	8 node element with 6 DOFs per node	Linear layered structural shell capable of modeling sandwich structures
Beam 188	2 node element with 6 DOFs per node	3-D Linear Finite Strain Beam: including shear deformations
MPC 184	Rigid link with no mass	Provides a physical connection between 2 nodes

The SPS deck was modeled utilizing Shell 99 elements that were able to predict behavior over a wide range of aspect ratios as well as capable of modeling the sandwich structure of the SPS. User defined layers were able to represent the steel plates and the polyurethane core. The Shell 99 element was also used to model the flanges of the supporting girders, but linear layers were not used.

The bent "L" connection, girder web and diaphragms were modeled using Beam 188 elements. It is important to note that the Beam 188 element is a two node element that allows the addition of a node at the center of the element that is taken into consideration during the formulation and not in the modeling of the element. The two node element was chosen to simplify model generation when compared to the similar three node element, while the addition of the extra node allowed for quadratic strain compatibility between the Beam 188 element and the Shell 99 elements.

The third element required for modeling was the MPC 184 or rigid link element. This element was used to model the composite action between the deck and the girders by connecting nodes of the deck elements the beam and shell elements for the bent "L" and flange connections, respectively. The MPC 184 element allowed elements to deform and rotate relative to each other.

The model geometry closely represented the actual bridge configuration. The SPS deck was modeled using shell elements. Each girder was modeled utilizing shell elements for the flanges and beam elements for the web. The model geometry only differed based on the deck-to-girder connections. The bent "L" connection was represented by a beam element and was connected by a rigid link at the center of the beam to the corresponding shells elements that represented the SPS deck and the supporting girder flange. The welded flange connection utilized rigid links that connected corresponding nodes of the supporting girder flange directly to the SPS deck. Both model geometries and finite element representations are illustrated in Figure 6.1

The actual support restraint conditions of the bridges can be difficult to model. Several researchers have suggested utilizing a spring with known stiffness that limits translational and rotational degrees of freedom at the support, but for simplicity only simply supported boundary conditions were assumed in this study. To accurately represent the actual restraint located at the bottom of the girder flange, a series of dummy nodes was created at the bearing locations under each girder flange. These nodes were then connected to the centroid of the corresponding shell element using the MPC 184, to effectively restrain the model. Simply supported boundary conditions were then applied directly to the dummy nodes. The dummy nodes and corresponding restraints are shown in Figure 6.1

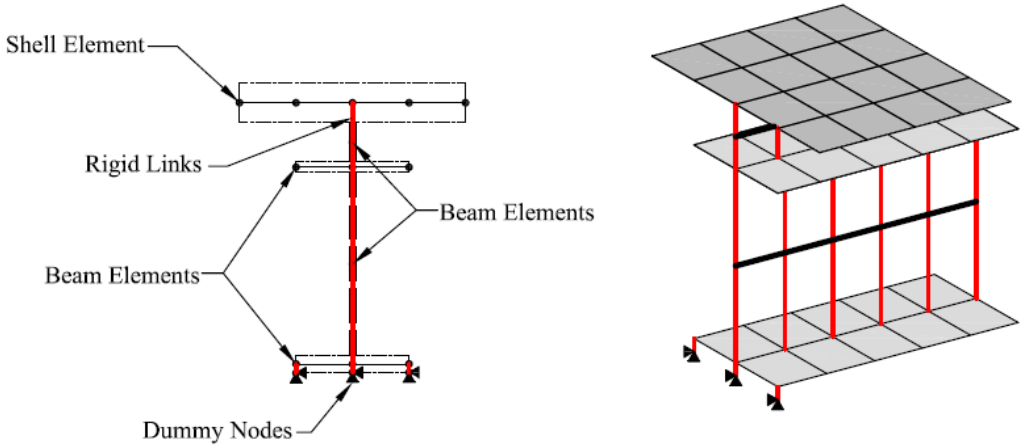

(a) Bent "L" connection

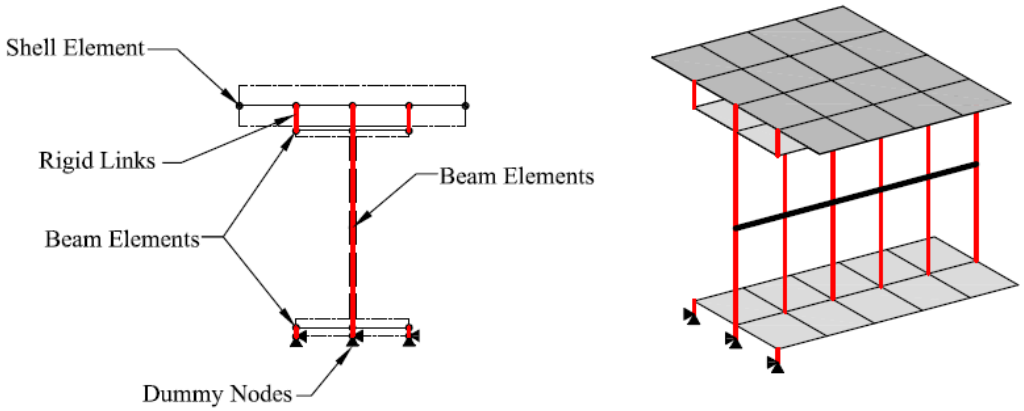

(b) Flange connection

Figure 6.1: Basic model geometry and finite element representation

The loads were applied to the system utilizing the method of equivalent nodal loading. This method distributes the load through the use of the element shape functions, in the case of the Shell 99, a quadratic shape function. This method does not require the loads to be coupled to the element mesh and allows the application of loads anywhere on the bridge deck.

6.2.1 Validation of Initial Models

The first model developed closely represented the actual laboratory bridge configuration so that the results from Load Case 1 and 2 from Chapter 3 could be used to validate the results. After verification that the FEA provided reasonable results, the Shenley Bridge model was developed and validated using results of field testing by Harris (2007). Complete description of the laboratory bridge and the Shenley Bridge are in Section 3.1 and Section 2.2.1, respectively, but condensed reviews are presented for reference.

The 40 ft simple span laboratory bridge system consisted of the SPS deck with top and bottom plates bonded to an elastomer core with specified dimensions of 1/8 in. and 3/4 in. thick, respectively. The bent "L" plates were nominally 3/16 in. by 7-7/8 in. and connected the deck to the girders. The SPS bridge deck was supported by two plate girders. Each girder was a built-up member with a top flange measuring 5/8 in. by 6-3/8 in., a web 1/4 in. by 21-3/8 in., and a bottom flange 1 in. by 7 in. The girders were connected by a steel angle diaphragms spaced at 10 ft. center to center. Each diaphragm consisted of steel angles nominally 2 in. by 2 in. by 5/16 in.

The Shenley Bridge utilizes 1/4 in. steel plates separated by a 1-1/2 in. elastomer core. The bridge has a span of 73.8 ft and a transverse width of 23.3 ft. Each built-up girder consists of a top flange measuring 3/4 in. by 11-13/16 in., a web 15/32 in. by 36-7/32 in. and a bottom flange 1 in. by 13-13/16 in. The bent "L" used for the deck-to-girder connections are 7-7/8 by 4-9/16 by 3/8 in.

6.2.2 Load Case 1 Validation

The first load case, Load Case 1, used to validate the initial laboratory FEA model consisted on four loading areas located at the centerline of each girder and offset 2 ft on each side from mid-span of the bridge. Each load patch measured 9 in. by 18 in. and had a corresponding load of 25.9 kips each. The deflection data was recorded from the mid-span nodes of each girder while the strain data was recorded from nodes that were offset 30 in. from mid-span, corresponding to the center of the panel adjacent to mid-span. This gauge pattern was chosen to match the laboratory setup as explained in detail in Section 3.3.4. Figure 6.2 shows the ANSYS model of Load Case 1. The arrows represent the loading of each patch area.

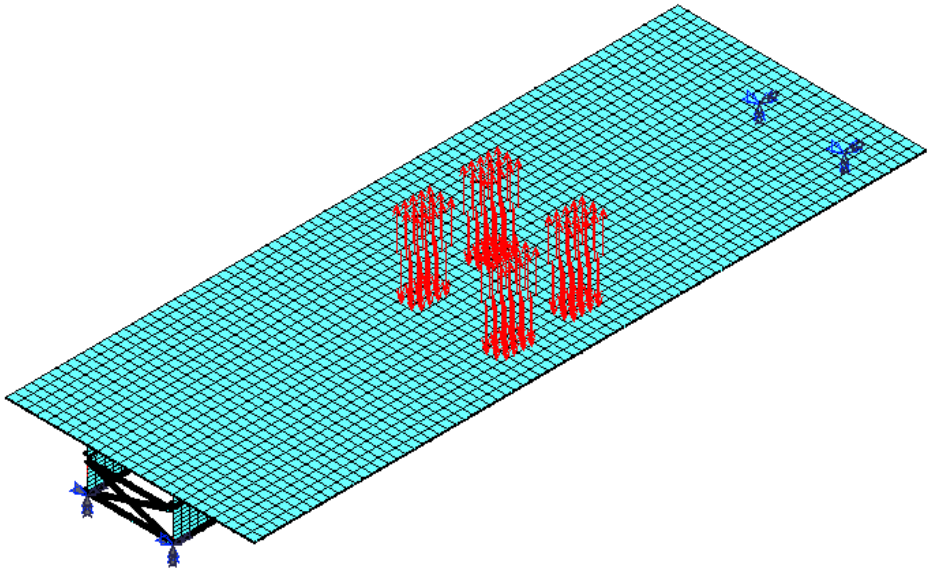

Figure 6.2: ANSYS model of Load Case 1

The results from the finite element analysis closely represented the data collected in the laboratory. Table 6.2 summarizes the deflections and strain results from the model and the corresponding percent difference from the measured laboratory data. Notice that the maximum mid-span deflection measured from the laboratory specimen was used. Unlike the laboratory results, the end condition deflections were not averaged and subtracted from the mid-span deflection (See Section 4.1.1 for complete description of the experimental vertical displacement results). The small percent errors of approximately five percent, from the maximum recorded displacement in the laboratory, suggest that the laboratory specimen resting on the neoprene pads acted similar to a theoretical pin-roller boundary condition. The scope of this project limited additional research in the actual boundary conditions and the maximum deflections measured in the laboratory were used to validate the finite element model. To ensure accuracy, the strains calculated from the model were also compared to the measured strains from the laboratory specimen. The calculated strains in the bottom of the girders are within approximately seven percent of the measured strains. There is a significant difference in strains at the bent "L" and girder interface but this can be contributed to the small strain levels at this location. Figure 6.3 better illustrates the strains throughout the cross section of the model as compared to the actual girder data. The calculated deflection and strain data from the model closely represents the

measured data and the finite element model was considered valid for modeling the global behavior of the bridge.

Table 6.2: Deflection and strains comparison for Load Case 1

Location	FEA	Lab Test (Girder 1)	% Diff.	Lab Test (Girder 2)	% Diff.
Deflections (in.)					
Bottom of Girder	-0.86	-0.90	-4.6%	-0.91	-5.7%
Strains (με)					
Top of Bent "L"	-271.2	-187.2	44.8%	-231.9	16.9%
Bottom of Bent "L"	-44.0	-20.8	111.1%	40.2	-209.2%
Top of Girder	-24.0	-61.8	-61.2%	-30.1	-20.3%
Bottom of Girder	663.4	714.8	-7.2%	676.6	-2.0%

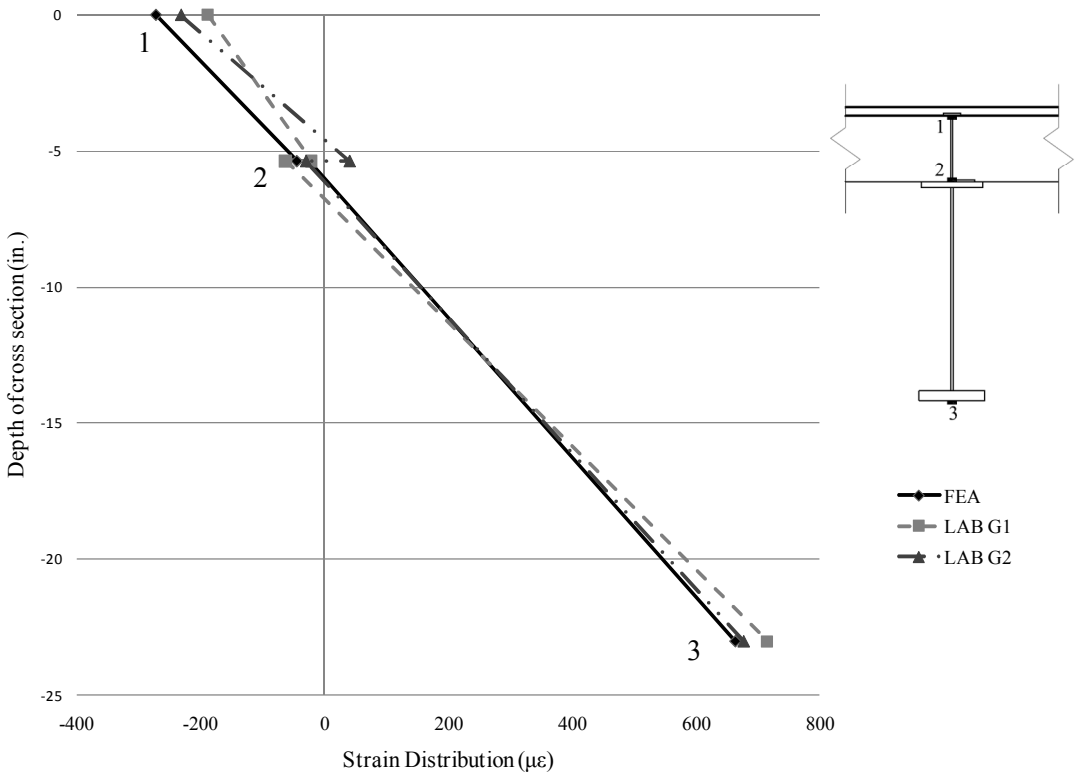

Figure 6.3: Strain throughout cross section depth for Load Case 1

6.2.3 Load Case 2 Validation

The second load case consisted of only two loading areas located at mid-span of the laboratory bridge with a corresponding load of 46.6 kips per patch as shown in Figure 6.4. Again, the deflections were measured at the mid-span while the strains were measured at a 30 in. offset. This gauge pattern was chosen to match the laboratory setup as explained in detail in Section 3.3.4. The same validation approach was used for this load case as previous described. Table 6.3 shows the calculated and measured data and the percent difference of each. It is important to note that the deflections were within 5 percent and the strains measured at the bottom of the girders were within 10 percent of the laboratory test results. The strains throughout the cross section are shown in Figure 6.5.

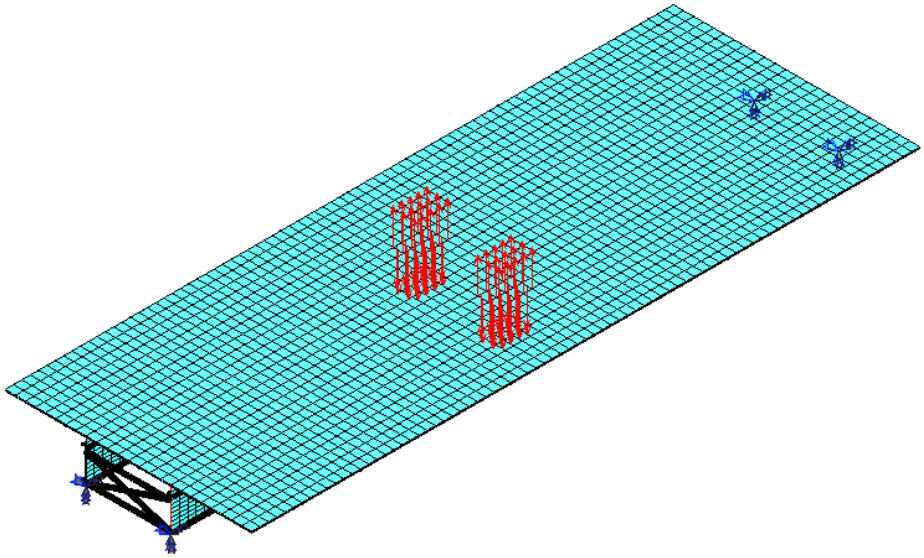

Figure 6.4: ANSYS model of Load Case 2

Table 6.3: Deflection and strains comparison for Load Case 2

Location	FEA	Lab Test (Girder 1)	% Diff.	Lab Test (Girder 2)	% Diff.
Deflections (in.)					
Bottom of Girder	-0.80	-0.85	-5.8%	-0.84	-4.6%
Strains (με)					
Top of Bent "L"	-282.6	-250.9	12.6%	-187.0	51.2%
Bottom of Bent "L"	-52.0	-24.1	115.5%	-6.0	763.2%
Top of Girder	-31.9	-32.7	-2.4%	-43.0	-25.8%
Bottom of Girder	665.4	737.0	-9.7%	669.1	-0.6%

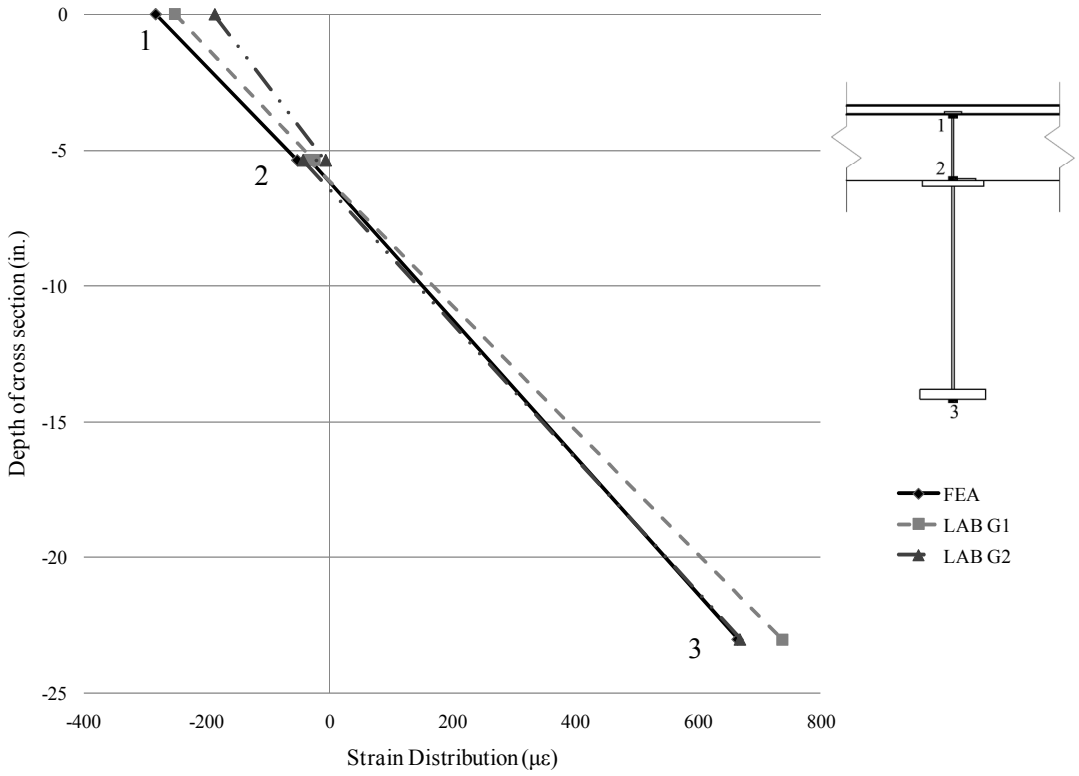

Figure 6.5: Strain throughout cross section depth for Load Case 1

6.2.4 Shenley Bridge Validation

After validation of the laboratory bridge specimen, a model representing the Shenley Bridge was developed. Load Cases 1 and 2, from the previous validation, were limited to loading directly over the girder locations and the affects of eccentric loading were not validated. To ensure that the models were able to accurately represent a truck loading anywhere on the bridge deck, the Shenley Bridge model was loaded with three loading cases that corresponded to previous field testing by Harris (2007). The lateral load distribution factors for the loading cases were then calculated and compared.

During the field test of the Shenley Bridge, instrumentation was setup to investigate lateral load distribution and dynamic load allowance of the in service conditions of the bridge. Strain gauges as well as deflectometers were placed at mid-span of the bridge at the extreme tension face of the girders to measure longitudinal strain and girder deflections, respectively. A series of load cases was used to determine the global effects of a three-axle dump truck driving

over the bridge. For this research only three of the load cases were considered. The load from the truck was applied at "crawl" speeds of approximately 5 mph or less. This allowed a representative static load to be applied to the bridge model. The three-axle dump truck and corresponding loading diagram as well as the three load cases are illustrated in Figures 6.6 and 6.7.

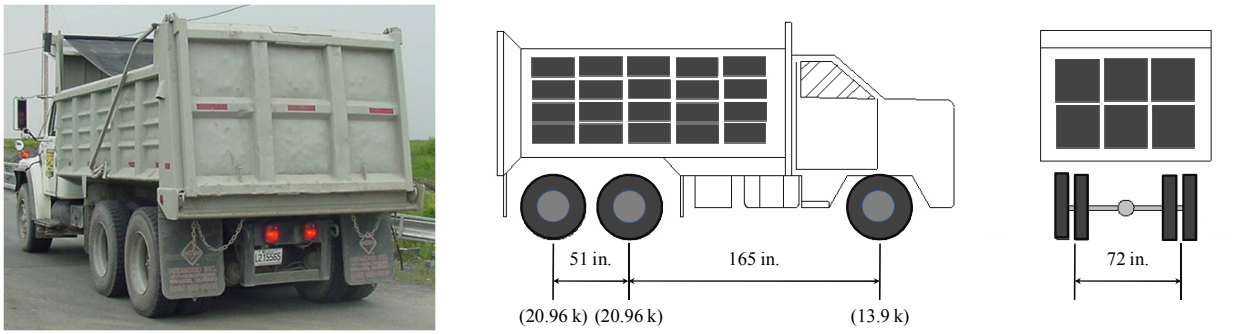

Figure 6.6: Three Axle Dump Truck used for Shenley Bridge Testing (Harris 2007)

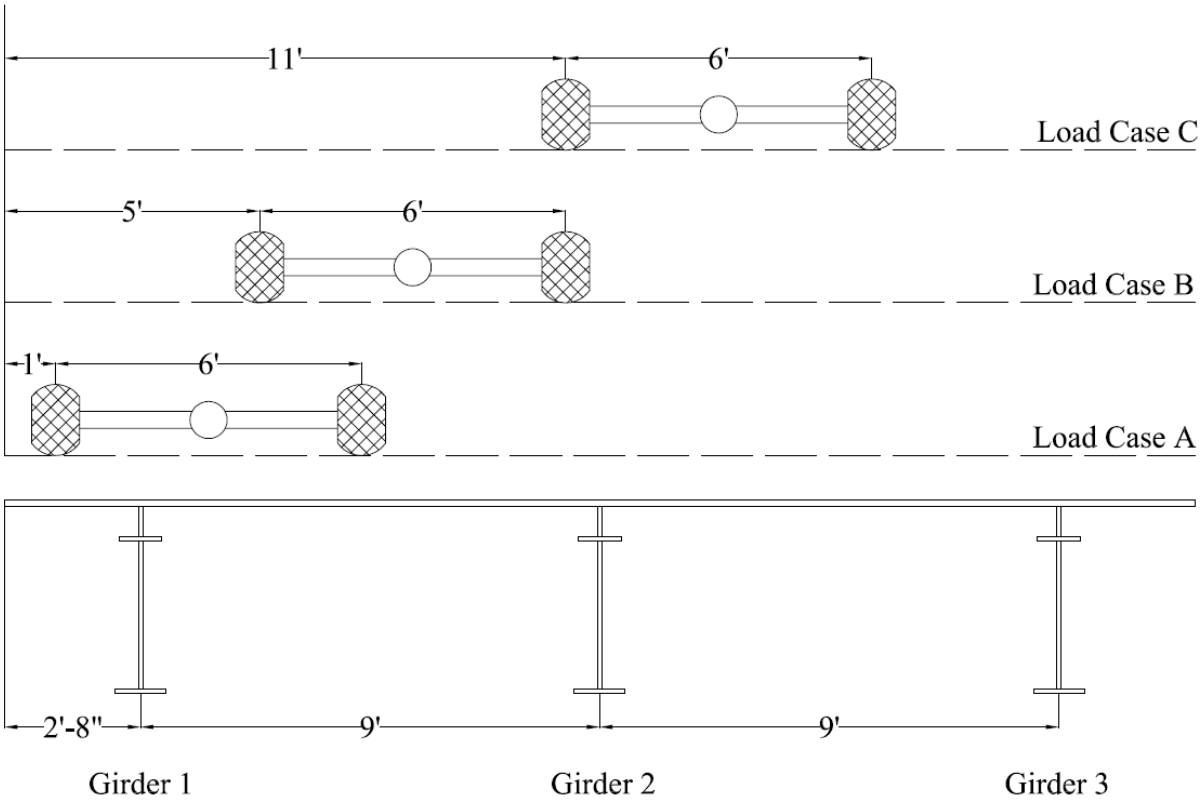

Figure 6.7: Loading Cases used for validation of Shenley Bridge model

Deflection data from previous testing of the Shenley Bridge was used to calculate lateral load distribution factors (LDF). The distribution factors from the Shenley Bridge were then compared to the calculated LDF from the finite element model. For multiple girder bridges the lateral load distribution factors represent a fraction of the force effect for a particular girder. The measurements from the field testing by Harris used in this study were taken at mid-span; therefore, only the LDF for moment were investigated. Several methods of calculating lateral load distribution have been utilized by researches, but the most common consider strains and deflections in the calculations (Eom and Nowak 2001; Stallings and Yoo 1993). The method utilized in this study was a ratio of the maximum displacement/strain response in a particular girder to the summation of the displacement/strain response of all the girders as shown in Equation (6.1). Notice that each distribution factor was also based on the number of trucks present on the bridge. This allowed the lateral load distribution factor to represent the fraction of the load from a single truck supported by a girder in any load configuration.

$$DF_i = \frac{\Delta_{max\,i}}{\sum_{i=1}^{\#girders} \Delta_{max\,i}} N_{trucks} = \frac{\varepsilon_{max\,i}}{\sum_{i=1}^{\#girders} \varepsilon_{max\,i}} N_{trucks} \tag{6.1}$$

Where: DF_i = lateral load distribution for girder "i"
Δ = deflection
ε = strain
N = number of trucks

To validate the lateral load distribution factors for the Shenley Bridge model, a simulated truck load representing the three-axle dump truck shown in Figure 6.6 was applied to the bridge model. The location of the truck that caused the maximum deflection of the girders was found by moving the truck load at 6 in. increments along the length of the bridge. At this location the truck load was placed 1 ft, 5 ft, and 11 ft, from the edge of the bridge specimen as shown in Figure 6.7. Deflection and strain data was then collected from the mid-span nodes at the extreme tension flange of the girders. The deflection and strain data is compared to the field test data in Tables 6.4 and 6.5, respectively. The deflection readings offer similar results with an approximate percent error of 10 percent when the truck is in close proximity to the girders. The high percent differences at some of the load cases may be attributed to the small deflection and strain readings at those locations.

Table 6.4: Displacement validation based on field test data

	Load Case A			Load Case B			Load Case B		
	Field (in.)	FEA (in.)	% Diff	Field (in.)	FEA (in.)	% Diff	Field (in.)	FEA (in.)	% Diff
Girder 1	-0.616	-0.678	10.0%	-0.436	-0.480	10.2%	-0.107	-0.235	119.3%
Girder 2	-0.302	-0.340	12.6%	-0.326	-0.414	27.1%	-0.285	-0.431	51.1%
Girder 3	-0.023	-0.073	215.7%	-0.145	-0.191	31.4%	-0.370	-0.419	13.3%

Table 6.5: Strain validation based on field test data

	Load Case A			Load Case B			Load Case B		
	Field (με)	FEA (με)	% Diff	Field (με)	FEA (με)	% Diff	Field (με)	FEA (με)	%Diff
Girder 1	243	275.6	13.4%	157	186.4	18.7%	44.0	87.629	99.2%
Girder 2	97	133.4	37.5%	115	188.8	64.2%	122.0	201.007	64.8%
Girder 3	-11	42.0	-481.4%	32	73.5	129.6%	127.0	159.725	25.8%

The lateral load distribution factors (LDF) were calculated for the three girders using both deflections and strains. The load distribution factors based on displacement and strain data are shown in Tables 6.6 and 6.7 respectively. The model closely represented the lateral load distribution factors for the girders in close proximity to the loading configuration. It also appears that displacements offer a better representation of the actual bridge response and result in overall lower percent differences.

Load Case A of Figure 6.7 was consider, as it was intended to produce the worst case loading scenario for the exterior girder and ultimately the largest lateral load distribution factor. As the truck was moved away from the exterior girder an increase of load sharing occurred between the girders and the load distribution factors decreased. The percent differences in the deflection results for Girder 1 and 2 were both less than 10 percent and are considered reasonable. The percent difference in deflection for Girder 3 in Load Case A is considerably higher however, and is most likely due to the small deflections and strains measured at that location. Based on the comparison of the Shenley Bridge field testing and the developed model, the finite element model appears to accurately model global behavior of the SPS system with any loading configuration, and is most accurate when measurements are taken in close proximity to the loading points.

Table 6.6: LDF validation based on displacements

	Load Case A			Load Case B			Load Case B		
	Field	FEA	% Diff.	Field	FEA	% Diff.	Field	FEA	% Diff.
Girder 1	0.654	0.622	-5.0%	0.479	0.443	-7.6%	0.146	0.216	48.2%
Girder 2	0.321	0.312	-2.8%	0.359	0.382	6.4%	0.372	0.397	6.7%
Girder 3	0.024	0.067	177.4%	0.162	0.176	8.4%	0.482	0.387	-19.8%

Table 6.7: LDF validation based on strains

	Load Case A			Load Case B			Load Case B		
	Field	FEA	% Diff.	Field	FEA	% Diff.	Field	FEA	% Diff.
Girder 1	0.654	0.611	-6.5%	0.479	0.415	-13.3%	0.146	0.195	33.9%
Girder 2	0.321	0.296	-7.9%	0.359	0.421	17.2%	0.372	0.448	20.5%
Girder 3	0.024	0.093	287.7%	0.162	0.164	1.1%	0.482	0.356	-26.1%

6.3 Global Response of Connections

After careful validation of the laboratory and Shenley bridge specimens the global behavior of the Shenley and Martin Branch bridges was investigated. Two models of each bridge configuration, the bent "L" connection and the welded flange connection, were developed and compared.

The Martin Branch Bridge was models were developed similarly to the previous models of the laboratory and Shenley bridges. A complete description of the Martin Branch Bridge can be found in Section 2.2.2, but a condensed review is presented for reference.

The entire bridge has of three 50 ft simply supported spans of SPS sections for a total length of 150 ft. A typical span consists of six longitudinal girders (W27x114) welded to the underside of SPS panels utilizing 5/16 in. steel faceplates separated by a 1 in. elastomer core. Each girder is transversely connected at each end and at mid-span by C15x50 and C15x33.9 sections, respectively.

The same procedure for calculating lateral load distribution factors that was used for validation of the models was utilized. The location resulting in the largest deflection due to a three-axle dump truck moving along the length of the bridges was found. At the location of maximum deflection, the truck was placed at 12 in. intervals along the transverse width of the bridge to simulate all possible loading configurations in the transverse direction. The finite

element models and the corresponding loading configurations for the Shenley and Martin Branch bridges are illustrated in Figures 6.8 and 6.9, respectively. The arrows represent the middle of each tire patch from the three-axle dump truck. Deflection and strain data was then collected from the mid-span nodes at the extreme tension flange of the girders, and Equation (6.1) was used to calculate load distribution factors for all loading configurations. The deflection and strain data as well as the calculated lateral load distribution factors for each 12 in. interval for each model are presented in Appendix C.

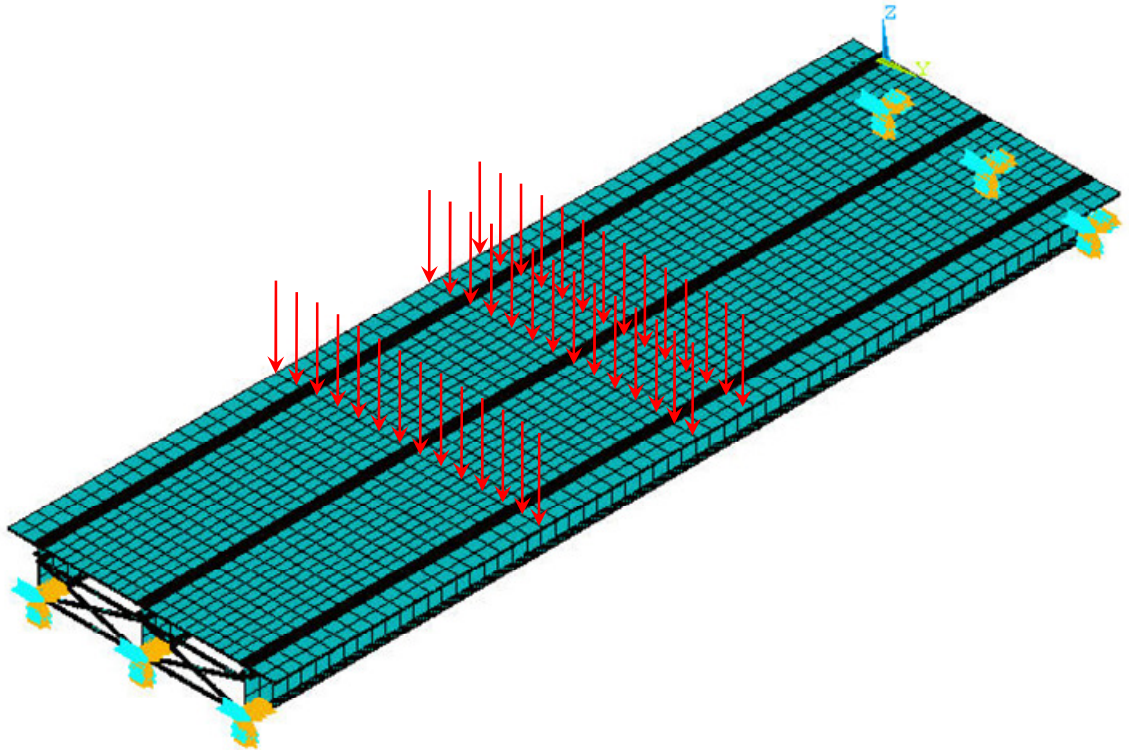

Figure 6.8: Finite element model of Shenley Bridge

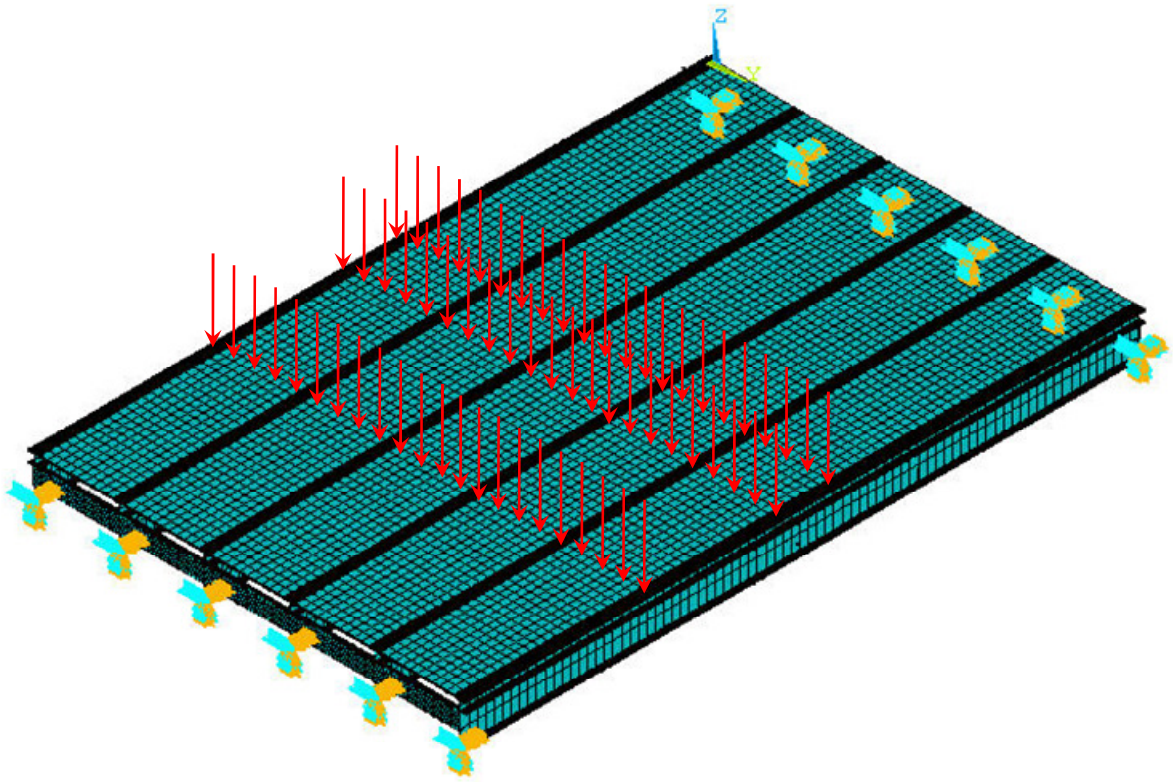

Figure 6.9: Finite element model of Martin Branch Bridge

6.3.1 Shenley Bridge Load Distribution Factors (LDF)

Two models of the Shenley Bridge were developed to represent both connection types. For comparison purposes, the same Load Cases A, B, and C of Figure 6.7used for the validation of the models, were used to compare the influence of the different connections. Table 6.8 compares the distribution factors calculated based on displacements, while Table 6.9 is based on strains. Notice that there was no significant change in the load distribution factors for any of the cases for the Shenley Bridge model with the bent "L" as compared to the model with the flange connection. There is slight change in the deflection results at Girder 3 for Load Case A, but this is most likely due to the small displacements measured at this location, and there is relatively no difference between the LDF when calculated based on strains.

Table 6.8: Shenley Bridge LDF based on displacements

	Load Case A			Load Case B			Load Case B		
	Bent "L" (in.)	Flange (in.)	% Diff.	Bent "L" (in.)	Flange (in.)	% Diff.	Bent "L" (in.)	Flange (in.)	% Diff.
Girder 1	0.622	0.607	-2.4%	0.443	0.442	-0.2%	0.216	0.227	4.8%
Girder 2	0.312	0.317	1.5%	0.382	0.371	-2.7%	0.397	0.384	-3.3%
Girder 3	0.067	0.077	15.1%	0.176	0.187	6.3%	0.387	0.389	0.7%

Table 6.9: Shenley Bridge LDF based on strains

	Load Case A			Load Case B			Load Case B		
	Bent "L" (με)	Flange (με)	% Diff.	Bent "L" (με)	Flange (με)	% Diff.	Bent "L" (με)	Flange (με)	% Diff.
Girder 1	0.611	0.601	-1.7%	0.415	0.418	0.7%	0.195	0.205	5.0%
Girder 2	0.296	0.301	1.9%	0.421	0.408	-3.0%	0.448	0.433	-3.5%
Girder 3	0.093	0.098	5.0%	0.164	0.173	5.9%	0.356	0.362	1.6%

6.3.2 Martin Branch Bridge Load Distribution Factors (LDF)

For consistency, Load Cases A, B and C of Figure 6.7 were used for comparison purposes of the Martin Branch Bridge as well. All relative data and calculations are presented in Appendix C. The lateral load distribution factors for the load cases are presented based on displacements and strains in Table 6.10 and 6.11, respectively. Again, there is no significant change in the distribution factor for the types of connections, suggesting that the change in flexural stiffness caused by the connections do not have a significant influence on the global behavior of the SPS bridge systems.

Table 6.10: Martin Bridge LDF based on displacements

	Load Case A			Load Case B			Load Case B		
	Bent "L"	Flange	% Diff.	Bent "L"	Flange	% Diff.	Bent "L"	Flange	% Diff.
Girder 1	0.386	0.374	-3.1%	0.254	0.249	-2.0%	0.130	0.128	-1.4%
Girder 2	0.300	0.287	-4.5%	0.286	0.273	-4.5%	0.191	0.193	0.9%
Girder 3	0.170	0.172	1.0%	0.227	0.223	-1.4%	0.256	0.248	-2.9%
Girder 4	0.092	0.097	5.3%	0.128	0.136	6.8%	0.214	0.214	0.1%
Girder 5	0.046	0.053	14.8%	0.074	0.080	9.2%	0.128	0.136	6.2%
Girder 6	0.005	0.017	233.0%	0.033	0.038	17.2%	0.081	0.080	-0.6%

Table 6.11: Martin Bridge LDF based on strains

	Load Case A			Load Case B			Load Case B		
	Bent "L"	Flange	% Diff.	Bent "L"	Flange	% Diff.	Bent "L"	Flange	% Diff.
Girder 1	0.374	0.370	-0.9%	0.264	0.262	-1.0%	0.131	0.125	-4.6%
Girder 2	0.266	0.255	-4.0%	0.245	0.235	-4.0%	0.203	0.207	1.9%
Girder 3	0.188	0.187	-0.5%	0.219	0.218	-0.6%	0.226	0.223	-1.4%
Girder 4	0.100	0.102	2.0%	0.153	0.162	5.5%	0.213	0.216	1.7%
Girder 5	0.053	0.056	6.0%	0.081	0.085	5.7%	0.152	0.160	5.5%
Girder 6	0.020	0.030	49.7%	0.038	0.039	2.0%	0.075	0.069	-8.7%

6.4 Summary

Two different types of deck-to-girder connections were investigated to determine if the type of connection influenced the global behavior of SPS bridge systems. The bent “L” connection provides little support at the connection location and acts similar to a pinned connection, while the flange connection provides a significant increase in surface area contact with the bridge deck and increases the stiffness of the bridge deck. After several validations of different models from laboratory and field tests, four models were developed for comparison. The Shenley and Martin Branch bridges were both modeled with the bent “L” and the flange connection. The lateral load distribution factors determined from each connection type was compared. Initial findings from the study suggest that the different connection types, do not affect the load distributing behavior of SPS bridges.

Chapter 7: Conclusions and Recommendations

7.1 Conclusions

An innovative bridge construction technique using the Sandwich Plate System has been investigated to assess the performance and behavior of the SPS technology in bridge applications. The focus of the research was provided by two bridges utilizing SPS decking. The Shenley Bridge and the proposed Martin Branch Bridge utilized different connection techniques to achieve composite action between the deck-to-girder interfaces. The Shenley Bridge utilizes a bent "L" plate that was welded to the bridge deck and subsequently bolted to the supporting girders as the deck-to-girder connection, while the proposed Martin Branch Bridge's supporting girder are connected directly to the deck through continuous welding of the flanges to the underside of the deck, eliminating the need for the bent "L" plate and bolted connections. This research investigated the performance of the bent "L" connection and determined the effect of the different connections on the behavior of the bridge system.

7.1.1 Laboratory Testing Conclusion

A one-half scale SPS bridge utilizing the bent "L" connection was tested to determine the fatigue resistance of connections, especially the welded joint and the slip-critical connections. A testing program was developed for the study, consisting of cyclically loading the bridge with a simulated fatigue truck load to determine the fatigue performance of the connection between the deck and the supporting girders.

Two loading configurations were required to test the fatigue performance of the connections. Each load corresponded to the AASHTO-LRFD maximum fatigue moment for the one-half scale bridge of 466 kip-ft as determined by a ratio of the maximum moments from the AAHSTO- LRFD HL-93 fatigue and strength trucks on a full scale 80 ft bridge. Load Case 1 simulated a fatigue truck by using a spreader beam to distribute the 51.8 kip load to the supporting girders. This configuration caused weld failures to occur at approximately 30,000 cycles. The failures occurred directly under the loading patches and were most likely due to high transverse stresses due to load eccentricities. The second loading setup, Load Case 2, was developed to relive the strains at the cracked welds and distributed the 46.6 kip load at mid-span of the one-half scale bridge. Fatigue cracks were observed at 743,000 cycles at the intersection of

the panel-to-panel connection and the bent “L” connection. The cracks initiated at the intersection of the three fillet welds, and it appears that this type of weld detailing significantly decreased the fatigue resistance of the system and subsequently was the limiting state of the fatigue test.

No slip in the slip critical connection was measured during the testing program to 743,000 cycles. The fatigue resistance of the bridge specimen was not limited by the slip-critical connection, but rather by the unanticipated weld failures.

7.1.2 Local Behavior

High localized stresses at the weld toe location due to possible eccentricities in the loading configuration of Load Case 1 may have caused weld failure during the laboratory testing. An investigation using finite element analysis allowed a comparison of two deck-to-girder connections to determine the effect on the stresses at the weld location. Two models of a SPS bridge deck panel were developed; one utilizing the bent “L” connection, and the other utilizing the welded flange connection to investigation the influence of the connections on deck deflections and transverse stresses at the weld locations.

The change in deformations between the two connections was minimal, but the welded flange connection appeared to provide a more rigid end condition, limiting the rotation of the connection and increasing the stiffness, when compared to the bent “L” connection. The comparison of stresses at the location of the weld toe between the two connection types showed a significant decrease in stresses due to the flange connection. The welded flange connection resulted in an average of 38 percent decrease in stresses at the weld toe location. This comparison suggests that the welded flange connection would increase the fatigue life of the structure based on lower stresses due to eccentric loading at the fillet weld locations.

7.1.3 Global Behavior

The use of the different connections in the Shenley and proposed Martin Branch bridges was studied to determine if a change in the connection type at the supporting girders influenced the global behavior of the bridges. The bent “L” connection has a small contact area with the SPS, while the flange connection increases the contact area and ultimately the stiffness off the deck. The change in flexural stiffness of SPS decks based on different end conditions caused by the connection type was investigated by comparing the load sharing behavior of the different

bridge systems. Loading combinations of a simulated three-axle dump truck were placed on the bridge in the longitudinal direction at 12 in. intervals. The location resulting in maximum deflection was found and at this location the truck was placed at 6 in. interval across the transverse width of the bridge. The strains and deflections at mid-span of the bridge were recorded and used to compute transverse lateral load distribution factors. A comparison of the load distribution factors of each bridge utilizing the different deck-to-girder connections found that the type of connection type used in SPS bridge decks does not significantly influence the global behavior of the bridge.

7.2 Summary

The performance and behavior of two types of SPS deck-to-girder connections, a bent "L" plate that is welded to the deck and subsequently bolted to the supporting girder utilizing slip-critical connections and a flange that is welded directly to the SPS deck, was considered. An evaluation of the laboratory testing along with a comparative study from finite element analysis allowed for the following conclusions to be drawn.

- The slip-critical connections used to connect the bent "L" to the supporting girders did not slip after approximately 730,000 cycles, but weld failures occurred due to tri-axial stresses at a three point intersection of fillet welds.
    - Special attention should be given to transverse loading on the weld locations. The inclusion of transverse loading on fillet weld reduces the fatigue category of the welded connection and ultimately the bridge system.
- Small eccentricities due to the loading setup caused high transverse stresses at the weld connecting the bent "L" to the SPS deck, resulting in fatigue failure of the weld.
    - The fillet weld connecting the bent "L" plate to the SPS deck was shown to be a category "E" based on the AASHTO-LRFD fatigue categories.
    - Careful detailing of the welded deck-to-girder connection should be considered. Three point intersections of fillet welds should be avoided, as they may reduce the fatigue life of the bridge system.
- The connection type has a significant influence on the transverse stresses at the weld toe location.

- The welded flange connection significantly reduced the stresses at the weld location and may provide a prolong fatigue life for the structure.

- The connection type does not significantly influence the load sharing capabilities of a SPS bridge system.

7.3 Recommendations for future research

The innovative technology of the Sandwich Plate System appears to offers a viable alternative to traditional slab-girder bridges. Based on the investigation of the deck-to girder connections used in two SPS bridge decks, the following observations and recommendations are suggested.

- The use of alternate shear connections other than conventional connections that do not use concrete as a component of the composite action was investigated. High local stresses at the weld toe located at the bottom plate of the SPS deck were studied. The flexibility of SPS bridge decks compared to other types of bridge deck system may also have an influence on the fillet weld used to connect the web of a plate girder to the flange. Additional studies should compare the use of built up members, especially the fillet weld connecting the top flange to the web, in SPS applications as compared to other types of bridge decks.

- Finite element analysis results from the global modeling of the SPS bridges suggest that the connection detail does not influence the load sharing capabilities of the system. Additional field testing of the proposed Martin Brach Bridge will allow validation of the finite element models and provide addition insight into the global behavior of a SPS bridge that utilizes the welded flange connection as the deck-to-girder connection.

References

American Association of State Highway and Transportation Officials (AASHTO). (2002). *Standard specifications for highway bridges 17th Edition*, American Association of State Highway and Transportation Officials, Washington, D.C.

American Association of State Highway and Transportation Officials (AASHTO). (2007). *AASHTO LRFD bridge design specifications*, American Association of State Highway and Transportation Officials, Washington, D.C.

Bakht, B., and Jaeger, L. G. (1988). "Bearing Restraint in Slab-on-Girder Bridges." *Journal of Structural Engineering*, 114(12), 2724-2740.

Barker, R. M., and Puckett, J. A. (2007). *Design of highway bridges : An LRFD Approach*, John Wiley and Sons, Inc., Washington, D.C.

Brockenbrough, R. L. (1986). "Distribution factors for curved I-girder bridges." *Journal of Structural Engineering*, 112(10), 2200-2215.

Campbell Scientific. (2007). "CR9000 Measurement and Control System." http://www.campbellsci.com/cr9000, Acessed: June 7,2006.

Celesco Transducer Products. (2007). "Cable-Extention Position Transducer." http://www.celesco.com/_datasheets/pt101.pdf, Acessed June 18, 2007.

Chen, Y. (1995). "Refined and simplified methods of lateral load distribution for bridges with unequally spaced girders: I. Theory." *Computers & Structures*, 55(1), 1-15.

Chung, W., and Sotelino, E. D. (2006). "Three-dimensional finite element modeling of composite girder bridges." *Engineering Structures*, 28(1), 63-71.

Cook, R. D., Malkus, D. S., Plesha, M. E., and Witt, R. J. (2001). *Concepts and applications of finite element analysis*, Wiley, New York, NY.

Cousins, T., and Stallings, J. (1998). "Laboratory Test of Bolted Diaphragm-Girder Connections." *Journal of Bridge Engineering*, 3(2), 56-63.

Eom, J., and Nowak, A. S. (2001). "Live load distribution for steel girder bridges " *Journal of Bridge Engineering*, 6(6), 489-497.

Federal Highway Administration (FHwA). (2006). *2006 Status of the Nation's Highways, Bridges, and Transit: Conditions and Performance*, FHwA, Washington D.C.

Grigg, W. R. (2006). "Post-Injection Welded Joint Fatigue Tests of Sandwich Plate System Panels," M.S. Thesis, Virginia Polytechnic Institute and State University, Blacksburg, VA.

Harris, D. K. (2007). "Lateral Load Distribution and Deck Design Recommendations for the Sandwich Plate System (SPS) in Bridge Applications," Virginia Polytechnic Institute and State University, Blacksburg.

Hays, C. O., Sessions, L. M., and Berry, A. J. (1986). "Further studies on lateral load distribution using FEA." *Transportation Research Record* (1072), 6-14.

Higgins, C., and Mitchell, H. (2001). "Behavior of Composite Brdige Decks with Alternative Shear Connectors." *Journal of Bridge Engineering*, 6(1), 17-22.

Holt, J. (2007). "Re: Virginia Tech Research on Texas SPS Bridge." Email interview to the author, 6 Dec. 2007.

Imbsen, R. A., and Nutt, R. V. "Load distribution study on highway bridges using STRUDL FEA." *Conference on Computing in Civil Engineering*, Atlanta, GA.

Intelligent Engineering (IE). (2007). "SPS: The Sandwich Plate System - Civil Engineering." http://www.ie-sps.com/civil_engineering.html Accessed: October 31, 2007.

Kennedy, D. J. L., Dorton, R. A., and Alexander, S. B. D. (2002). "The Sandwich Plate System for bridge decks." 2002 International Bridge Conference, Pittsburgh, PA.

Kennedy, D. J. L., Ferro, A., Dorton, R. A., Vincent, R. B., Cousins, T., and Murray, T. M. (2005). "Accelerated Construction of Bridges with Decks of Prefabricated Sandwich Plate System Panels Acting Compositely with the Girders." Accelerated Bridge Construction 2005, Federal Highway Administration, San Diego, CA.

Kim, S., and Nowak, A. S. (1997). "Load distribution and impact factors for I-girder bridges." *Journal of Bridge Engineering*, 2(3), 97-104.

Kulak, G. L., Fisher, J. W., and Struik, J. H. (1987). *Guide to design criteria for bolted and riveted joints*, 2nd Ed., Wiley, New York.

Lachemi, M., Hossain, K., Ramcharitar, M., and Shehata, M. (2007). "Bridge Deck Rehabilitation Practices in North America." *Journal of Infrastructure Systems*, 13(3), 225-234.

Mabsout, M. E., Tarhini, K. M., Frederick, G. R., and Kesserwan, A. (1998). "Effect of continuity on wheel load distribution in steel girder bridges." *Journal of Bridge Engineering*, 3(3), 103-110.

Martin, D. (2005). "Sandwich Plate System Bridge Deck Tests," M.S. Thesis, Virginia Polytechnic Institute and State University, Blacksburg.

Moses, J. P., Harries, K. A., Earls, C. J., and Yulismana, W. (2006). "Evaluation of effective width and distribution factors for GFRP bridge decks supported on steel girders." *Journal of Bridge Engineering*, 11(4), 401-409.

Schulz, J. L., Commander, B., Goble, G. G., and Frangopol, D. M. (1995). "Efficient Field Testing and Load Rating of Short-Span and Medium-Span Bridges." *Structural Engineering Review*, 7(3), 181-194.

Shahawy, M., and Huang, D. (2001). "Analytical and field investigation of lateral load distribution in concrete slab-on-girder bridges." *ACI Structural Journal*, 98(4), 590-599.

Stallings, J. M., and Yoo, C. H. (1993). "Tests and Ratings of Short-Span Steel Bridges." *Journal of Structural Engineering*, 119(7), 2150-2168.

Tarhini, K. M., and Frederick, G. R. (1992). "Wheel load distribution in I-girder highway bridges." *Journal of Structural Engineering*, 118, 1285-1294.

Tonias, D. E., and Zhao, J. J. (2007). *Bridge Engineering*, Mc Graw Hill, New York.

Trans-Tek. (2007). "Series 350." http://www.transtekinc.com/Catalog%20PDFs%2004C/Gagings/Ser350_04c.pdf, Accessed: June 18, 2007.

Vanderzee, P. (2005). "A Bridge too Near." *Bridges*, 8(1), 18-21.

Vincent, R., Boilard, A., and Pilon, N. (2005). "Then Shenley Bridge." *Bridges*, 8(1), 22-24.

Vincent, R., and Ferro, A. "A New Orthotropic Bridge Deck: Design, Fabrication and Construction of the Shenley Bridge Incorporating an SPS Orthotropic Bridge Deck." *Proceedings of the Annual Transportation Association of Canada*, Quebec City, Quebec.

Xiao, Z., and Yamada, K. (2005). "Fatigue Strength of Intersection Attachments." *Journal of Structural Engineering*, 131(6), 924-932.

Yousif, Z., and Hindi, R. (2007). "AASHTO-LRFD Live Load Distribution for Beam-and-Slab Bridges: Limitations and Applicability." *Journal of Bridge Engineering*, 12(06), 765-773.

Zhou, Y. (2004). "Fatigue Problems in Steel Bridge Structures." Structures Congress, Nashville, Tennessee.

Zokaie, T. (2000). "AASHTO-LRFD live load distribution specifications." *Journal of Bridge Engineering*, 5(2), 131-138.

Appendix A: Additional Laboratory Supporting Calculations

A.1 Load Calculation Example

Determination of Load due to yield stress in bottom flange

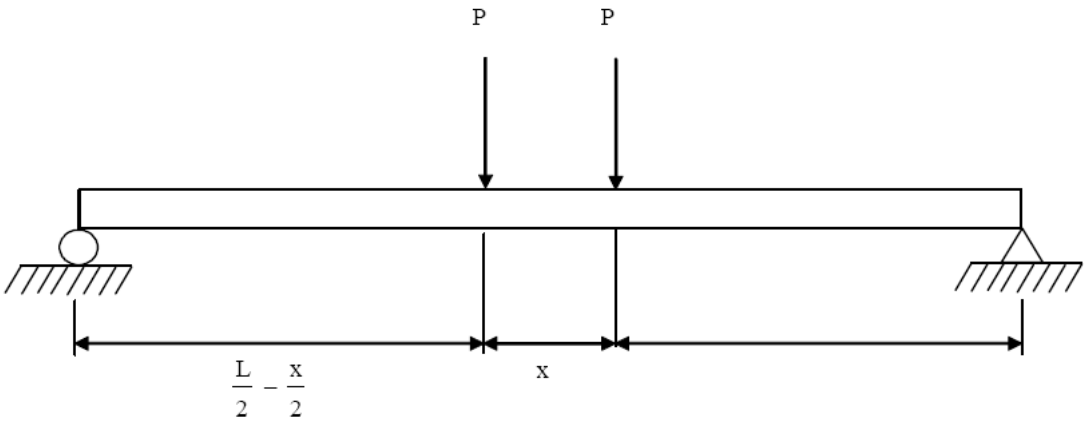

Defining Moment $M = Fy \cdot Sb$

Substituting for M $P \cdot \left(\frac{L}{2} - \frac{x}{2}\right) = Fy \cdot Sb$

Solving for P $P = -2 \cdot Fy \cdot \frac{Sb}{(-L + x)}$

SPS half-scale composite section properties

$I := 5097.4in^4$	Moment of Inertia	
$yb := 19.94in$	Centroid from bottom	
$Sb := 255.67in^3$	Section modulus	
$As := 33.7in^2$	Area of steel	
$\gamma s := 490pcf$	Weight of Steel	
$w := As \cdot \gamma s$	Dead load of bridge	$w = 0.115\,klf$
$L := 40ft$	Length of bridge	
$Fy := 50ksi$	Yield strength	
$x := 4ft$	Spacing of load	

Determining Max Moment for fatigue due to HL-93 fatigue truck on a full scale 80' bridge

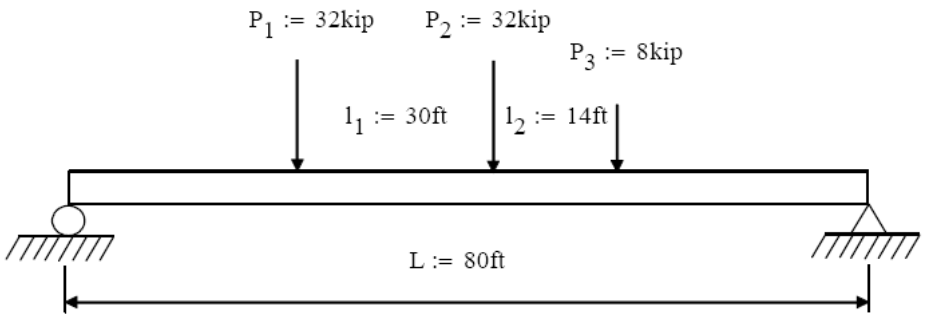

$P_1 := P_1 \qquad P_2 := P_2 \qquad P_3 := P_3 \qquad P_t := P_1 + P_2 + P_3$

Finding centroid of Loads

$$y := \frac{P_1 \cdot (0 \cdot ft) + P_2 \cdot (l_1) + P_3 \cdot (l_1 + l_2)}{P_t} \qquad y = 18.222\,ft$$

Distance from centroid to nearest load case

$$L_2 := l_1 - y \qquad L_2 = 11.778\,ft$$

Solving for distance from left support to max moment

$$X := \frac{L}{2} - \frac{L_2}{2} \qquad X = 34.111\,ft$$

Solving for shear

$$V_L := (P_t) - \frac{(P_t) \cdot X}{L}$$

Solving for max moment without load factors

$$M_{max} := V_L \cdot (X + L_2 - l_1) + (V_L - P_1) \cdot (l_1) \qquad M_{max} = 935.2\,kip \cdot ft$$

Load factors

Dynamic Load Allowance, IM (AASHTO Table 3.6.2.1-1)	IM := 1.15
Load Combinations and Load Factors (AASHTO Table 3.431-1)	LL := 0.75
Fatigue Resistance (AASHTO 6.6.1.2.5)	R := 2

Solving for maximum moment due to fatigue truck

$$M_{fatigue} := M_{max} \cdot IM \cdot LL \cdot R \qquad M_{fatigue} = 1613\,kip \cdot ft$$

Determining Max Moment for strength due to HL-93 truck on a full scale 80' bridge

$P_1 := 32kip$ $P_2 := 32kip$ $P_3 := 8kip$

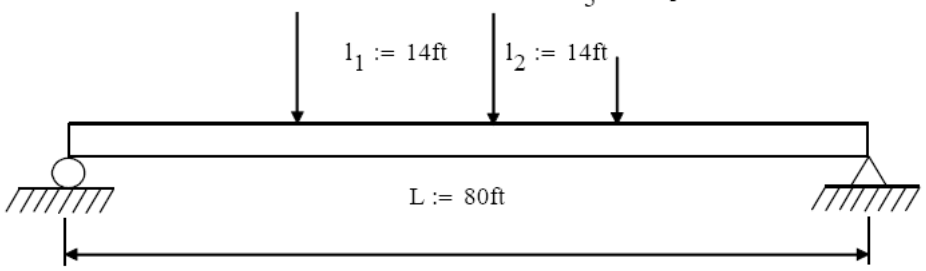

$P_1 := P_1$ $P_2 := P_2$ $P_3 := P_3$ $P_t := P_1 + P_2 + P_3$

Finding centroid of loads

$$y := \frac{P_1 \cdot (0 \cdot ft) + P_2 \cdot (l_1) + P_3 \cdot (l_1 + l_2)}{P_t} \qquad y = 9.333\,ft$$

Distance from centroid to nearest load case

$$L_2 := l_1 - y \qquad L_2 = 4.667\,ft$$

Solving for distance from left support to max moment

$$X := \frac{L}{2} - \frac{L_2}{2} \qquad X = 37.67\,ft$$

Solving for shear

$$V_L := (P_t) - \frac{(P_t) \cdot X}{L}$$

Solving for max moment

$$M_{max} := V_L \cdot (X + L_2 - l_1) + (V_L - P_1) \cdot (l_1) \qquad M_{max} = 1164.9\,kip \cdot ft$$

Lane Loading (AASHTO 3.6.1.2.4) $w := 0.64klf$

Moment Due to Lane Load

$$M_{lane} := \frac{w \cdot L \cdot X}{2} - \frac{w \cdot X^2}{2} \qquad M_{lane} = 510\,kip \cdot ft$$

Dynamic Load Allowance, IM (AASHTO Table 3.6.2.1-1) $IM := 1.33$

Load Combinations and Load Factors (AASHTO Table 3.431-1) $LL := 1.75$

Solving for maximum moment due to strength truck

$$M_{strength} := M_{max} \cdot IM \cdot LL + M_{lane} \cdot LL \qquad M_{strength} = 3604\,kip \cdot ft$$

Determining point load that causes yielding due to bending

$$P := -2 \cdot Fy \cdot \frac{Sb}{(-L + x)} \qquad P = 59.2\,kip$$

Determining Max Moment due to dead load

$$M_{dead} := \frac{w \cdot L^2}{4} - \frac{w \cdot \left(\frac{L}{2}\right)^2}{2} \qquad M_{dead} = 22.935\,kip \cdot ft$$

Finding stress due to dead load

$$F_{dead} := \frac{M_{dead}}{Sb} \qquad F_{dead} = 1.076\,ksi$$

Finding the stress at fatigue

$$\frac{M_{fatigue}}{M_{strength}} = 0.448 \quad \text{Ratio of Max moments}$$

$$F_{fatigue} := \left(Fy - F_{dead}\right) \cdot \left(\frac{M_{fatigue}}{M_{strength}}\right) \qquad F_{fatigue} = 21.9\,ksi$$

Max moment due to fatigue stress

$$M_{test} := F_{fatigue} \cdot Sb \qquad M_{test} = 466.552\,kip \cdot ft$$

Reaction to create max moment due to fatigue stress on half-scale bridge

$$P := 2 \cdot \left[-2 \cdot F_{fatigue} \cdot \frac{Sb}{(-L + x)}\right]$$

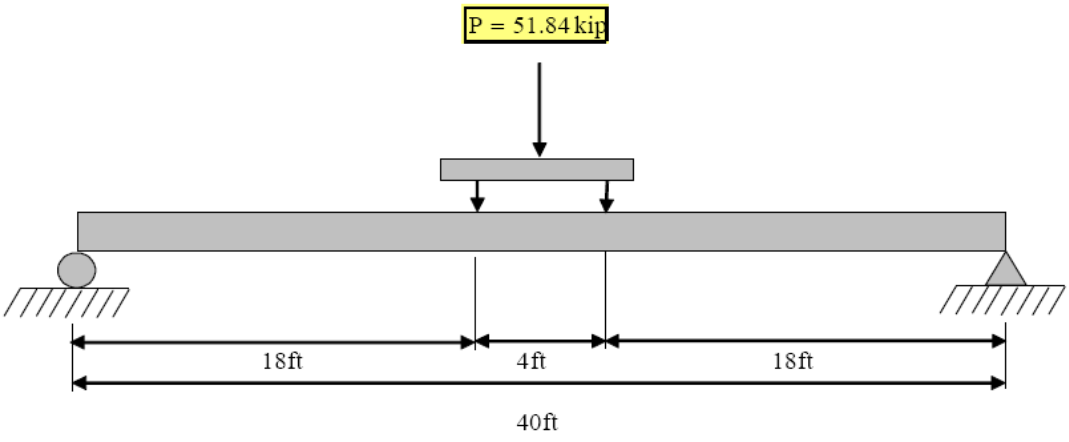

Appendix B: Additional Local Behavior Results

B.1 Displacement contour plots from finite element panels

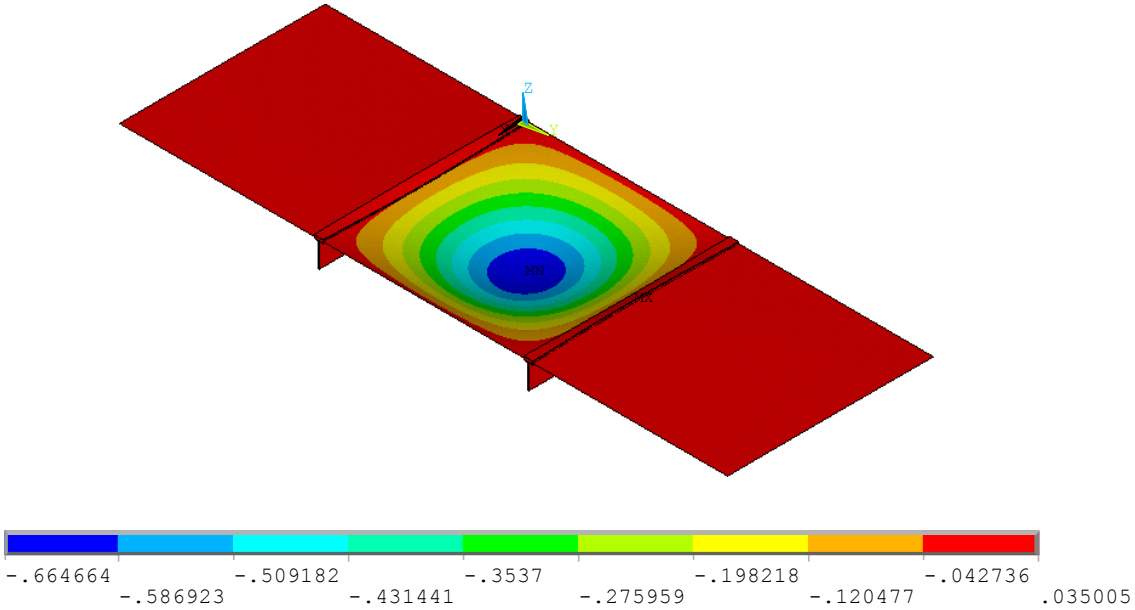

Figure B.1: Contour plot of deck displacement for bent "L" panel

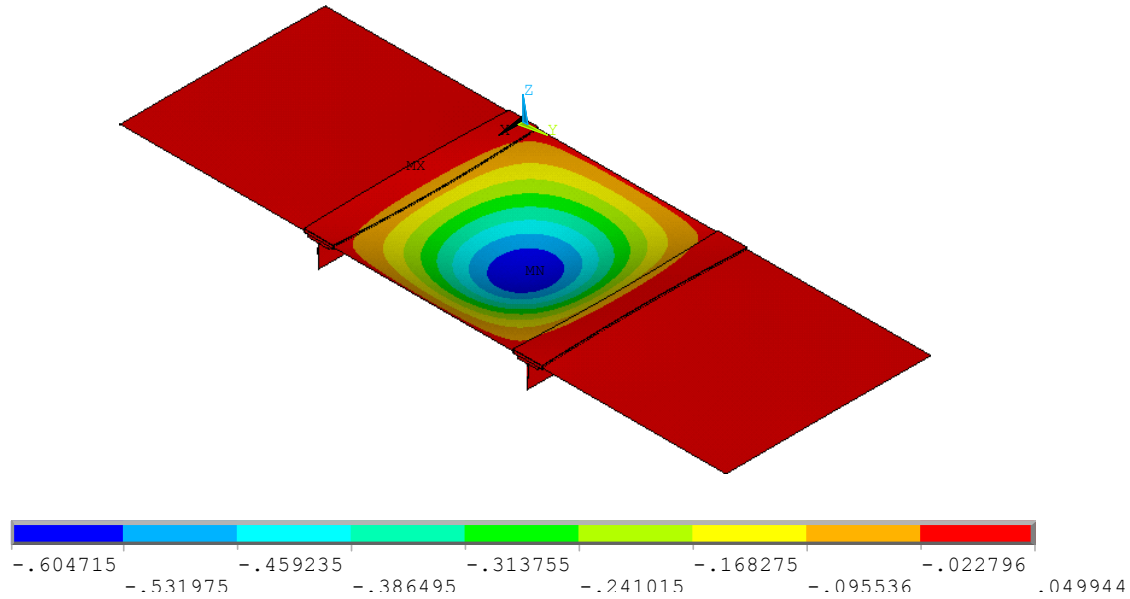

Figure B.2: Contour plot of deck displacement for welded flange panel

B.2 Average finite element transverse stresses at weld toe

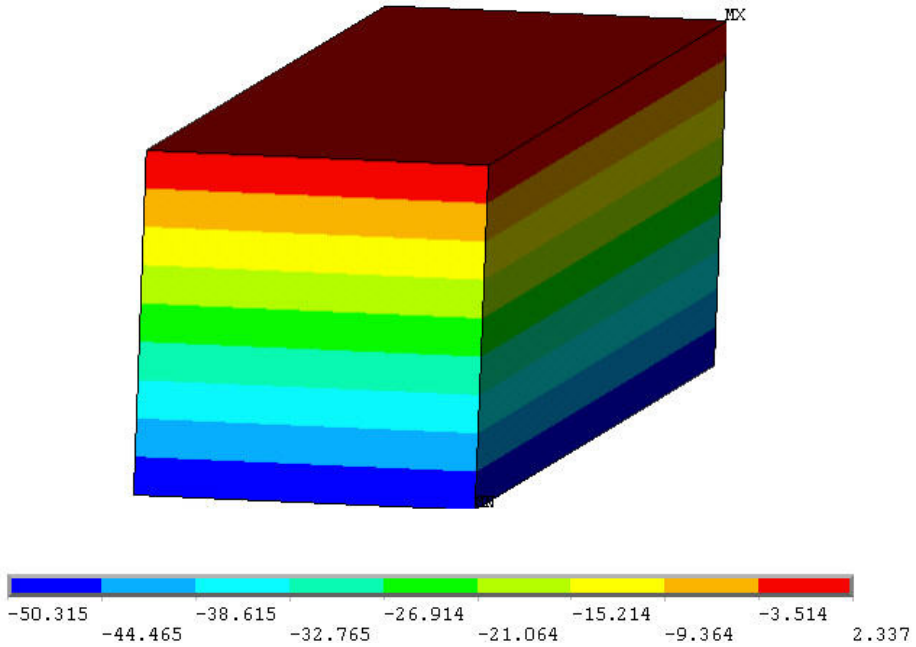

Figure B.3: Average transverse stress at 30 in. for bent "L" connection

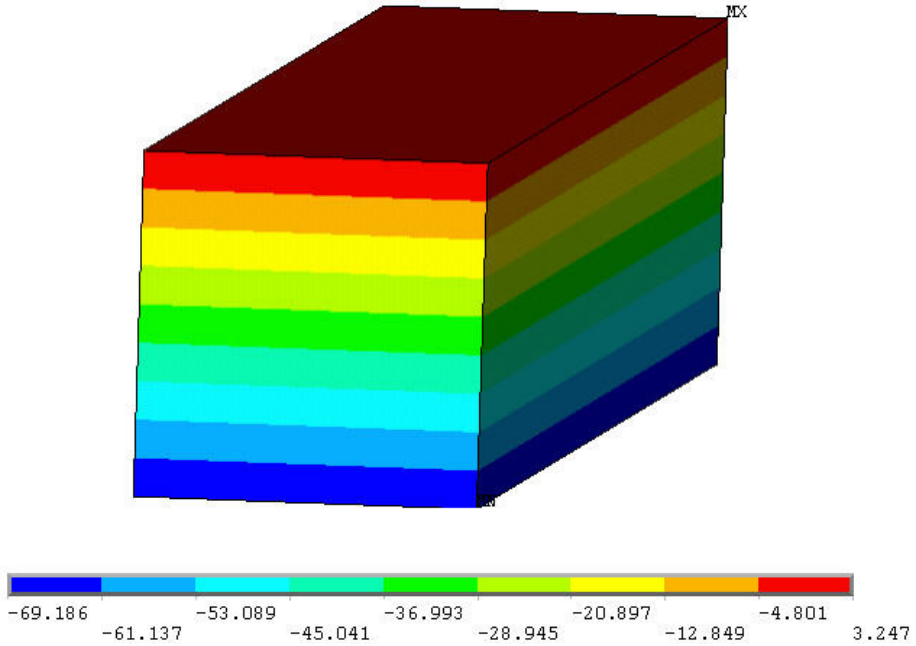

Figure B.4: Average transverse stress at 24 in. for bent "L" connection

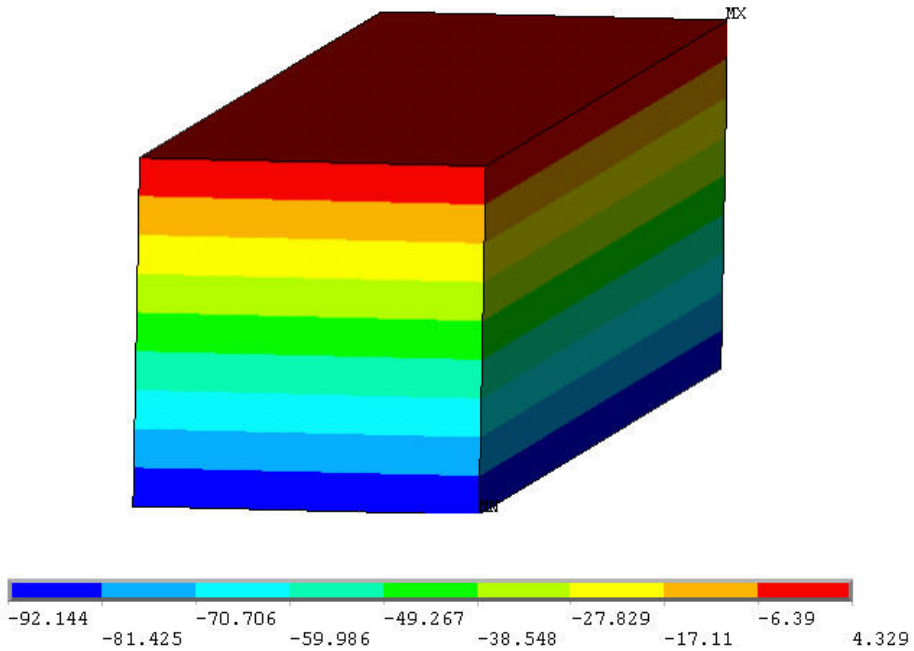

Figure B.5: Average transverse stress at 18 in. for bent “L” connection

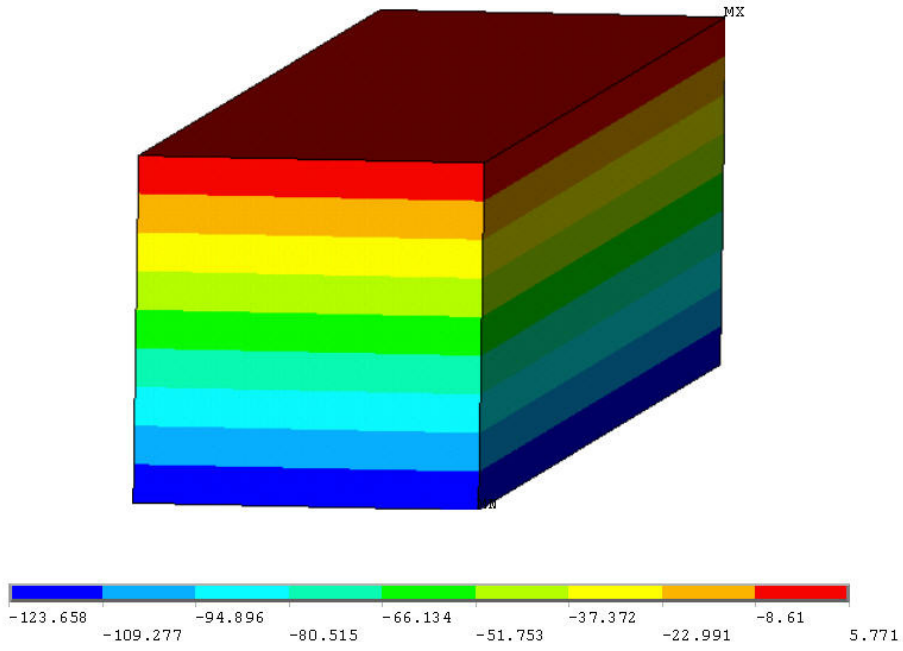

Figure B.6: Average transverse stress at 12 in. for bent “L” connection

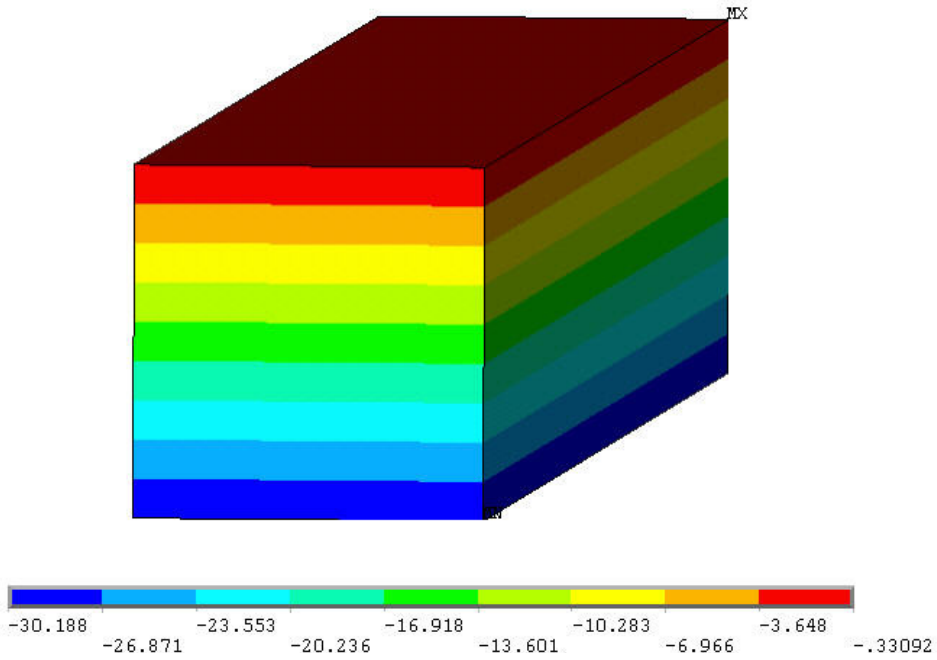

Figure B.7: Average transverse stress at 30 in. for welded flange connection

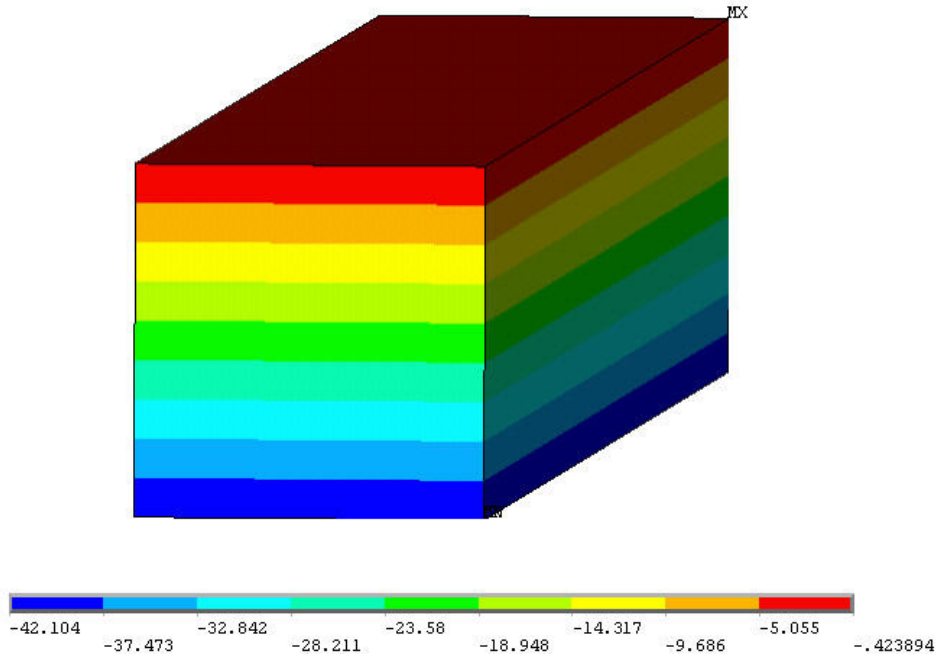

Figure B.8: Average transverse stress at 24 in. for welded flange connection

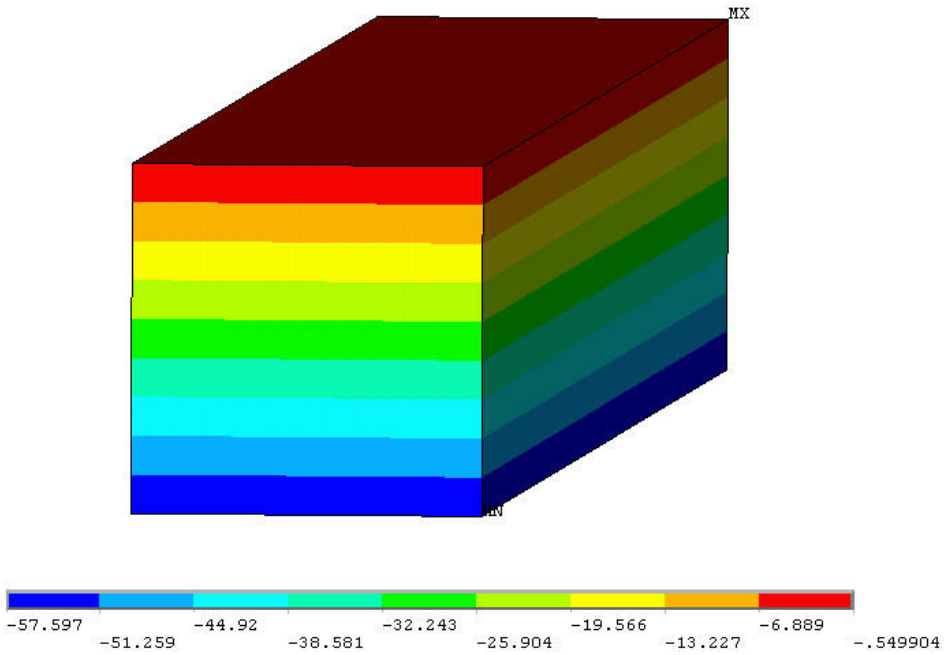

Figure B.9: Average transverse stress at 18 in. for welded flange connection

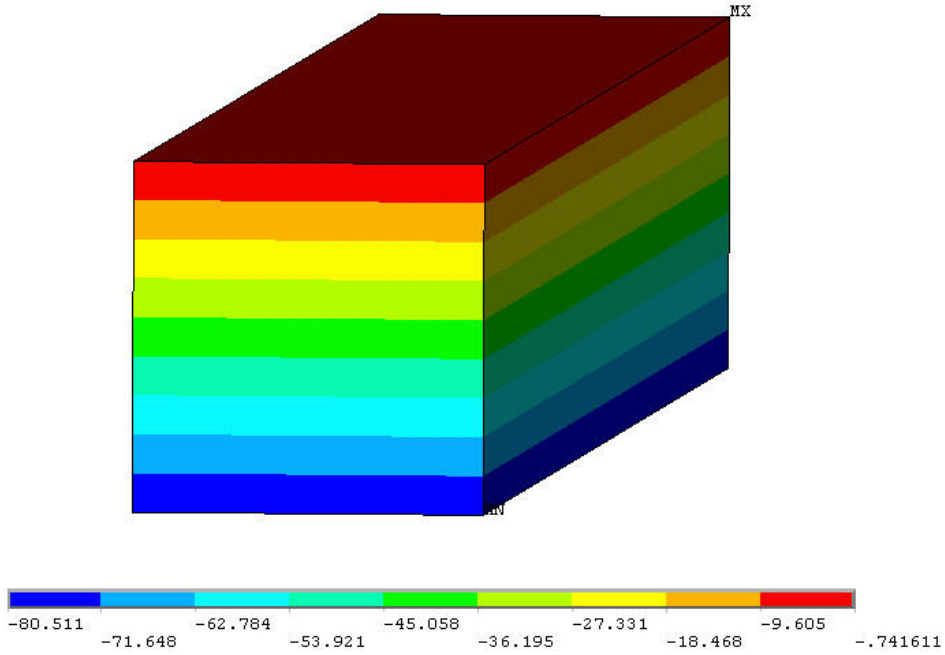

Figure B.10: Average transverse stress at 12 in. for welded flange connection

Appendix C: Additional Global Behavior Supporting Calculations

C.1 Load Distribution Factor calculations

Table C.1: FEA deflections and calculated LDF for Shenley bent "L" connection

Location from edge to tire center	Girder 1	Girder 2	Girder 3	Sum	Girder 1	Girder 2	Girder 3
(ft)	Deflections (in.)				LDF		
12	-0.678	-0.340	-0.073	-1.090	0.622	0.312	0.067
24	-0.627	-0.361	-0.101	-1.089	0.576	0.331	0.093
36	-0.577	-0.380	-0.130	-1.087	0.531	0.350	0.119
48	-0.528	-0.399	-0.160	-1.086	0.486	0.367	0.147
60	-0.480	-0.414	-0.191	-1.085	0.443	0.382	0.176
72	-0.434	-0.427	-0.223	-1.085	0.400	0.394	0.206
84	-0.390	-0.436	-0.258	-1.084	0.360	0.402	0.238
96	-0.348	-0.441	-0.295	-1.084	0.321	0.407	0.272
108	-0.308	-0.441	-0.335	-1.084	0.284	0.407	0.309
120	-0.270	-0.438	-0.376	-1.084	0.249	0.404	0.347
132	-0.235	-0.431	-0.419	-1.085	0.216	0.397	0.387
144	-0.201	-0.419	-0.465	-1.085	0.185	0.386	0.428
156	-0.170	-0.404	-0.512	-1.086	0.156	0.372	0.472
168	-0.139	-0.387	-0.561	-1.087	0.128	0.356	0.516
180	-0.110	-0.368	-0.610	-1.088	0.101	0.338	0.561
192	-0.082	-0.347	-0.661	-1.090	0.075	0.319	0.606

Table C.2: FEA strains and calculated LDF for Shenley bent "L" connection

Location from edge to tire center	Girder 1	Girder 2	Girder 3	Sum	Girder 1	Girder 2	Girder 3
(ft)	Strains (με)				LDF		
12	275.6	133.4	42.0	450.9	0.611	0.296	0.093
24	251.6	149.0	48.8	449.5	0.560	0.332	0.109
36	228.8	163.8	56.3	448.9	0.510	0.365	0.125
48	207.5	177.5	64.4	449.4	0.462	0.395	0.143
60	186.4	188.8	73.5	448.7	0.415	0.421	0.164
72	166.2	198.3	83.8	448.2	0.371	0.442	0.187
84	147.4	205.6	95.8	448.8	0.328	0.458	0.213
96	130.1	209.4	109.4	449.0	0.290	0.466	0.244
108	114.3	209.9	124.7	449.0	0.255	0.468	0.278
120	100.2	207.3	141.4	448.9	0.223	0.462	0.315
132	87.6	201.0	159.7	448.4	0.195	0.448	0.356
144	76.8	192.2	179.5	448.4	0.171	0.429	0.400
156	67.3	181.6	200.4	449.3	0.150	0.404	0.446
168	58.9	168.5	221.6	449.0	0.131	0.375	0.493
180	51.3	154.0	243.8	449.1	0.114	0.343	0.543
192	44.2	138.7	267.6	450.5	0.098	0.308	0.594

Table C.3: FEA deflections and calculated LDF for Shenley flange connection

Location from edge to tire center	Girder 1	Girder 2	Girder 3	Sum	Girder 1	Girder 2	Girder 3
(ft)	Deflections (in.)				LDF		
12	-0.940	-0.490	-0.119	-1.548	0.607	0.317	0.077
24	-0.873	-0.514	-0.159	-1.546	0.565	0.332	0.103
36	-0.808	-0.535	-0.201	-1.544	0.523	0.347	0.130
48	-0.744	-0.555	-0.244	-1.542	0.482	0.360	0.158
60	-0.681	-0.572	-0.288	-1.541	0.442	0.371	0.187
72	-0.620	-0.587	-0.333	-1.540	0.402	0.381	0.216
84	-0.560	-0.598	-0.381	-1.539	0.364	0.388	0.248
96	-0.503	-0.604	-0.432	-1.539	0.327	0.392	0.281
108	-0.449	-0.605	-0.485	-1.539	0.292	0.393	0.315
120	-0.398	-0.601	-0.541	-1.540	0.258	0.390	0.351
132	-0.349	-0.591	-0.600	-1.540	0.227	0.384	0.389
144	-0.303	-0.578	-0.660	-1.541	0.196	0.375	0.429
156	-0.258	-0.561	-0.723	-1.542	0.167	0.364	0.469
168	-0.215	-0.542	-0.786	-1.543	0.139	0.351	0.510
180	-0.173	-0.521	-0.851	-1.545	0.112	0.337	0.551
192	-0.132	-0.498	-0.917	-1.547	0.085	0.322	0.593

Table C.4: FEA strains and calculated LDF for Shenley flange connection

Location from edge to tire center	Girder 1	Girder 2	Girder 3	Sum	Girder 1	Girder 2	Girder 3
(ft)	Strains (με)				LDF		
12	337.2	169.1	54.8	561.2	0.601	0.301	0.098
24	309.2	186.1	64.1	559.4	0.553	0.333	0.115
36	282.6	201.9	74.1	558.7	0.506	0.361	0.133
48	257.9	216.2	85.0	559.1	0.461	0.387	0.152
60	233.5	228.0	96.8	558.3	0.418	0.408	0.173
72	209.6	238.3	109.9	557.8	0.376	0.427	0.197
84	187.0	247.1	124.4	558.5	0.335	0.442	0.223
96	166.0	251.8	140.9	558.8	0.297	0.451	0.252
108	146.9	252.5	159.4	558.8	0.263	0.452	0.285
120	129.7	249.2	179.8	558.7	0.232	0.446	0.322
132	114.5	241.5	201.9	558.0	0.205	0.433	0.362
144	101.0	231.5	225.4	558.0	0.181	0.415	0.404
156	88.8	220.4	249.7	559.0	0.159	0.394	0.447
168	77.7	206.9	274.2	558.8	0.139	0.370	0.491
180	67.4	191.5	300.1	559.0	0.121	0.343	0.537
192	57.8	174.9	327.9	560.6	0.103	0.312	0.585

Table C.5: FEA deflections and calculated LDF for Martin Branch bent “L” connection

Location from edge to tire center	Girder 1	Girder 2	Girder 3	Girder 4	Girder 5	Girder 6	Sum	Girder 1	Girder 2	Girder 3	Girder 4	Girder 5	Girder 6
(ft)	Deflections (in.)							LDF					
12	-0.281	-0.219	-0.124	-0.067	-0.034	-0.004	-0.728	0.386	0.300	0.170	0.092	0.046	0.005
24	-0.255	-0.219	-0.133	-0.073	-0.038	-0.009	-0.726	0.351	0.301	0.183	0.100	0.053	0.012
36	-0.229	-0.216	-0.143	-0.079	-0.043	-0.014	-0.724	0.317	0.299	0.197	0.109	0.060	0.019
48	-0.205	-0.212	-0.154	-0.085	-0.048	-0.019	-0.722	0.284	0.293	0.212	0.118	0.066	0.026
60	-0.183	-0.206	-0.163	-0.092	-0.053	-0.024	-0.721	0.254	0.286	0.227	0.128	0.074	0.033
72	-0.163	-0.198	-0.172	-0.100	-0.058	-0.029	-0.720	0.226	0.275	0.239	0.139	0.081	0.040
84	-0.145	-0.189	-0.178	-0.109	-0.064	-0.034	-0.719	0.202	0.263	0.248	0.151	0.089	0.048
96	-0.129	-0.177	-0.183	-0.119	-0.070	-0.040	-0.718	0.180	0.247	0.254	0.165	0.098	0.056
108	-0.116	-0.164	-0.185	-0.130	-0.077	-0.046	-0.717	0.162	0.229	0.258	0.181	0.107	0.063
120	-0.104	-0.151	-0.185	-0.142	-0.084	-0.051	-0.716	0.145	0.210	0.258	0.198	0.117	0.072
132	-0.093	-0.137	-0.183	-0.153	-0.092	-0.058	-0.716	0.130	0.191	0.256	0.214	0.128	0.081
144	-0.083	-0.124	-0.180	-0.164	-0.101	-0.065	-0.716	0.117	0.173	0.251	0.229	0.141	0.090
156	-0.074	-0.112	-0.174	-0.172	-0.110	-0.073	-0.716	0.104	0.157	0.243	0.241	0.154	0.102
168	-0.066	-0.102	-0.166	-0.179	-0.121	-0.082	-0.716	0.092	0.143	0.231	0.249	0.170	0.114
180	-0.059	-0.094	-0.156	-0.183	-0.134	-0.091	-0.716	0.082	0.131	0.217	0.255	0.187	0.127
192	-0.053	-0.085	-0.144	-0.185	-0.148	-0.102	-0.716	0.073	0.119	0.201	0.258	0.206	0.142
204	-0.047	-0.078	-0.132	-0.185	-0.162	-0.113	-0.717	0.065	0.109	0.184	0.258	0.225	0.158
216	-0.041	-0.071	-0.121	-0.183	-0.175	-0.127	-0.718	0.057	0.099	0.168	0.255	0.244	0.176
228	-0.035	-0.065	-0.110	-0.179	-0.187	-0.142	-0.719	0.049	0.091	0.153	0.250	0.260	0.197
240	-0.030	-0.059	-0.102	-0.173	-0.197	-0.159	-0.720	0.041	0.083	0.141	0.241	0.273	0.221
252	-0.025	-0.054	-0.094	-0.165	-0.205	-0.179	-0.721	0.034	0.075	0.130	0.229	0.284	0.248
264	-0.020	-0.049	-0.086	-0.156	-0.211	-0.201	-0.722	0.027	0.068	0.120	0.215	0.292	0.278
276	-0.015	-0.044	-0.080	-0.145	-0.216	-0.224	-0.724	0.020	0.061	0.110	0.200	0.298	0.310
288	-0.010	-0.039	-0.074	-0.135	-0.218	-0.250	-0.726	0.014	0.054	0.102	0.186	0.301	0.344
300	-0.005	-0.035	-0.068	-0.125	-0.219	-0.276	-0.728	0.007	0.048	0.094	0.172	0.301	0.379

Table C.6: FEA strains and calculated LDF for Martin Branch bent “L” connection

Location from edge to tire center	Girder 1	Girder 2	Girder 3	Girder 4	Girder 5	Girder 6	Sum	Girder 1	Girder 2	Girder 3	Girder 4	Girder 5	Girder 6
(ft)	Strains (με)							LDF					
12	182.8	130.0	92.1	48.8	25.8	9.8	489.3	0.374	0.266	0.188	0.100	0.053	0.020
24	169.2	127.4	97.2	55.0	29.1	12.2	490.2	0.345	0.260	0.198	0.112	0.059	0.025
36	155.6	124.8	101.3	61.7	32.3	14.4	490.2	0.318	0.255	0.207	0.126	0.066	0.029
48	142.4	122.4	104.7	68.5	35.8	16.4	490.1	0.290	0.250	0.214	0.140	0.073	0.034
60	129.5	120.1	107.3	75.2	39.5	18.6	490.2	0.264	0.245	0.219	0.153	0.081	0.038
72	116.8	117.2	108.7	81.5	43.9	21.1	489.2	0.239	0.240	0.222	0.167	0.090	0.043
84	104.4	114.4	109.4	87.2	48.9	24.0	488.3	0.214	0.234	0.224	0.179	0.100	0.049
96	92.8	112.0	110.6	92.3	54.6	26.9	489.3	0.190	0.229	0.226	0.189	0.112	0.055
108	82.3	108.5	111.1	96.8	60.9	29.9	489.5	0.168	0.222	0.227	0.198	0.124	0.061
120	72.7	104.2	111.0	100.7	67.6	33.0	489.2	0.149	0.213	0.227	0.206	0.138	0.067
132	64.0	99.5	110.6	104.0	74.4	36.8	489.1	0.131	0.203	0.226	0.213	0.152	0.075
144	56.0	94.3	109.4	106.3	81.0	41.5	488.4	0.115	0.193	0.224	0.218	0.166	0.085
156	48.8	88.5	107.8	107.5	87.3	47.4	487.3	0.100	0.182	0.221	0.221	0.179	0.097
168	42.6	82.3	106.6	109.0	93.2	54.5	488.2	0.087	0.169	0.218	0.223	0.191	0.112
180	37.6	75.7	104.5	110.4	98.5	62.3	489.1	0.077	0.155	0.214	0.226	0.201	0.127
192	33.7	68.9	101.4	110.9	103.3	70.9	489.1	0.069	0.141	0.207	0.227	0.211	0.145
204	30.4	62.2	97.6	111.1	107.7	80.3	489.4	0.062	0.127	0.199	0.227	0.220	0.164
216	27.5	55.8	93.3	110.8	111.4	90.7	489.4	0.056	0.114	0.191	0.226	0.228	0.185
228	24.6	50.0	88.3	109.6	113.9	102.1	488.4	0.050	0.102	0.181	0.224	0.233	0.209
240	21.6	44.8	82.6	108.9	116.6	114.3	488.9	0.044	0.092	0.169	0.223	0.239	0.234
252	19.1	40.3	76.4	107.7	119.6	127.0	490.1	0.039	0.082	0.156	0.220	0.244	0.259
264	16.8	36.5	69.8	105.3	121.9	139.8	490.1	0.034	0.074	0.142	0.215	0.249	0.285
276	14.8	33.0	63.0	102.1	124.3	153.0	490.2	0.030	0.067	0.129	0.208	0.254	0.312
288	12.7	29.7	56.3	98.1	126.9	166.6	490.3	0.026	0.061	0.115	0.200	0.259	0.340
300	10.3	26.5	50.0	93.2	129.4	180.1	489.5	0.021	0.054	0.102	0.190	0.264	0.368

Table C.7: FEA deflections and calculated LDF for Martin Branch flange connection

Location from edge to tire center	Girder 1	Girder 2	Girder 3	Girder 4	Girder 5	Girder 6	Sum	Girder 1	Girder 2	Girder 3	Girder 4	Girder 5	Girder 6
(ft)	Deflections (in.)							LDF					
12	-0.446	-0.342	-0.205	-0.116	-0.063	-0.021	-1.191	0.374	0.287	0.172	0.097	0.053	0.017
24	-0.405	-0.341	-0.219	-0.126	-0.071	-0.027	-1.188	0.341	0.287	0.184	0.106	0.060	0.023
36	-0.366	-0.337	-0.234	-0.137	-0.078	-0.033	-1.185	0.308	0.284	0.197	0.116	0.066	0.028
48	-0.328	-0.331	-0.250	-0.149	-0.086	-0.039	-1.183	0.277	0.280	0.211	0.126	0.073	0.033
60	-0.294	-0.322	-0.264	-0.161	-0.095	-0.045	-1.181	0.249	0.273	0.223	0.136	0.080	0.038
72	-0.263	-0.311	-0.276	-0.174	-0.104	-0.052	-1.179	0.223	0.264	0.234	0.147	0.088	0.044
84	-0.235	-0.298	-0.284	-0.187	-0.113	-0.060	-1.178	0.199	0.253	0.241	0.159	0.096	0.051
96	-0.210	-0.283	-0.290	-0.202	-0.124	-0.068	-1.176	0.178	0.241	0.247	0.172	0.105	0.058
108	-0.187	-0.265	-0.294	-0.218	-0.135	-0.076	-1.175	0.159	0.226	0.250	0.186	0.115	0.065
120	-0.168	-0.246	-0.294	-0.235	-0.147	-0.085	-1.175	0.143	0.209	0.250	0.200	0.125	0.072
132	-0.151	-0.226	-0.292	-0.252	-0.160	-0.094	-1.174	0.128	0.193	0.248	0.214	0.136	0.080
144	-0.135	-0.208	-0.286	-0.266	-0.174	-0.105	-1.174	0.115	0.177	0.244	0.226	0.148	0.090
156	-0.121	-0.192	-0.278	-0.276	-0.189	-0.118	-1.174	0.103	0.163	0.237	0.235	0.161	0.101
168	-0.108	-0.177	-0.268	-0.285	-0.205	-0.132	-1.174	0.092	0.150	0.228	0.243	0.174	0.113
180	-0.096	-0.163	-0.255	-0.291	-0.223	-0.147	-1.174	0.082	0.138	0.217	0.248	0.190	0.126
192	-0.086	-0.149	-0.239	-0.294	-0.242	-0.164	-1.174	0.073	0.127	0.203	0.250	0.206	0.140
204	-0.078	-0.137	-0.222	-0.294	-0.262	-0.183	-1.175	0.066	0.117	0.189	0.250	0.223	0.156
216	-0.070	-0.126	-0.205	-0.291	-0.280	-0.205	-1.176	0.059	0.107	0.174	0.247	0.238	0.174
228	-0.062	-0.115	-0.190	-0.285	-0.296	-0.230	-1.178	0.052	0.098	0.161	0.242	0.251	0.195
240	-0.054	-0.106	-0.177	-0.277	-0.309	-0.257	-1.179	0.046	0.090	0.150	0.235	0.262	0.218
252	-0.047	-0.097	-0.164	-0.266	-0.320	-0.287	-1.181	0.040	0.082	0.139	0.226	0.271	0.243
264	-0.040	-0.088	-0.151	-0.253	-0.329	-0.321	-1.182	0.034	0.074	0.128	0.214	0.279	0.272
276	-0.034	-0.080	-0.139	-0.237	-0.336	-0.358	-1.185	0.029	0.068	0.118	0.200	0.284	0.302
288	-0.028	-0.072	-0.128	-0.222	-0.340	-0.397	-1.187	0.024	0.061	0.108	0.187	0.286	0.334
300	-0.022	-0.065	-0.118	-0.207	-0.342	-0.438	-1.191	0.018	0.054	0.099	0.174	0.287	0.367

Table C.8: FEA strains and calculated LDF for Martin Branch flange connection

Location from edge to tire center	Girder 1	Girder 2	Girder 3	Girder 4	Girder 5	Girder 6	Sum	Girder 1	Girder 2	Girder 3	Girder 4	Girder 5	Girder 6
(ft)	Strains (με)							LDF					
12	248.4	171.2	125.7	68.3	37.6	20.2	671.3	0.370	0.255	0.187	0.102	0.056	0.030
24	230.5	167.1	133.3	78.2	42.2	21.8	673.1	0.342	0.248	0.198	0.116	0.063	0.032
36	212.3	163.6	139.2	88.6	46.9	23.1	673.7	0.315	0.243	0.207	0.132	0.070	0.034
48	194.2	160.7	143.6	99.0	51.9	24.4	673.7	0.288	0.239	0.213	0.147	0.077	0.036
60	176.2	158.4	146.6	108.9	57.4	26.1	673.6	0.262	0.235	0.218	0.162	0.085	0.039
72	158.3	155.8	147.8	117.8	63.9	28.3	672.0	0.236	0.232	0.220	0.175	0.095	0.042
84	140.8	153.5	148.4	125.4	71.3	31.3	670.7	0.210	0.229	0.221	0.187	0.106	0.047
96	124.4	151.7	149.5	132.1	79.7	34.6	671.9	0.185	0.226	0.222	0.197	0.119	0.051
108	109.5	148.7	150.0	137.6	88.8	37.8	672.4	0.163	0.221	0.223	0.205	0.132	0.056
120	96.0	144.4	149.9	142.0	98.3	41.5	672.1	0.143	0.215	0.223	0.211	0.146	0.062
132	83.8	139.2	149.7	145.3	107.8	46.1	671.9	0.125	0.207	0.223	0.216	0.160	0.069
144	72.7	133.1	148.8	147.0	116.7	52.4	670.7	0.108	0.198	0.222	0.219	0.174	0.078
156	62.6	126.1	147.7	147.5	124.6	60.8	669.2	0.094	0.188	0.221	0.220	0.186	0.091
168	53.9	118.3	147.2	148.6	131.7	70.6	670.3	0.080	0.177	0.220	0.222	0.197	0.105
180	47.2	109.6	145.8	149.6	138.1	81.5	671.8	0.070	0.163	0.217	0.223	0.206	0.121
192	42.3	100.2	142.7	149.9	143.5	93.5	672.1	0.063	0.149	0.212	0.223	0.213	0.139
204	38.5	90.6	138.6	150.0	147.9	106.8	672.4	0.057	0.135	0.206	0.223	0.220	0.159
216	35.2	81.4	133.2	149.7	151.2	121.4	672.1	0.052	0.121	0.198	0.223	0.225	0.181
228	32.0	72.9	126.8	148.5	153.1	137.5	670.8	0.048	0.109	0.189	0.221	0.228	0.205
240	28.9	65.3	119.4	147.9	155.3	154.8	671.5	0.043	0.097	0.178	0.220	0.231	0.231
252	26.4	58.6	110.8	147.0	157.9	172.7	673.4	0.039	0.087	0.164	0.218	0.235	0.256
264	24.7	52.9	101.0	144.3	160.2	190.6	673.8	0.037	0.079	0.150	0.214	0.238	0.283
276	23.4	47.8	90.7	140.1	162.9	208.7	673.7	0.035	0.071	0.135	0.208	0.242	0.310
288	22.1	43.1	80.2	134.5	166.4	226.9	673.3	0.033	0.064	0.119	0.200	0.247	0.337
300	20.5	38.5	70.2	127.3	170.3	244.9	671.6	0.031	0.057	0.104	0.189	0.254	0.365